# STRUCTURAL, THERMAL, AND ACOUSTIC PERFORMANCE OF POLYURETHANE FOAMS FOR GREEN BUILDINGS

Mangesh Nar, B.E., M.S.

Dissertation Prepared for the Degree of

DOCTOR OF PHILOSOPHY

UNIVERSITY OF NORTH TEXAS

December 2014

APPROVED:

Nandika D'Souza, Major Professor
Yong Tao, Minor Advisor
Witold Brostow, Committee Member
Jincheng Du, Committee Member
Jaehyung Ju, Committee Member
Sheldon Shi, Committee Member
Nigel D. Shepherd, Chair of the Department of Materials Science and Engineering
Costas Tsatsoulis, Dean of the College of Engineering
Mark Wardell, Dean of the Toulouse Graduate School

Nar, Mangesh. Structural, Thermal and Acoustic Performance of Polyurethane Foams for Green Buildings. Doctor of Philosophy (Materials Science and Engineering), December 2014, 159 pp., 18 tables, 52 figures, chapter references.

Decreasing the carbon footprint through use of renewable materials has environmental and societal impact. Foams are a valuable constituent in buildings by themselves or as a core in sandwich composites. Kenaf is a Southeast USA plant that provides renewable filler. The core of the kenaf is porous with a cell size in a 5-10 micrometer range. The use of kenaf core in foams represents a novel multiscalar cellular structural composite. Rigid polyurethane foams were made using free foaming expansion with kenaf core as filler with loadings of 5, 10 and 15 %. Free foaming was found to negatively affect the mechanical properties. An innovative process was developed to introduce a constraint to expansion during foaming. Two expansion ratios were examined: 40 and 60 % (decreasing expansion ratio). MicroCT and SEM analysis showed a varying structure of open and closed cell pores. The mechanical, thermal insulation, acoustic properties were measured. Pure PU foam showed improved cell size uniformity. Introducing kenaf core resulted in decreasing the PU performance in the free expansion case. This was reversed by introducing constraints. To understand the combined impact of having a mixed close cell and open cell architecture, finite element modeling was done using ANSYS. Models were created with varying percentages of open, closed, and bulk cells to encompass entire range of foam porosities. Net zero energy building information modelling was conducted using EnergyPlus was conducted using natural fiber composite skins. Environmental impacts for instance global warming potential, acidification, eutrophication, fossil fuel consumption, ozone depletion, and

smog potential of the materials used in construction was studied using life cycle assessment. The results showed improvement on energy consumption and carbon footprint.

ACKNOWLEDGEMENTS

My sincere gratitude towards Dr. Nandika Anne D‘Souza, for she has been my mentor, guide, and philosopher in a true sense. She inculcated in me research curiosity by initiating intellectually stimulating discourses which made research a lifetime of experience. A profound statement she made while I made a mistake was —don‘t ever worry about making mistakes, you can always correct them, and that‘s the reason pencils have erasers‖. This statement freed me to try all possible things for research ever worrying about going wrong. This dissertation would not have been possible without her support, tutelage, and guidance. I will always remain indebted to her.

I would like to thank Dr. Yong Tao and Dr. Junghyon Mun for letting me do the building simulation study on Zero Net Energy lab. Thanks to Suraj Talele and Naimee Hasib for guiding me through the simulation process. My special thanks to Wael Zaitouni for helping me in setting up acoustics system; without whom the acoustics chapter would not have been possible. Thanks to Noe who helped me in acoustics measurements.

I will never forget the loud laughter that reverberated the passage way of material science and engineering department with Shailesh Vidhate and Sandeep Manandhar, it was fun, and I still miss you both. Thank you Andres Garcia, Shunli Zhao, Gerrit Staufenberg, Mickey Richardson, Bing Yang, Gabriel Viscondi, Hugo Diaz, Hussain Rizvi, Worasak Klongthong, Changlei Xia, Jeerapan Teingtong, and Fancine Mascarenhas.

Lastly to my family and Rachana Akhade who supported me throughout unconditionally.

TABLE OF CONTENTS

Page

LIST OF FIGURES

Page

LIST OF TABLES

# GLOSSARY

| | |
|---|---|
| AEP | Aquatic eutrophication potential |
| Al | Aluminum |
| AP | Acidification potential |
| APP | Aromatic polyester polyols |
| ASTM | American Society for Testing and Materials |
| CFC-11 | trichlorofluoromethane |
| CFC-12 | dichlorodifluoromethane |
| CI | Category indicator |
| DOE | Department of Energy |
| EPP | Expanded polypropylene |
| EPS | Expanded polystyrene foams |
| EPW | Weather data format |
| ESEM | Environmental scanning electron microscopy |
| GWP | Global warming potential |
| HCFCs | Hydrochlorofluorocarbon(s) |
| HCs | Hydrocarbons |
| HDPE | High density polyethylene |
| IDF | Input data files |
| ISO | International Organization for Standardization |
| LCA | Life-cycle assessment |
| LCIA | Life-cycle impact assessment |
| LDPE | Low density polyethylene |

| | |
|---|---|
| MDI | Methylene diphenyl diisocyanate |
| MMDI | di-cyclic monomeric MDI |
| Ni | Nickel |
| NREL | National Research Energy Laboratory |
| PEO | Polyethylene oxide |
| PLA | Poly-lactic acid |
| PMDI | Polycyclic polyisocyanates |
| POPC | Photooxidant formation potential |
| PPE | Personal protective equipment |
| PTFE | Polytetrafluoroethylene |
| PU | Polyurethanes |
| PVC | Polyvinyl chloride |
| QBtu | Quadrillion Btu |
| RPUFs | Rigid polyurethane foams |
| SIP | Structural insulated panel |
| SOD | Stratospheric ozone depletion |
| TDI | Toluene diisocyanate |
| TEP | Terrestrial eutrophication potential |
| Tg | Teragrams |
| Ti | Titanium |
| UVR | Ultraviolet radiation |
| VOC | Volatile organic compounds |
| WAHP | Water-to-air heat pump |

| | |
|---|---|
| WHO | World Health Organization |
| WWHP | Water-to-water heat pump |
| ZOE | Zero Energy Research Lab |

# CHAPTER 1

# INTRODUCTION

## 1.1 Porous Materials

Porous materials are used in a number of applications such as structural insulation panels, fuel cells, filters, sieves, membranes, scaffold development for tissue engineering etc. Natural zeolite was discovered over 250 years ago by Swedish mineralogist Axel F. Cronstedt first described its porous nature [1]. This high porosity made zeolite a natural filter [2], molecular sieve [3], catalysts adsorbers [4], and ion exchangers [5]. This porosity inspired scientists to make synthetic zeolites as an alternative to natural zeolite [6]. Another example of natural porosity inspiration was bone implants. These implants initially were made from titanium due to its biocompatibility as well as non-corrosive nature [7,8]. However, porosity needed to be introduced in-order to reduce the high stiffness of titanium to match the stiffness of bone [9]. Polymer composites materials were then developed to replace titanium in most of the bone implant applications. Polymers such as highly porous high density polyethylene (HDPE) [10], polytetrafluoroethylene (PTFE) [11], poly-lactic acid (PLA) [12], polyethylene oxide (PEO) [13] are widely used as porous scaffolds for bone regeneration and growth.

Recent development in porous material is use of metals such as aluminium (Al), titanium (Ti), and nickel (Ni). The applications that demands low weight, high strength such as automotive and aerospace industries have started to explore a possibility to incorporate porous metals into their design. Aluminium foam alloy with closed cells (Alporas™) is used for shielding electromagnetic field [14].

## 1.2 Eiffel Tower: Bio-Inspired Engineering Design

Man has always looked up to nature for designs that are efficient and innovative. Amongst such myriad examples, the one that stands out in a literal sense is Eiffel tower in Paris. The design engineer Gustavo Eiffel derived inspiration in an attempt to come up with an innovative design he was inclined towards the work of anatomist Herman von Meyer for his work on human femur, and ball and socket joint [15].

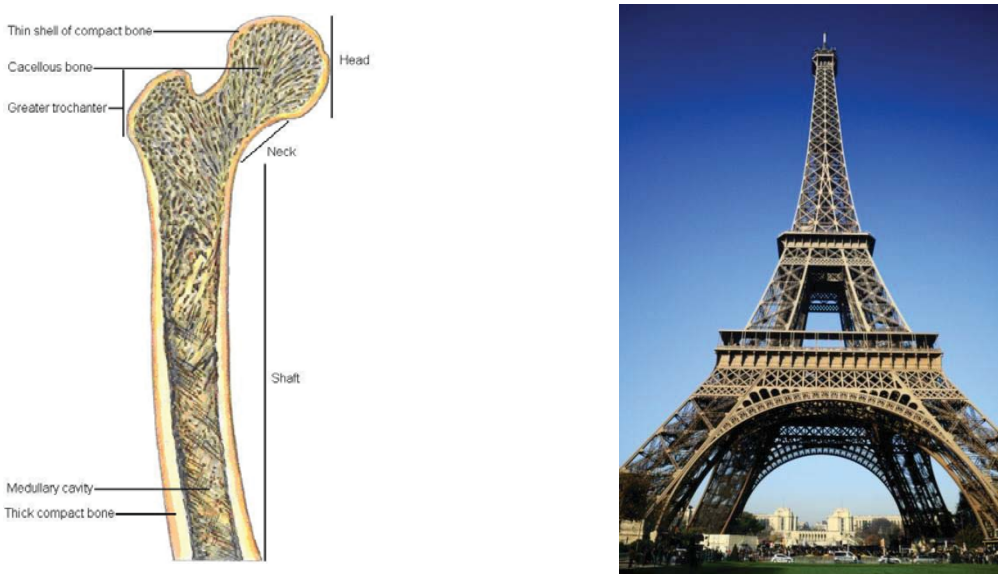


A B

*Figure 1-1* (A) longitudinal section of the human femur bone to reveal the interconnectivity of trabecular and cortical bone [16], (B) photo of Eiffel Tower [17].

Later when the design and construction were completed, contemporary architects predicted the fall of Eiffel tower by collapsing under its own weight. However even today it still stands. Karl Cullman derived model on the basis of femur design and made a startling discovery of resemblance of use of struts and braces used typically in construction of buildings. Gustavo Eiffel then designed the tower on the basis of the research of anatomist Herman von Meyer and engineer Karl Cullman.

### 1.2.1 Hierarchical Natural Cellular Structure – Bone

Bone is hierarchical [18] natural foam composite that functions as a structural element for framework for body and as a cage to house, and protects internal organs. In a process to continuously modify for the distribution of the applied load, during the course of evolution and natural selection the bone developed into a structure that we see today. One of the studies that we did was to look at the influence of collagen crosslink's on the mechanical properties [19]. At the end of microfibrills of collagen the hydroxyappatite crystallizes and as the bone ages the collagen crosslink's increases to give higher stiffness and less deformation. The mineral content increases thereby increasing the strength of the bone however rendering them brittle. Response of bone to the impact is very interesting. The bone is termed as live composite. This is because the porous structure of the bone aids it to distribute the impact of the load. When the bone is loaded the tissues responds to this load and the osteoclast dissolves the bone, the osteoblast forms the bone in response to the load to make it more tolerable to the higher impacts, thereby increasing the strength of the bone.

### 1.2.2 Naturally Occurring Porous and Cellular Materials

Pumice is naturally occurring rigid closed cell foam. It is mainly composed of 60 % of silica ($SiO_2$) and 16 % alumina ($Al_2O_3$) [20]. The volcanic eruption of molten lava is ejected into air. In this process the air gets mixed with the lava. When the rock cools down the air inside becomes the closed pores and the rock becomes the struts of the rigid foam. The pumice cell morphology can be seen from the Figure 1-1.

A

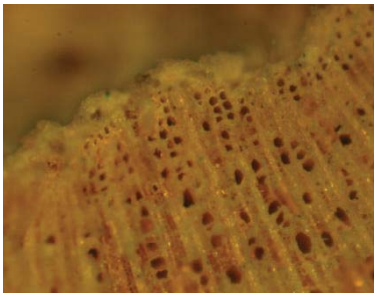

B

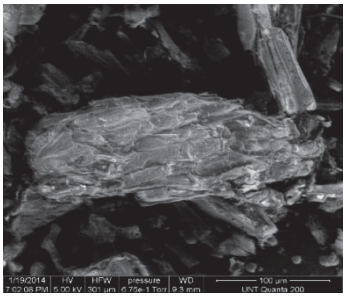

C

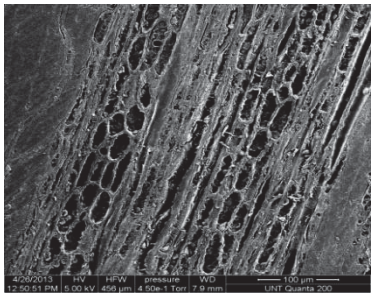

D

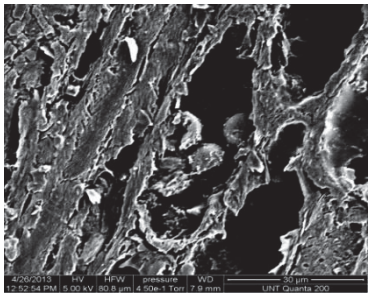

E

F

G

H

I

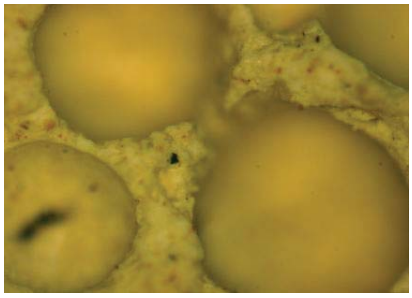

J

*Figure 1.2.* Naturally occurring porous materials (A) kenaf core dried stalk with powdered kenaf core, (B) optical microscope image of stalk cross section, (C) scanning electron microscope image for powdered kenaf core, (D) and (E) cross section of kenaf core revealing the micro-pores. (F), (G), (H), (I), and (J) are kenaf fibers, bacterial retted kenaf fibers, sugarcane fibers, pumice stone, and optical image of pumice stone showing its closed foam cell morphology.

## 1.3 Polyurethane Foams

Polyurethanes (PU) were discovered in 1937 by Otto Bayer, which got developed into versatile material with potential use in variety of applications. In addition to the incorporation of urethane linkages, they can contain on the basis of raw material linkages with urea, ether, and ester [21]. The urethane linkage (-NH-CO-O-) which is typically an ethyl carbamate (ethyl carbamate is also called as urethane and that's where the polyurethane name was derived from) is formed from the reaction of hydroxyl group of one component with isocyanate group of other component. Polyurethane finds applications in foams, coatings, upholstery etc.

Rigid polyurethane foams (RPUFs), which are basically closed cell foams, find applications in wide range of products. Applications such as insulation panel for buildings, and refrigerators being of main importance. Rigid closed cells impart superior thermal insulation property to the material that can be further improved by using low thermal conductive blowing gas [22]. Apart from thermal insulation rigid polyurethane foams perform well in compression load and also is very easily processable [23]. Its low viscous pour in place characteristics is useful in molding complex shapes. Later the low viscous two part (polyol and isocyanate) components start reacting. A two step exothermic reaction takes place where the translucent mixture starts becoming opaque. This loss of translucency is due to the fact that the polyol and isocyanate reacts to liberate $CO_2$ gas. This step is also termed as gelling. Later the curing of polyurethane takes place to give dimensional stability as well as full attainment of the mechanical properties. Alternate method to the exothermic expansion of the blowing agent is to use the agent that has boiling point below room temperature. This agent is mixed in one of

the component and is stored in pressurized vessel. When the mixture is depressurized the blowing agent comes in form of gas and foams the reaction mixture.

### 1.3.1 Isocyanates

All most all polyurethanes are made from toluene diisocyanate (TDI) and methylene diphenyl diisocyanate (MDI) including rigid as well as flexible PU. Initially phosgenation of aromatic or aliphatic amines was used to synthesize isocyanates. Phosgene free routes have been recently used to prepare isocyanates.

$$R\text{-}NO_2 + 3CO + R'\text{-}OH \rightarrow R\text{-}NH\text{-}CO\text{-}O\text{-}R' + 2CO_2\uparrow$$

Nitro compound is reduced in presence of alcohol and carbonyl group to give an unstable urethane.

$$R\text{-}NH\text{-}CO\text{-}O\text{-}R' \rightarrow R\text{-}NCO + R'\text{-}OH$$

In the above step the unstable urethane is thermally decomposed to give isocyanate.

MDI is a mixture of di-cyclic monomeric MDI (MMDI) and polycyclic polyisocyanates (PMDI) with proportions respectively 48% of 2 ring monomeric MDI, 27, 5, 4, and16% of 3-ring, 4-ring, 5-ring, and higher homologues ring compounds [24].

TDI that is produced using toluene diamine which is a mixture of 2,4 and 2,6 isomers in ratio of 20:80 or 65:35.

### 1.3.2 Polyol

Polyols are oligomers, which has at least two hydroxyl groups. Polyols can be polyether polyols, polyester polyols, aromatic polyester polyols, or can be a combination of polyether-polyester polyol.

#### 1.3.2.1 Polyether Polyols

For rigid polyurethane polyether polyol that is used is of high functionality. These polyols are therefore produced using glycerol, sorbitol, and sucrose initiators. The functionality should be inbetween 3 to 8 [25].

#### 1.3.2.2 Polyester Polyols

These are produced using di-basic acids with glycols, an alternate route of ring opening polymerization of lactones can also be utilized to synthesize polyester polyols.

#### 1.3.2.3 Aromatic Polyester Polyols

Aromatic polyester polyols (APP) are widely used for rigid polyurethane foams, and have found applications in building construction as insulating board [26]. APP is manufactured from carboxylic acids with alcohols. These polyols family was found to perform better as flame resistant foams due to the presence of aromatic ring in the main chain of the chemical [27].

### 1.3.3 Blowing Agents and Environmental Concerns

CFC-11 (trichlorofluoromethane) was the first blowing agent ever used around 1960s for making rigid polyurethane foams. The thermal conductivity depended on the material as well as the blown gas into the closed cell [28]. The gas was retained in the closed cell for longer helped to keep the thermal conductivity lower for longer period of time. With CFC-11 the thermal conductivity of the foams were measured to be 15 mW/m.K. Although CFC-11 and CFC-12 (dichlorodifluoromethane) being a very effective blowing agent were discovered to be ozone depleting. NASA detected a hole in stratospheric ozone layer and the depletion was attributed to CFCs [29]. World wide it

was agreed upon to slowly reduce the consumption of CFCs and replace by more environmentally friendly blowing agents; this effort today is well known by the Montreal Protocol [30].

The phasing out of CFCs led to other blowing agent development such as hydrochlorofluorocarbon(s) (HCFCs). HCFCs required greater control on processing of foams and these foams were dimensionally less stable which required the foams to be of higher densities [31].

Water when used as blowing agent liberates $CO_2$ gas. This gives better insulation than when air is used as physical blowing agent but performs poor when subjected to aging. However, diffusion of $CO_2$ from within the cells of the foams can be delayed by additionally gluing impervious film on the outside of the foams [32], which is also used in expanded polystyrene foams (EPS) [33].

## 1.4 Scope of Dissertation

Rigid PU foams are valuable in many construction applications. Kenaf is a bast fiber plant where the surface stem skin provides bast fibers whose strength-to-weight ratio competes with glass fiber. The higher volume product of the kenaf core is an under-investigated area in composite applications. The naturally porous structure of kenaf-core provides a novel reinforcement particle. In chapter 2, foams of rigid polyurethane with 5, 10, and 15% kenaf-core were formed. To date efforts at using it as reinforcement have proven largely unsuccessful. This was mirrored in this effort when free expansion of the foam was utilized. However introducing constrained foaming as described in chapter 2, resulted in reinforcement. The environmental scanning electron microscopy is used in conjunction with in–situ microCT compression to capture the

change in void fractions before and after deformation. The results show that free foaming resulted in poor reinforcement while a constrained expansion on the foam increased the reinforcement potential of the kenaf core.

In-order to capture detailed deformation mechanism which could not be studied via microCT, ANSYS simulation was employed in chapter 4. Rigid low density polyurethane foam geometries were modeled. Model design was done considering the porosity, and void volume of the foams. Design was developed to include increasing porosity with open and closed cells, and void volume taking account for bulk material distributed with open, and closed cells with uniform cell face thickness. The inner edge radius was adjusted according to the foam type; this is called as edge spread. Uniaxial compression test was modeled as a typical foam product usually is loaded in compression. In this test initial plastic deformation of faces predominantly hexagonal was observed. For closed cell foam apart from material gas phase too provides compressive resistance, therefore $CO_2$ gas filled closed cells were modeled for gas contribution for compressive stress.

The foam composites were tested for acoustics properties in chapter 4 such as normal sound absorption coefficient, reflection, and normal transmission loss. An acoustics system was built according to ASTM standards. Two standards were used to measure acoustics properties, one being two microphone impedance tube methods (ASTM 1050) and second being four microphone impedance tube methods (ASTM E2611-09). These properties of the foam showed correlation with the viscoelastic properties of the PU material. The cell size distribution showed an influence on the sound absorption coefficient whereas the normal transmission loss was a result of

storage modulus and tan delta of the materials. A combination of foam with different cell size distribution is recommended in order to achieve higher acoustics properties in frequency range of 100 to 5000 Hz.

Thermal conductivities of the foam composites were measured before and after aging for 90 days in chapter 5. Negligible change in thermal conductivity is observed due to low diffusion of CO2 from within the cells of foams to the atmosphere. This low diffusion was attributed to the homogeneous distribution of urea hard domains in the matrix of polyurethane soft domains. The Raman spectroscopy was done to measure the urea-urethane ratio and its influence on the diffusion of $CO_2$ and ultimately its influence on thermal conductivity.

Further in Chapter 5 we have made rigid polyurethane foams by incorporating kenaf core which is plant based and hence environmentally less impactful material than PU. A volume expansion method was employed to improve the thermal properties of the foam. Further sandwich foam composites were made using kengro kenaf fiber – polyester, bacterial kenaf fiber polyester, sugarcane polyester, and fiberglass polyester. Panels have shown to improve thermal properties of foam even further. Energy consumption was simulated using the experimentally measured thermal conductivity of foams and sandwich foam composites for Zero Energy Research Lab (ZOE) model using energyplus software (Chapter 6). Life cycle assessment (LCA) was done to measure environmental impact. Results show that sandwich foam composites with sugarcane panels show lower thermal conductance and hence superior thermal properties with minimal environmental impact.

## 1.5 References


[1] Colella, Carmine, and Alessandro F. Gualtieri. "Cronstedt's zeolite." Microporous and Mesoporous Materials 105, no. 3 (2007): 213-221.

[2] Sheng-Bing, Gang Xue, and Hai-Nan Kong. "The performance of BAF using natural zeolite as filter media under conditions of low temperature and ammonium shock load." Journal of hazardous materials 143, no. 1 (2007): 291-295.

[3] Davis, Mark E., and Raul F. Lobo. "Zeolite and molecular sieve synthesis." Chemistry of Materials 4, no. 4 (1992): 756-768.

[4] Bernal, M. P., and J. M. Lopez-Real. "Natural zeolites and sepiolite as ammonium and ammonia adsorbent materials." Bioresource Technology 43, no. 1 (1993): 27-33.

[5] Ćurković, Lidija, Štefica Cerjan-Stefanović, and Tugomir Filipan. "Metal ion exchange by natural and modified zeolites." Water research 31, no. 6 (1997): 1379-1382.

[6] Sherman, John D. "Synthetic zeolites and other microporous oxide molecular sieves." Proceedings of the National Academy of Sciences 96, no. 7 (1999): 3471-3478.

[7] Albrektsson, T., P-I. Brånemark, H-A. Hansson, and J. Lindström. "Osseointegrated titanium implants: requirements for ensuring a long-lasting, direct bone-to-implant anchorage in man." Acta Orthopaedica 52, no. 2 (1981): 155-170.

[8] Davidson, James A., and Paul Kovacs. "Biocompatible low modulus titanium alloy for medical implants." U.S. Patent 5,169,597, issued December 8, 1992.

[9] Krishna, B. Vamsi, Susmita Bose, and Amit Bandyopadhyay. "Low stiffness porous Ti structures for load-bearing implants." Acta biomaterialia 3, no. 6 (2007): 997-1006.

[10] Spector, M., W. R. Flemming, A. Kreutner, and B. W. Sauer. "Bone growth into porous high-density polyethylene." Journal of biomedical materials research 10, no. 4 (1976): 595-603.

[11] Urban, Istvan A., Jaime L. Lozada, Sascha A. Jovanovic, Heiner Nagursky, and Katalin Nagy. "Vertical Ridge Augmentation with Titanium-Reinforced, Dense-PTFE Membranes and a Combination of Particulated Autogenous Bone and Anorganic Bovine Bone-Derived Mineral: A Prospective Case Series in 19 Patients." International Journal of Oral & Maxillofacial Implants 29, no. 1 (2014).

[12] Montjovent, Marc-Olivier, Laurence Mathieu, Boris Hinz, Lee Laurent Applegate, Pierre-Etienne Bourban, Pierre-Yves Zambelli, Jan-Anders Månson, and Dominique P. Pioletti. "Biocompatibility of bioresorbable poly (L-lactic acid) composite scaffolds obtained by supercritical gas foaming with human fetal bone cells." Tissue engineering 11, no. 11-12 (2005): 1640-1649.

[13] Frenkel, Sally R., and Paul E. Di Cesare. "Scaffolds for articular cartilage repair." Annals of biomedical engineering 32, no. 1 (2004): 26-34.

[14] Wang, Lin Biao, Kye Yak See, Yong Ling, and Wee Jin Koh. "Study of Metal Foams for Architectural Electromagnetic Shielding." Journal of Materials in Civil Engineering 24, no. 4 (2011): 488-493.

[15] von Meyer, Georg Hermann. "The Classic: The Architecture of the Trabecular Bone (Tenth Contribution on the Mechanics of the Human Skeletal Framework)." Clinical Orthopaedics and Related Research® 469, no. 11 (2011): 3079-3084.

[16] http://teleanatomy.com/introductiontoanatomy-SkeletalSystem.html

[17] http://www.mapsofworld.com/travel/destinations/france/eiffel-tower

[18] Weiner S, Wagner HD (1998) Annu Rev Mater Sci 28:271

[19] Mangesh A. Nar, Nandika D'Souza, Reza Mirshams, and Victor Kosmopoulos, "Intraspecimen Nanomechanical Properties Across The Femoral Cortex Parallel Compositional Measures", SAMPE Fall Technical Conference Proceedings: Advanced Materials and Processes: Developing Scalable Material and Processes for our Future, Fort Worth, TX, October 17-20, 2011. Society for the Advancement of Material and Process Engineering, CD-ROM—6 pp

[20] Hossain, K. M. A. "Development of volcanic pumice based cement and lightweight concrete." Magazine of Concrete Research 56, no. 2 (2004): 99-109.

[21] Woods, G. The ICI Polyurethanes Book, 2nd ed.; ICI Polyurethanes and John Wiley and Sons: 1990.

[22] Grünbauer, H.J.M., Rigid polyurethane foams, in Polymeric Materials Encyclopaedia, vol. 10, ed. J.C. Salamone, CRC Press, Boca Raton, FL, 1996, 7504–7512.

[23] European Thermal Insulation Markets: The Current and Future Prospects for Polyurethane, UTECH 2000 (Urethanes Technology), Crain Communications Ltd, London, 2000.

[24] Dow Polyurethanes - Flexible Foams, 2nd Edition, Ed., R. Herrington, Dow Chemical Company, Midland, MI, USA, 1997.

[25] Landrock, Arthur H. Handbook of Plastic Foams. No. Plastec-R52. Plastics Technical Evaluation Center Dover NJ, 1985.

[26] R. Brooks, Urethanes Technology, 1999, 16, 1, 34.

[27] Ishiwaka, Takumi, Noboru Yamaguchi, and Toshio Yukuta. "Flame resistant polyurethane foam and the method for manufacturing the same." U.S. Patent 4,221,875, issued September 9, 1980.

[28] Klempner, Daniel, and Kurt Charles Frisch, eds. Handbook of polymeric foams and foam technology. Munich etc.: Hanser, 1991.

[29] Crutzen, Paul J., and Frank Arnold. "Nitric acid cloud formation in the cold Antarctic stratosphere: A major cause for the springtime ‘ozone hole’." (1986): 651-655.

[30] Salby, Murry, Evgenia Titova, and Lilia Deschamps. "Rebound of Antarctic ozone." Geophysical Research Letters 38, no. 9 (2011).

[31] Zipfel, L., W. Krucke, K. Borner, P. Barthtlemy, and P. Dournel. "HFC-365mfc and HFC-245fa progress in application of new HFC blowing agents." Journal of cellular plastics 34, no. 6 (1998): 511-525.

[32] R. Brooks, Urethanes Technology, 1999, 16, 1, 34.

[33] Petela, Grazyna, Michel Berghmans, and Thomas Chee. "Enhanced expanded polystyrene foam insulation." U.S. Patent Application 12/473,527, filed May 28, 2009.

# CHAPTER 2

## RIGID POLYURETHANE AND KENAF CORE COMPOSITES[1]

### 2.1 Introduction

Polyurethane foams (PUFs) are one of the most versatile thermosetting polymeric materials. They can be made into flexible and rigid PUs. Their application varies from heat and sound insulation for building structures, appliances like refrigerators and freezers. The vacuum heat insulation panels of RPUF provide energy efficiency by reducing the heat loss by 25 % leading to reduced power consumption [1]. PUs can also be tailored to make foams with a number of different foam cell characteristics; these foams can be open and closed cell structures and can affect their insulation properties [2 - 5]. The closed cell foam structure is widely used, laid under floors, so as to keep a building resistant to moisture. PUs have been reinforced with inorganic and organic materials to enhance their properties [6]. A recent study suggests that the incorporation of 0.1, 0.2, and 0.3 wt % of graphene nanosheets, and carbon nanotubes resulted in an increase in mechanical and thermal properties [7]. Much research is being carried out to substitute petroleum based polyols with a vegetable oil base like soy and castor [8] to make the PUs bio-polymers. These foams demonstrated comparable foam density and cellular morphology and an increase in compressive strength [9]. These natural materials provide encouraging avenues for their development for use as renewable sources for foams.

[1] This chapter is presented in entirety from Nar, M., Webber, C. and Anne D'Souza, N. (2014), Rigid polyurethane and kenaf core composite foams. Polym Eng Sci. doi: 10.1002/pen.23868 with permission from Wiley.

Using natural fibers such as Kenaf (Hibiscus cannabinus, L. family Malvaceae) is gaining value for reinforcing polymer composite materials. The kenaf plant is branchless and grows up to an average height of 5.5 meters in 5 months and is widely grown in sunbelt regions throughout the world. Kenaf is a multipurpose plant with components that are harvestable such as stalk core, stalk bark, seeds, and leaves. The stalk core, which is the woody core, can be used as a wood-product substitute and building material[10]. Most often kenaf bast fibers (these are obtained from the outer layer of the plant, i.e., phloem) are used in polymer composites. The low density of kenaf bast fiber as compared to glass fiber [11], carbon fiber, and hemp [12] has made kenaf frequently considered reinforcement filler. Kenaf fiber is a good replacement for such current reinforcements as glass fibers, due to its competitive strength-to-weight ratio contributions [13]. The advantages that natural fibers have over glass fibers are that no surface modification is required in order to provide polymer-fiber mechanical interlocking, which provides good adhesion and therefore superior properties, low cost, with renewability and biodegradability being some of the other merits over synthetic fibers [14]. Low density of kenaf makes it possible for it to make automobiles more fuel efficient [15].

In our earlier work we have studied the effect of low kenaf loading of about 5 % by weight having given similar benefits in mechanical properties of polylactic acid as that of 20 % by weight kenaf loading reported by many researchers [16]. A well dispersed low fiber fraction resulted in limited restriction for polymer crystal nucleation and growth, thereby increasing the mechanical properties. Further we studied the effect of kenaf fiber length and variation of bast fiber retting using chemical and enzymatic

retting in poly(hydroxybutyrate-co-valerate)/poly(butylene adipate-co-terephthalate) polymer blends. The enzymatic retted fibers produced higher reinforcement than chemical retting [17]. Kenaf fibers have been reported to improve tensile and flexural strength with 30 and 40 % by weight in poplypropylene [18]. Thermoforming of polyethylene, polypropylene and polyethylene terephthalate was improved by the addition of kenaf fibers for processablity [19].

Kenaf core particles are used to make panels with easy processing and with comparison to commercially available insulation panels, making it a potential raw material for low density insulation panels [20].The kenaf core has been investigated to reinforce unsaturated polyester to improve mechanical strength by Ishak et al. [21]. By incorporating 5, 10, 20, 30, and 40 % kenaf fibers and kenaf core in polyester to study the mechanical strength, Ishak et al. determined that kenaf fibers were required in addition to the core to provide reinforcement. Ismail et al. treated kenaf core with maleated polyethylene to improve interaction between kenaf core and HDPE to give better mechanical properties [22]. The addition of montmorillonite (MMT) was found necessary in composites of kenaf core with higher filler loadings of 40 to 60 % in composites with unsaturated polyester [23]. Agglomeration of kenaf core resulted in a decrease in mechanical performance while addition of MMT led to an increase in tensile strength. Extensive work has been done with kenaf as filler with thermoplastics and thermosets, but rarely has it been used in foam. RPUFs with vegetable oil substituted for petroleum based polyol have been reinforced with natural fibers like flax and hemp to obtain better mechanical and thermal properties [24]. The plant core remains an underutilized component, as reinforcement [25,26] Kenaf-core liquefied polyol has been

used to synthesize PU adhesive [27] and used in oil spillage absorption due to its hydrophobic nature [28,29].

## 2.2 Experimental

### 2.2.1 Materials

4,4'-Methylenebis (phenyl isocyanate) and polyester-block-polyether α, ω-diol were procured from Fiber Glast Developments. The average molecular weight for polyester-block-polyether α, ω-diol was 468. 100 g polyester-block-polyether α, ω-diol was mixed with 1% distilled water (i.e. 2.3 ml, which is 1% of total polymer weight considering 100 g of polyester-block-polyether α, ω-diol and 130 g of 4,4'-Methylenebis (phenyl isocyanate)) in a disposable cup and allowed to degas for 4 min, 130 g of 4,4'-Methylenebis (phenyl isocyanate) was added to the mixture [30] and mechanically stirred using cowless dissolver at 2500 rpm for 1 min and made to stand still. This mixture was then poured in mold and allowed to foam freely and cure for 72 h at room temperature. Fig 1A shows mold with length $L$, width $b$ and full depth $d_f$, the mixture is poured and allowed to expand freely. The foam obtained from this free expansion is termed henceforth as $d_i$.

Kenaf-core that was obtained from USDA was powdered using cryomilling for 30 min under liquid $NO_2$ bath. Kenaf-core had density of 0.28 g/cc and particle size of 150 ± 20 μm.

### 2.2.2 Preparation of Composites

Kenaf-core was preheated in a vacuum oven at 70 °C for 4 h to remove moisture. The composites were prepared with 5, 10 and 15 % kenaf-core by weight. The kenaf-

core was first mixed in polyester-block-polyether α, ω-diol which was premixed with 1% distilled water, and then mixed with 4,4'-Methylenebis (phenyl isocyanate) using cowless dissolver at 2500 rpm. This mixture was then poured into a mold (150 x 120 x 20 $mm^3$) and allowed to foam and cure for 72 h at room temperature. Fig. 1B, and 1C shows a schematic for the constraint expansion when the mold is filled with 40%, and 60% of full depth $d_f$ of the mold and henceforth referred respectively as $d_{i40}$, and $d_{i60}$. The expansion ratio, i.e., the fully foamed height to the initial height, was calculated for free foam expansion which was found to be uneven with an average height of 60 mm. Test samples were taken from foams cured on different days.

The foams obtained from the free expansion were termed as $d_i$ and these were made with 0, 5, 10, and 15 % kenaf-core. Above 15% by weight extensive segregation of the kenaf core to the surface resulted from the low kenaf density and thus this weight fraction was taken as the upper limit. In addition to free expansion, constrained expansion was used to influence the cell density. Introducing a constraint where the volume expansion was limited to 40% and 60% is denoted by ($d_{i40}$ and $d_{i60}$). This was done by setting the initial volume of unfoamed material at heights of 8 mm and 12 mm in the mold and limiting their expansion to the 20mm full-mold height. An expansion ratio of 2.5 and 1.7 resulted from these constraints.

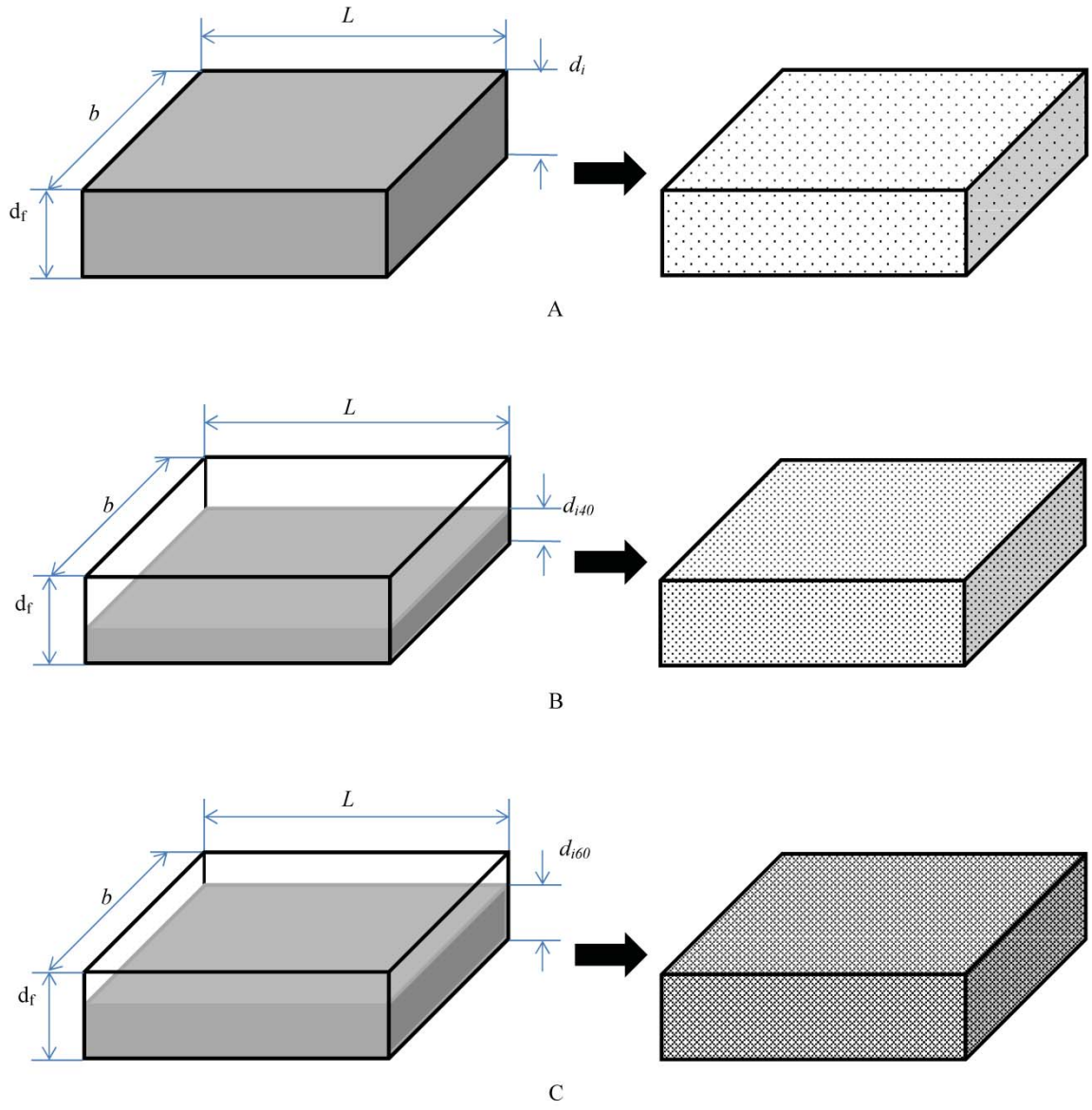


*Figure 2-1.* Schematic representation for (A) $d_i$, (B) $d_{i40}$, and (C) $d_{i60}$ foam preparation method.

## 2.3 Method

### 2.3.1 Flexural Test

Samples measuring 16.5 x 10.5 x 100 $mm^3$ were used. The test was carried out according to ASTM C – 393-11 in displacement control at room temperature. The rate of

displacement was set to 1 mm/min and maximum deflection was set to 15 mm. Flexural modulus was calculated from this test, where E is flexural modulus, L is span length, m is slope of the initial straight line, b and d are, respectively, the width and depth of the foam sample.

$$E = (L^3 m)/(4bd^3) \quad (1)$$

2.3.2 X-Ray Micro Tomography (μCT)

The machine used to μCT was Skyscan 1172. Voltage of 61 kV and current of 163 μA were used to give better contrast between the sample and background. Flat field correction was performed for dark and bright field, and later scanned with large resolution settings of 5 microns. Raw images were corrected for ring artifacts and beam hardening and analyzed for porosity before and after compression.

2.3.3 Compression Test

2.3.3.1 MTS

A sample measuring 25mm in length and 27 mm in diameter was used. The MTS machine was used in displacement control with strain rate of 0.5 mm/min. Samples were compressed to 85% of the original height. Compression strength and modulus were calculated.

2.3.3.2 μCT

A 10X10X10 $mm^3$ cubic sample was used. Machine was used in displacement control with strain rate of 0.5 mm/min. This test gave change in foam structure and cell structure and porosity during testing. Fig. 2 (A) and (B) show the microCT compression

stage with the foam sample. Fig. 2 (C) and (D) show before and after compression of the foam sample. The compression platens can be seen at top and bottom of the foam sample.

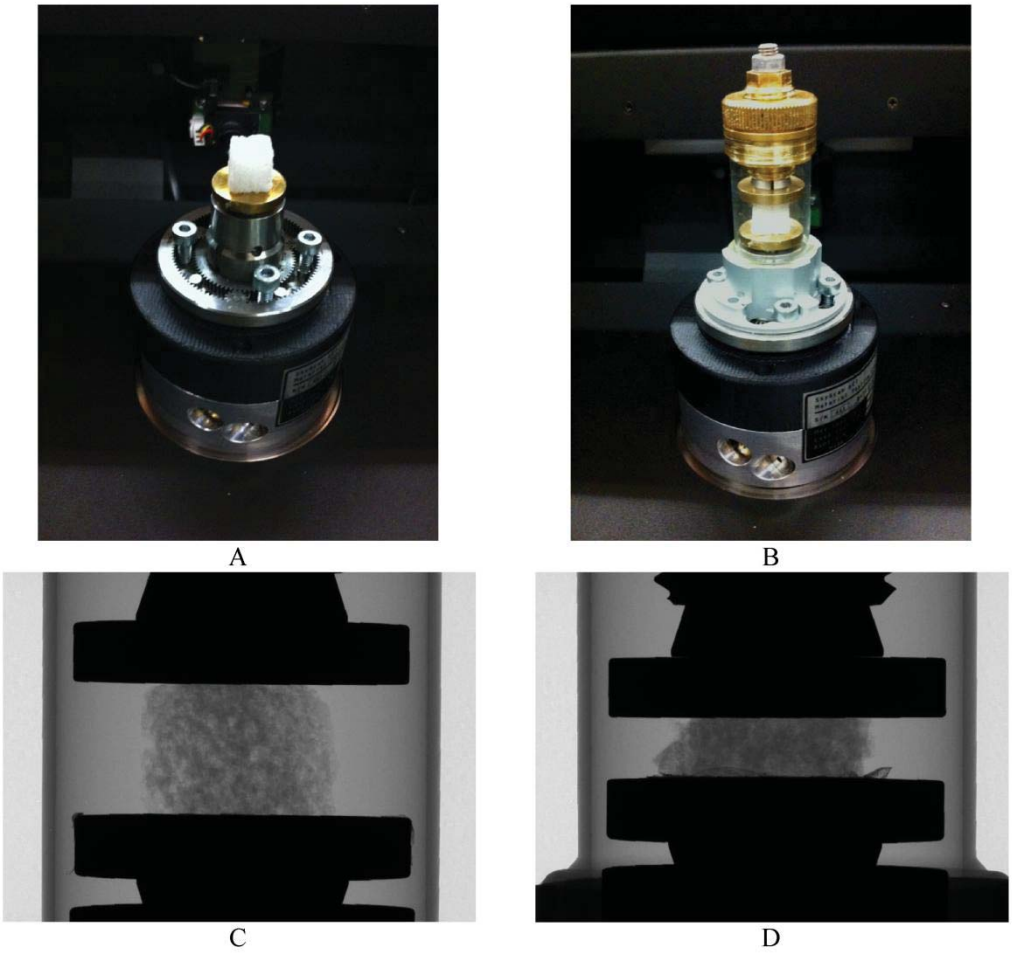


*Figure 2-2.* (A) foam sample on microCT compression fixture, (B) foam sample during compression test, (C) and (D) shows an in-situ image before and after the compression test respectively.

### 2.3.4 Microscopy

#### 2.3.4.1 Environmental Scanning Microscopy

FEI Quanta Environmental Scanning Electron Microscope (ESEM; FEI Company, Oregon, USA) was used. The foam was cryo-fractured using liquid nitrogen; to ensure

no surface yielding; this cryo-fracturing kept the micro-structure intact for analysis. The average cell diameter was determined using ImageJ, and counting on an average 50 cells. Cell density ($N_c$) was calculated from the micrographs using the following equation [31], where n is number of cells in ESEM image, A is the area of the micrograph in $cm^2$ and M is the magnification factor.

$$N_c \approx (nM^2/A)^{3/2} \quad (2)$$

2.3.4.2 Optical Microscopy

A Nikon Eclipse ME600 optical microscope was used to image fractured surface of the foams. These were cryo-fractured using liquid nitrogen (section 2.3.4.1). 5X Nikon Japan LU Plan objective was used to image surface of foams. A ruler tape was used to mark three random 1 $mm^2$ area for each foam sample and cells were counted to give linear cell density for 1 $cm^2$. The measurements were done in triplicate (Table 2-1).

2.3.5 Foam Density

Macro-foam densities were measured using Archimedes principle of water-displacement. Densities were calculated using volume of water displaced by sample divided by weight of sample. Measurements were done in triplicate using AEA/AAA Density kit from Adam Engineering.

2.4 Results and Discussions

Table 2.1

*Effect of kenaf-core loading of 5, 10 and 15 % and varying constraint volume expansion of $d_{i40}$ and $d_{i60}$ on foam density, cell density, linear cell density, and average cell diameter and void fraction change during compression test in microCT for rigid PU foam composites.*

| Kenaf core (%) | $d_i$ Foam density ($\rho_f$) (g/cc) | $d_i$ Cell density ($N_0$) (cells/cm$^3$) | $d_i$ Linear cell density (cells/cm$^2$) | $d_i$ Average cell diameter (D) (μm) | $d_{140}$ Foam density ($\rho_f$) (g/cc) | $d_{140}$ Cell density ($N_0$) (cells/cm$^3$) | $d_{140}$ Linear cell density (cells/cm$^2$) | $d_{140}$ Average cell diameter (D) (μm) | $d_{160}$ Foam density ($\rho_f$) (g/cc) | $d_{160}$ Cell density ($N_0$) (cells/cm$^3$) | $d_{160}$ Linear cell density (cells/cm$^2$) | $d_{160}$ Average cell diameter (D) (μm) |
|---|---|---|---|---|---|---|---|---|---|---|---|---|
| 0 | 0.057 ± 0.063 | 3.18 x $10^4$ | 600±81.65 | 316±28 | 0.008 ± 0.271 | 1.11 x $10^4$ | 833±47 | 350±50 | 0.197 ± 0.061 | 7.60 x $10^4$ | 1233±94 | 583±76 |
| 5 | 0.077 ± 0.092 | 1.18 x $10^4$ | 433±47.14 | 650±50 | 0.010 ± 0.484 | 1.03 x $10^4$ | 800±81 | 300±70 | 0.394 ± 0.086 | 8.14 x $10^4$ | 1200±81 | 300±86 |
| 10 | 0.077 ± 0.085 | 1.59 x $10^4$ | 633±125 | 250±132 | 0.017 ± 0.658 | 8.50 x $10^3$ | 800±163 | 283±76 | 0.514 ± 0.104 | 10.10 x $10^4$ | 1100±141 | 250±50 |
| 15 | 0.086 ± 0.107 | 1.12 x $10^4$ | 700±81 | 293±158 | 0.023 ± 0.899 | 1.28 x $10^4$ | 966±94 | 168±23 | 0.797 ± 0.131 | 11.42 x $10^4$ | 1266±47 | 150±50 |

| Kenaf core (%) | $d_i$ Compressive strength (g/mm$^2$) | $d_i$ Void fraction before ($V_f$) (%) | $d_i$ Void fraction after ($V_f$) (%) | $d_i$ Change in void fraction (%) | $d_{140}$ Compressive strength (g/mm$^2$) | $d_{140}$ Void fraction before ($V_f$) (%) | $d_{140}$ Void fraction after ($V_f$) (%) | $d_{140}$ Change in void fraction (%) | $d_{160}$ Compressive strength (g/mm$^2$) | $d_{160}$ Void fraction before ($V_f$) (%) | $d_{160}$ Void fraction after ($V_f$) (%) | $d_{160}$ Change in void fraction (%) |
|---|---|---|---|---|---|---|---|---|---|---|---|---|
| 0 | 218 | 54.46 | 43.3 | 20.49 | 225.05 | 73.92 | 67.73 | 8.37 | 227.86 | 64.28 | 59.18 | 7.93 |
| 5 | 83 | 44.9 | 38.71 | 13.79 | 187.14 | 74.57 | 37.37 | 49.89 | 231.42 | 67.61 | 62.52 | 7.53 |
| 10 | 110 | 43.96 | 39.24 | 10.74 | 176.83 | 66.21 | 53.07 | 19.85 | 235.78 | 59.73 | 56.81 | 4.89 |
| 15 | 280 | 41.75 | 37.88 | 9.27 | 196.14 | 57.68 | 51.99 | 9.86 | 237.1 | 54.27 | 49.15 | 9.43 |

### 2.4.1 Microstructure and Density of Foam

The ESEM images of pure PU foam for $d_i$ (Fig. 2-3) shows regular pore sizes with open cell structure. The 5% shows a foam structure that is regular as compared to 10% which shows agglomeration of kenaf-core which resulted in non-uniform distribution of foam cells with lower mechanical properties as compared to pure PU, 5 and 15% compositions. The 5% foam composition shows regular cell structure very similar to the pure PU foam; kenaf-core particles can be seen attached to the cell walls.

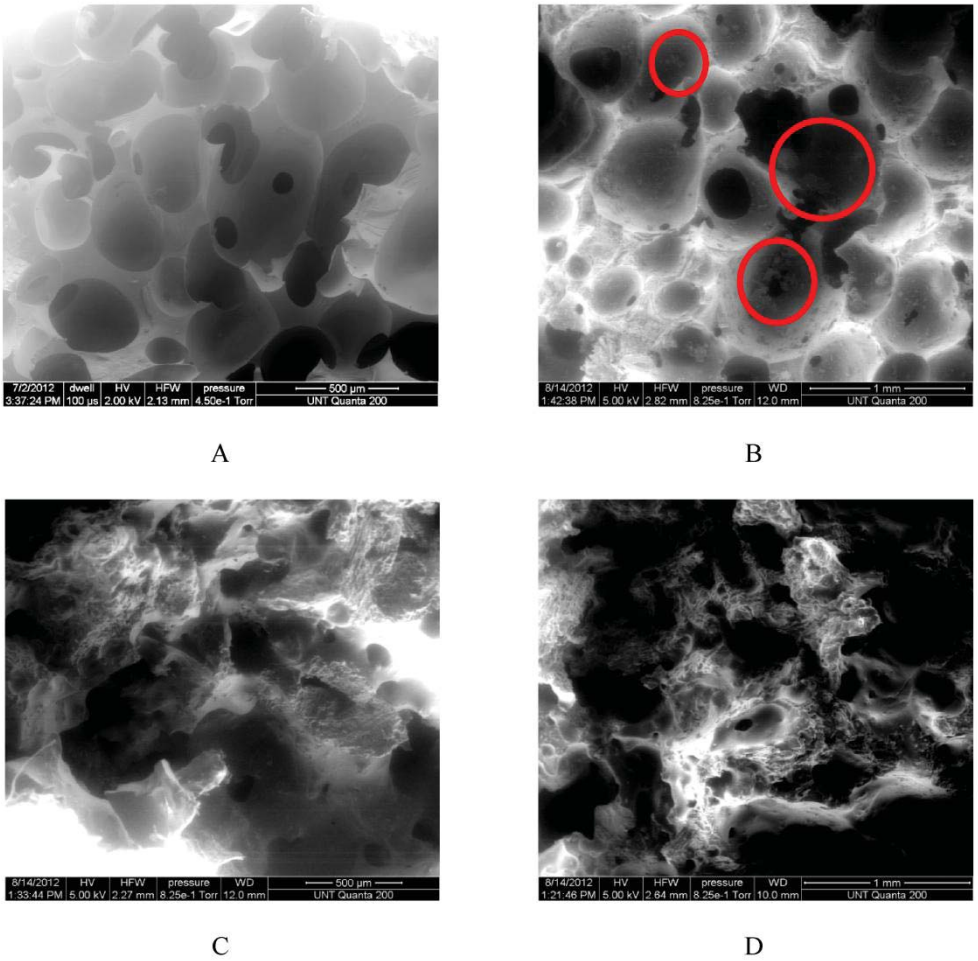


*Figure 2-3.* ESEM images for free volume expansion: $d_i$ (A) pure PU foam, (B) 5, (C) 10, and (D) 15% foam composites.

The micrograph (Fig. 2-4 and 2-5) for $d_{i40}$ and $d_{i60}$ shows the cell structure for foams when compared to 0 %; in all cases 0 % shows regular foam cells. In contrast to the $d_i$ foams the kenaf-core for 10 % can be seen inside the cells more than on the cell walls thereby reducing the mechanical properties like compression and flexural modulus and peak load. The 5, 10 and 15 % for $d_{i40}$ and $d_{i60}$ shows that since there is constraint in volume expansion the packing density causes more small cells in an equivalent volume. From Fig. 2-4, and 2-5 it can be seen that for $d_{i40}$ and $d_{i60}$ the cell size of $d_{i60}$ is much smaller. Hence, it can be seen that for $d_{i60}$ the cell packing is denser than $d_{i40}$.

This increases the density for all composites for $d_{i60}$ as compared to $d_{i40}$ as shown in Table 2-1 and Fig. 10B. Also, it can be noted that as the kenaf-core loading increases; the density increases.

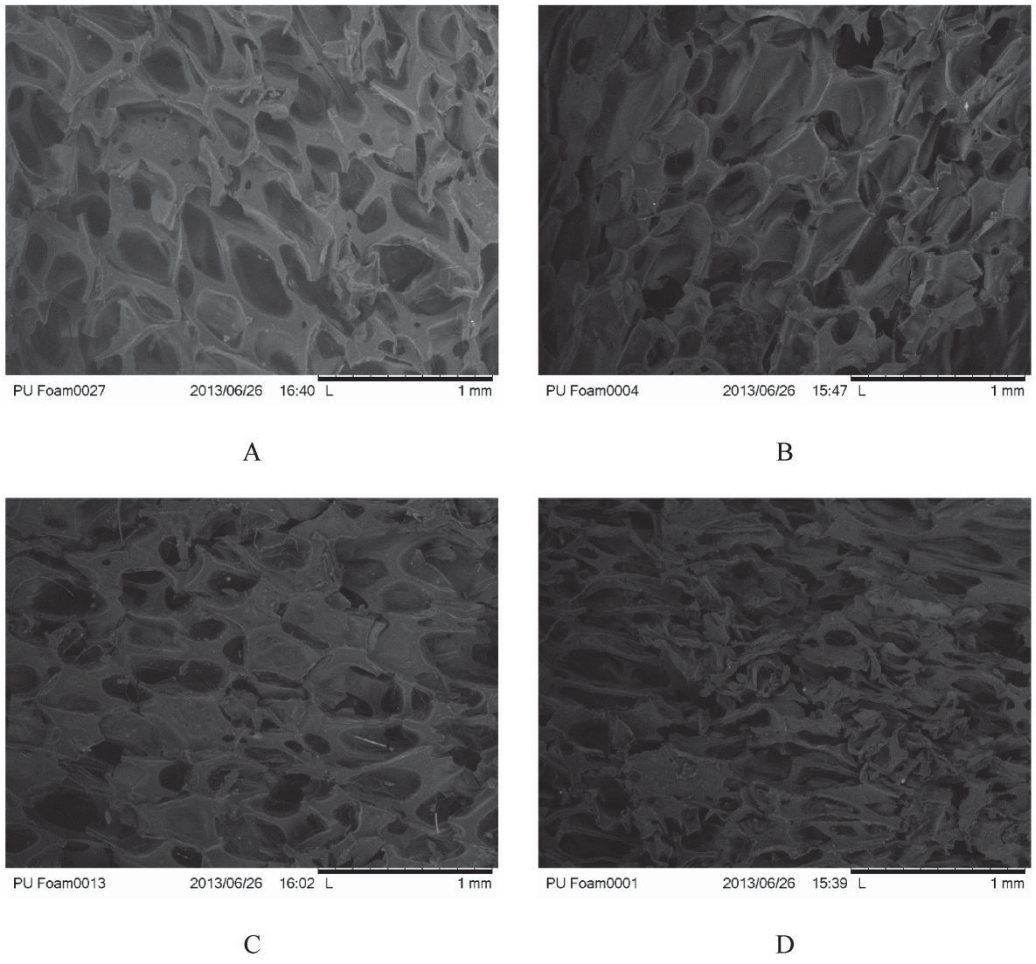


*Figure 2-4* ESEM images for $d_{i40}$ volume expansion (A) pure PU foam, (B) 5, (C) 10, and (D) 15% foam composites.

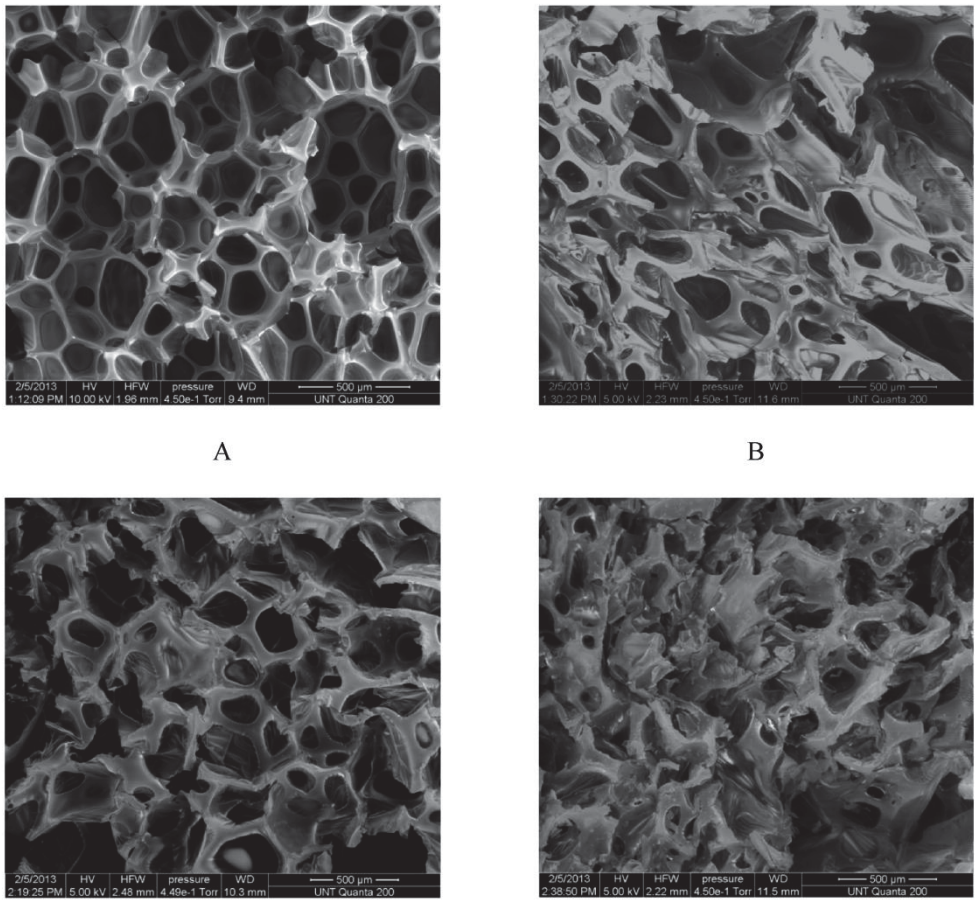


*Figure 2-5* ESEM images for $d_{i60}$ volume expansion (A) pure PU foam, (B) 5, (C) 10, and (D) 15% foam composites.

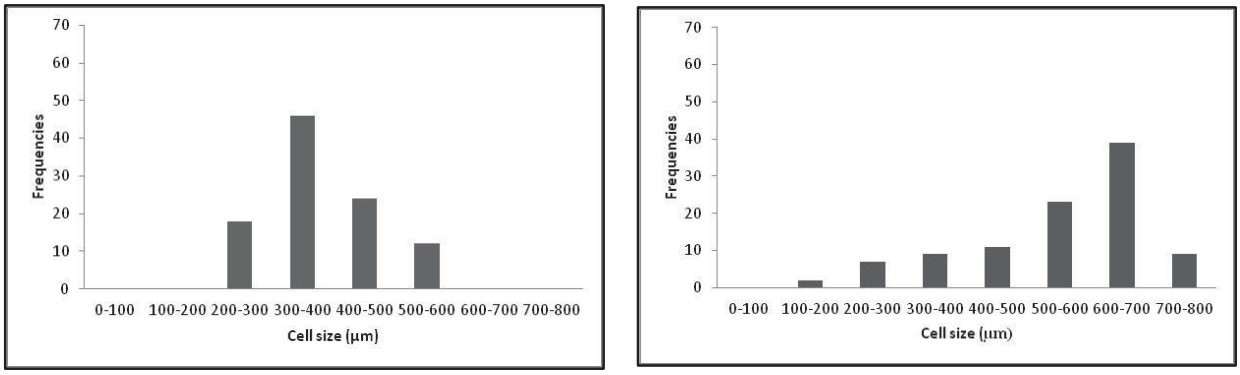

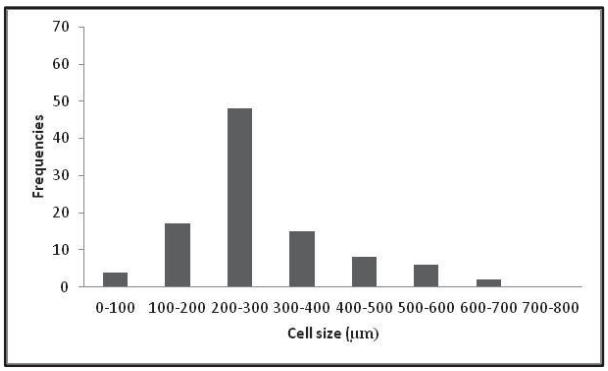
70
60
50
40
30
20
10
0
Frequencies
0-100 100-200 200-300 300-400 400-500 500-600 600-700 700-800
Cell size (µm)

C

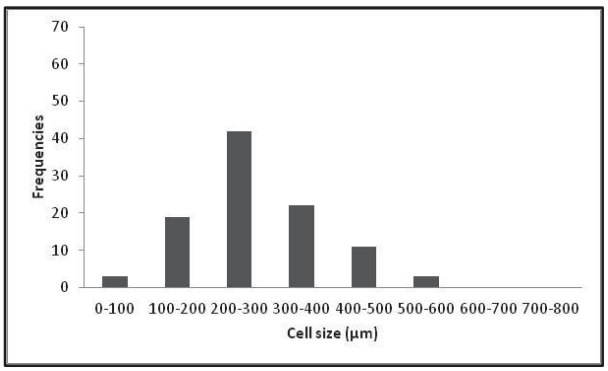
70
60
50
40
30
20
10
0
Frequencies
0-100 100-200 200-300 300-400 400-500 500-600 600-700 700-800
Cell size (µm)

D

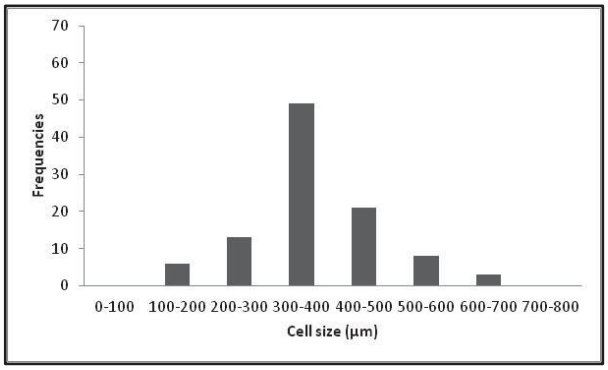
70
60
50
40
30
20
10
0
Frequencies
0-100 100-200 200-300 300-400 400-500 500-600 600-700 700-800
Cell size (µm)

E

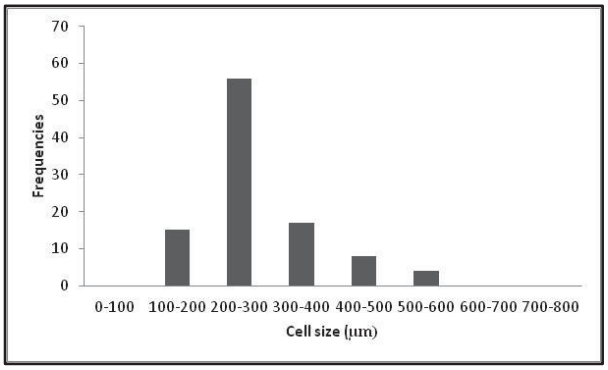
70
60
50
40
30
20
10
0
Frequencies
0-100 100-200 200-300 300-400 400-500 500-600 600-700 700-800
Cell size (µm)

F

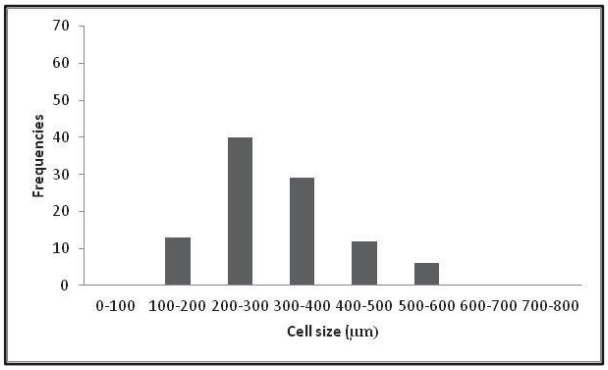
70
60
50
40
30
20
10
0
Frequencies
0-100 100-200 200-300 300-400 400-500 500-600 600-700 700-800
Cell size (µm)

G

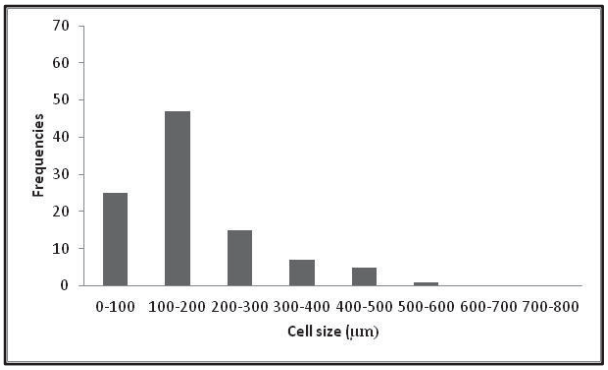
70
60
50
40
30
20
10
0
Frequencies
0-100 100-200 200-300 300-400 400-500 500-600 600-700 700-800
Cell size (µm)

H

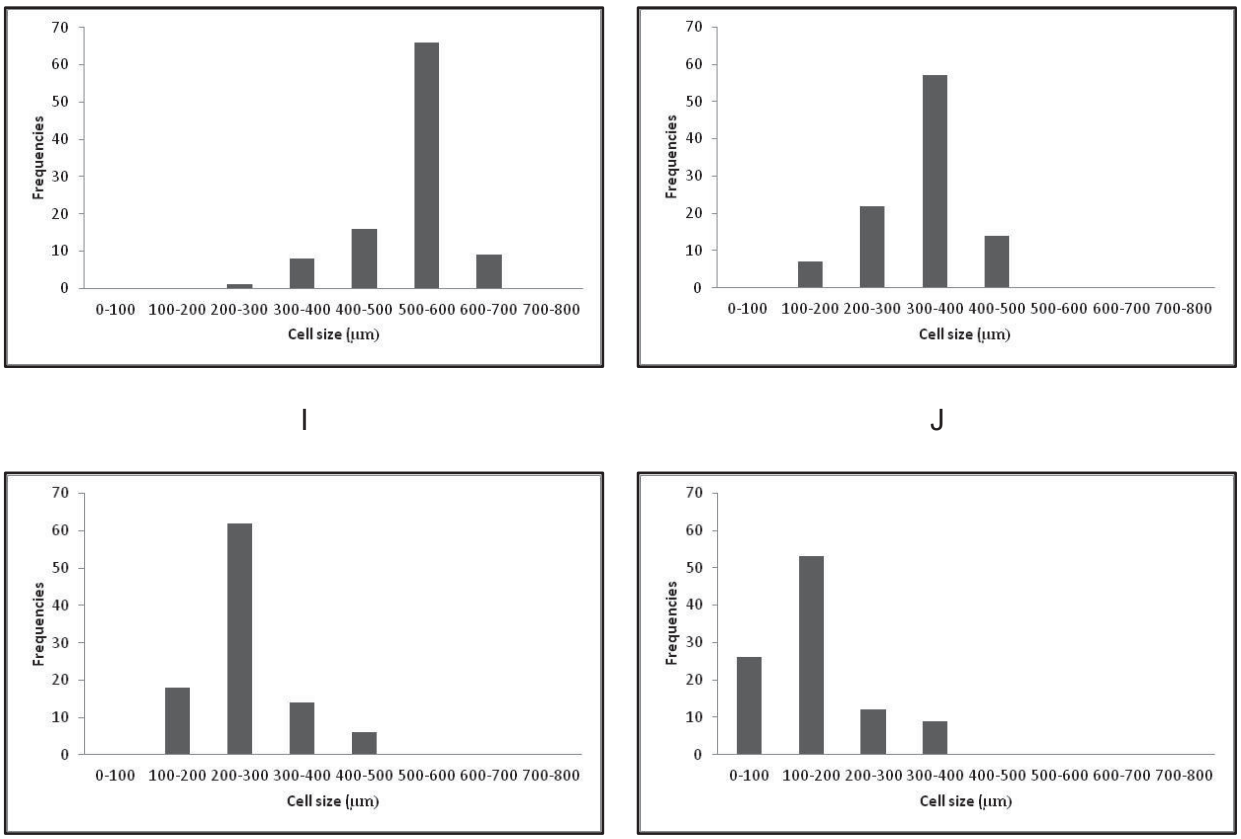


*Figure 2-6* Cell size distribution for rigid PU foam composites (A) di_0, (B) di_5, (C) di_10, (D) di_15, (E) di40_0, (F) di40_5, (G) di40_10, (H) di40_15, (I) di60_0, (J) di60_5, (K) di60_10, (L) di60_15

The linear cell density from Table 2-1 shows that the $d_{i60}$ has higher cell density followed by $d_{i40}$ and then $d_i$ foams. This increase in density is due to packing of higher material into same volume for $d_{i60}$ than $d_{i40}$. It can also be noted that when the kenaf-core loading is increased, the linear cell density increases. This increase can be seen in the case of 15 % kenaf-core loading in the three types of foams, which is due to kenaf-core particles acting as a barrier to foam expansion. This constraint in expansion gives a higher fraction of smaller cells. Since $d_{i40}$ has less material for occupying an equal volume as has $d_{i60,}$ this initial smaller amount of material gives rise to larger cells after complete volume expansion than $d_{i60}$ in all the kenaf-core loaded samples. But, within

$d_{i40}$ it shows similar trend as that of $d_{i60}$. The 15 % shows higher number of smaller cells than rest of the compositions. The same is the case with free foam volume expansion.

The average cell size for $d_i$, $d_{i40}$ and $d_{i60}$ for no kenaf core loading showed an increase. This might be due to the coalescing of the foam cells due to constraint in free expansion as seen from Table 2-1. The addition of kenaf core has acted as a nucleation site during the foaming process resulting in smaller cell sizes. Hence, 15 % kenaf core loaded foams shows smallest cell sizes followed by 10, and 5 % for $d_{i40,}$ and $d_{i60}$.

Figure 2-6 shows the cell size distribution for the foams with free foam expansion and constrained volume expansion. It can be seen for free foaming the distribution of cells are broad (Figure 2-6 A, B, C, and D). Constrained volume expansion shows narrow distribution in the sense of the larger cell size. For instance 40 % show probability of forming larger diameter is about 50 (Figure 2-6 E, F, G, and H) whereas with 60 % its ~60 (Figure 2-6 I, J, K and L). This indicates that as the constraint was increased to 60 % a narrower distribution was observed with about 60 % frequency of forming of average cell size diameter observed.

Thus as the foam cell packing increases for $d_{i60}$ compared to $d_{i40}$ the mechanical properties are seen found to increase for $d_{i60}$. Packing the cells in a dense manner has increased the foams resistance to compression, flexing and shear stress. Since the kenaf-core loading influences the packing and the regularity of the cell structure. The ESEM images show that the 5 and 10 % loading barely changes the cell structure in $d_{i40}$ and $d_{i60}$ volume expansion foam. It can be seen that 15 % loading has disrupted the regular cell structure for both $d_{i40}$ and $d_{i60}$ type of foams. However this did not influence the properties in adverse ways. As even though we can see that the cell structure for 15

% has changed the regular cell structure, the increase in compression and the flexural properties can be seen. This will be due to more kenaf-core particles supporting the foam cell from deforming as the compressive and shear forces are applied.

It can also be noted that the kenaf-core for $d_{i40}$ and $d_{i60}$ resides on the foam walls providing reinforcement to the foam cells. Hence as the loading increases more kenaf-core particles go to the walls of the foam cells thereby increasing the resistance to deformation and thereby increasing the strength of the foam composite. This is not seen in the foams processed with no constraint. From ESEM (Fig. 3 - C) the 10 % foam composite shows that the kenaf-core particles not only reside on the wall but also occupy the volume inside the cell, thereby decreasing the deformation and hence the strength of the composite. This can be seen from the compressive modulus and the flexural modulus and peak load for both Fig. 10 (A to D).

### 2.4.2 Mechanical Strength

Fig. 10A and 10B shows compressive modulus and strength for the three types of foam volume expansion, it can be seen that the $d_{i40}$ and $d_{i60}$ shows an increase in compressive modulus and strength for the foam composites when compared to pure. With free expansion and $d_{i60}$ there was a negative impact on compressive modulus of the foam. Fig. 6A, and B are micrographs for $d_i$ for 10 % and Fig. 6C is $d_{i40}$ for 10 %. They clearly show the presence of kenaf core inside the cell of the foams marked with red open circle. Kenaf core within the cell wall is not available for reinforcement leading to lower mechanical reinforcement. From the images it can be seen that the kenaf core is attached to the cell wall, but most of it extends into the void of the cell. This reduces the resistance imparted by kenaf core while deformation, thereby reducing the

compression strength by increasing the polymer mobility. Fig. 6D, and H for 15 % kenaf core loading shows kenaf core on the cell wall. Fig. 6E shows kenaf core protruding out of the fractured surface indicating good interface bonding between kenaf core and polyurethane. Fig. 6F, and G, it is very clear that the kenaf core is inside the pore which is formed during the foaming process. This type of kenaf core location was only seen in 15 %. These loosely held kenaf core does not impart any reinforcement to the foam, even though this is the case there are kenaf cores which are deeply embedded in the foam as seen from Fig. 6I (section taken at an angle to view the embedded kenaf core). There by giving good compression strength to the foams by giving resistance for the polymer mobility during deformation. For $d_{i60}$ an increase by 2.4, 6 and 7.9% as compared to pure foam for 5, 10 and 15% kenaf core loading was seen. And for compression strength it has increased by 3.5 and 6% for 10 and 15 % whereas 5% showed decreased strength by 4%.

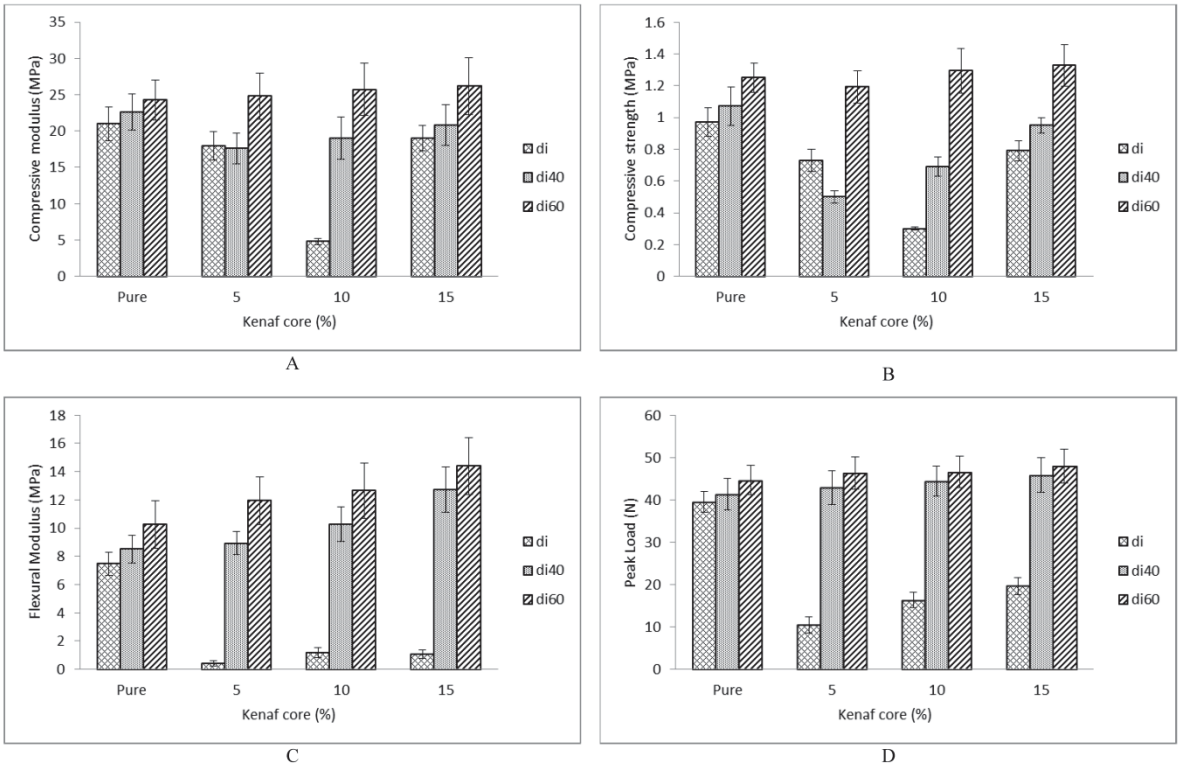


*Figure 2-7* (A) Compressive modulus, (B) compressive strength comparison (C) flexural modulus, and (D) peak load of rigid PU foam composites with increasing kenaf-core content of 5, 10, and 15 % and constraint volume expansion with $d_{i40}$ and $d_{i60}$.

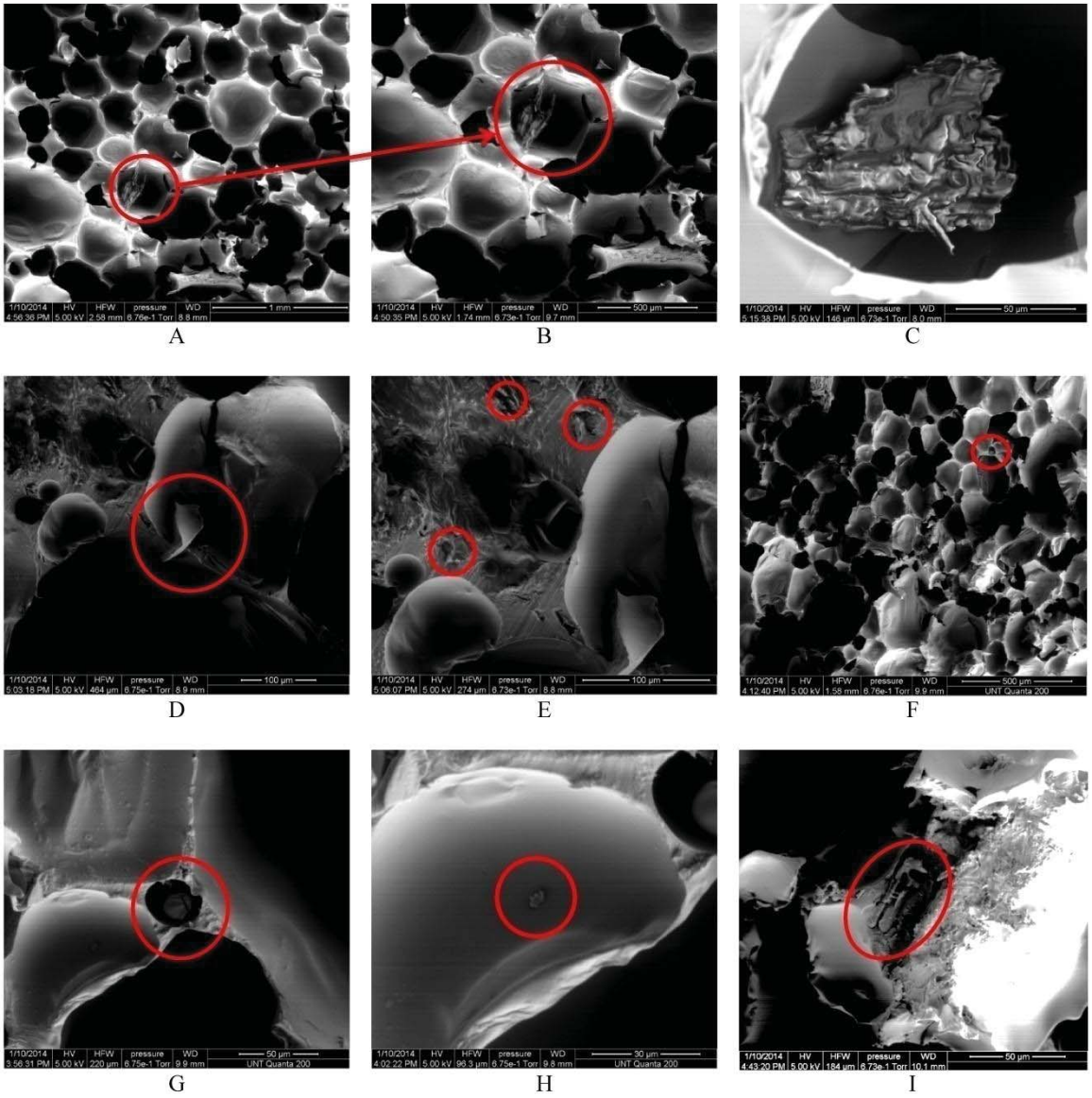


*Figure 2-8* ESEM images for 10 % kenaf core loaded foams (A), (B), and (C), and for 15 % kenaf core loaded foams (C), (D), (E), (F), (G), (H), and (I); with kenaf core marked with the open red circles.

Table 2-1 (Fig. 10C, and 10D) shows flexural modulus and peak load for the three types of foam volume expansion. It can be seen that the $d_{i40}$ and $d_{i60}$ shows an increase in flexural modulus and peak load for the foam composites when compared to pure. A positive increase by 4.8, 20.7 and 49% in modulus for foams prepared with an

expansion ratio of 2.5 ($d_{i40}$) and an increase by 16.5, 23.4 and 40.4 % in modulus is seen in $d_{i60}$ for 5, 10 and 15% kenaf core loading. Whereas free expansion, gave negative impact on flexural modulus.

Table 2-1 shows foam density comparison between three types of foam volume expansion. Free volume expansion shows an increase in foam density with increase in kenaf-core loading to 35, 35, and 50% for 5, 10, and 15% kenaf core loading. Cell density for $d_i$ was $3.18 \times 10^4$, $1.18 \times 10^4$, $1.59 \times 10^4$, and $1.12 \times 10^4$ cells/cm$^3$ for 0, 5, 10, and 15% kenaf-core loading respectively. The $d_{i40}$ volume expansion shows an increase in foam density by 100, 160 and 304 % for all composites. The cell densities for $d_{i40}$ are $1.11 \times 10^4$, $1.03 \times 10^4$, $8.50 \times 10^3$, $1.28 \times 10^4$ cells/cm$^3$ respectively. As compared to $d_i$ and $d_{i40}$, $d_{i60}$ show higher values for respective composites. The foam density increased in this case by 78, 142 and 231 %. The cell densities show a steady increase too in $d_{i60}$, $7.60 \times 10^4$, $8.14 \times 10^4$, $10.10 \times 10^4$, and $11.42 \times 10^4$, respectively for 0, 5, 10, and 15% kenaf-core loading.

Linear cell densities for free foaming samples are 600±81.65, 433±47.14, 633±125 and 700±81 cells/cm$^2$ for 0, 5, 10 and 15% kenaf-core loading. It can be seen that the $d_{i40}$ shows higher linear cell densities compared to free expansion of 833±47, 800±81, 800±163 and 966±94 cells/cm$^2$ for 0, 5, 10 and 15% kenaf-core loading respectively. Whereas $d_{i60}$ shows highest linear cell densities when compared to di and $d_{i40}$ with values of 1233±94, 1200±81, 1100±141 and 1266±47 cells/cm$^2$ for 0, 5, 10 and 15% kenaf-core loading.

### 2.4.3 MicroCT Analysis for Compressive Strength

Compression strength from microCT (Table 2-1) shows a similar trend as that shown from the MTS test. This shows that as the expansion ratio increases the compressive properties improves. For $d_{i60}$ there is a steady increase by 1.5, 3.5 and 4% with kenaf core loading of 5, 10 and 15%. The free expansion and $d_{i40}$ show a negative reinforcement impact on compression strength but increasing kenaf core loading has reduced the magnitude of the decrease in property. The microCT compression test and the before and after the test reconstructed 3D images show that the cell structure becomes more compact as seen in Figures 7 – 9. These images show the change in cells during the compression test. Table 2-1 shows void fraction and change in void fraction with increase in kenaf-core loading with the foam expansion as well as before and after the compression test. It can be seen that the void fraction before compression test is higher in all the three cases. The change in void fraction has reduced from $d_i$ to $d_{i40}$ to $d_{i60}$. $d_{i60}$ shows the lowest change in void fraction of 7.93, 7.53, 4.89 and 9.43% for 0, 5, 10 and 15% respectively indicating that under compressive load $d_{i60}$ offers more resistance to deformation. $d_{i40}$ shows 8.37, 49.89, 19.85 and 9.86% while $d_i$ shows 20.49, 13.79, 10.74 and 9.24 % for 0, 5, 10 and 15% respectively. This contributes towards the higher compressive strength of the $d_{i60}$ foam composites as compared to $d_{i40}$ and $d_i$. MicroCT void fraction changes clearly shows that as the kenaf-core is increased in foam the void fraction reduces. Also it can be noted that as the volume constraint foam expansion is compared for $d_{i40}$ and $d_{i60}$, the $d_{i60}$ shows lower porosity as expected than $d_{i40}$. This is due to higher material packed in $d_{i60}$ during foam expansion.

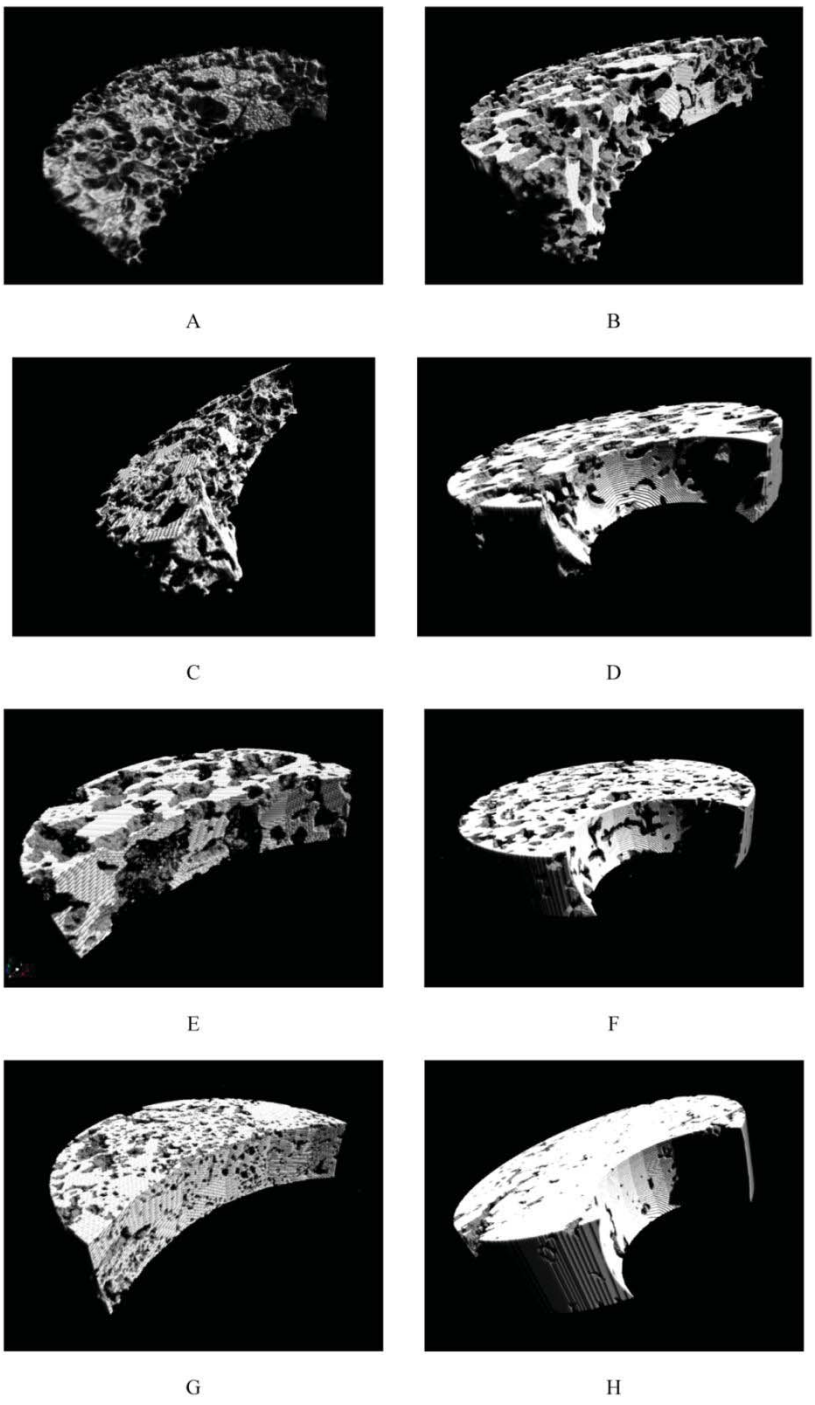


*Figure 2-9* Reconstructed and sectioned volume of $d_i$ pure foam (A and B) and foam composites 5% (C, D), 10% (E, F), 15% (G, H) before and after compression test in microCT

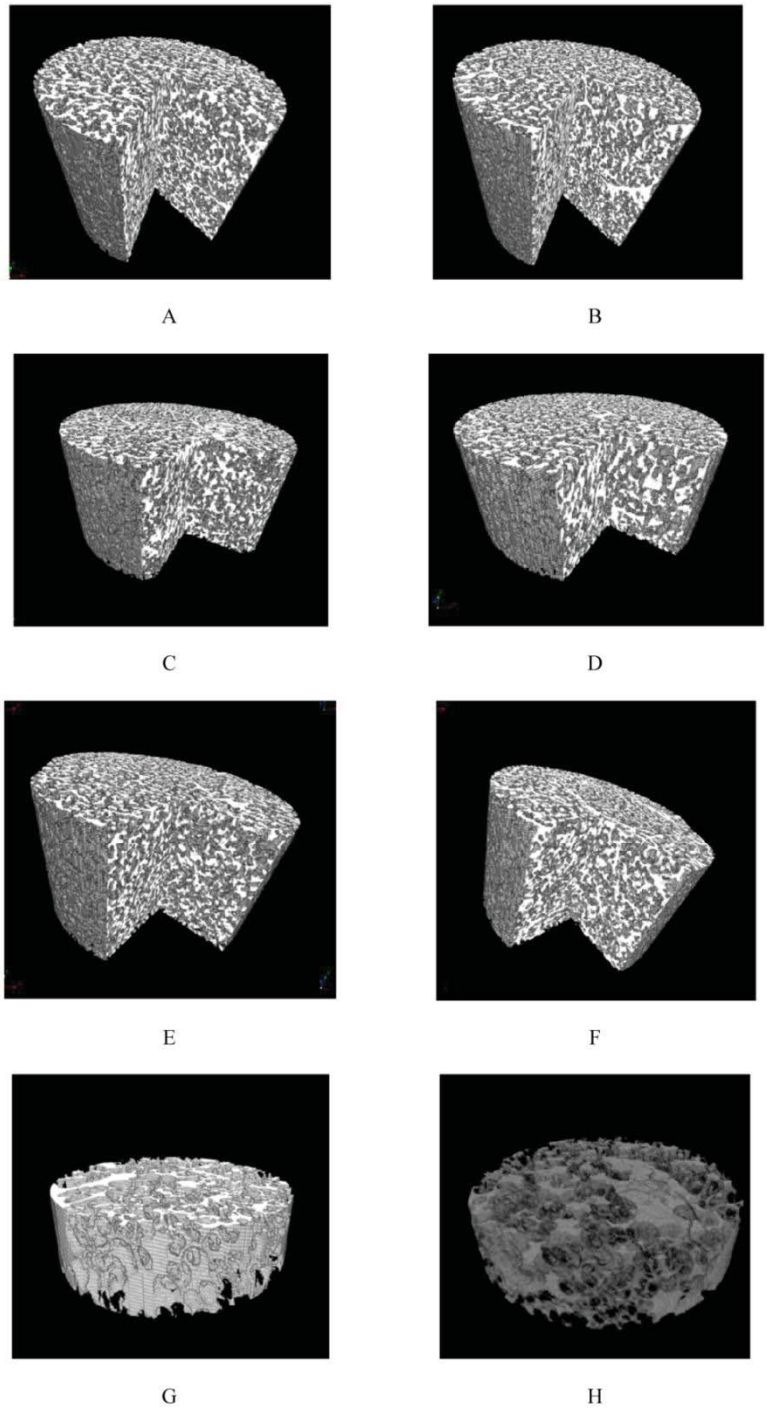


*Figure 2-10* Reconstructed and sectioned volume of $d_{i40}$ volume constraint foam expansion pure foam (A and B) and foam composites 5% (C, D), 10% (E, F), 15% (G, H) before and after compression test in microCT

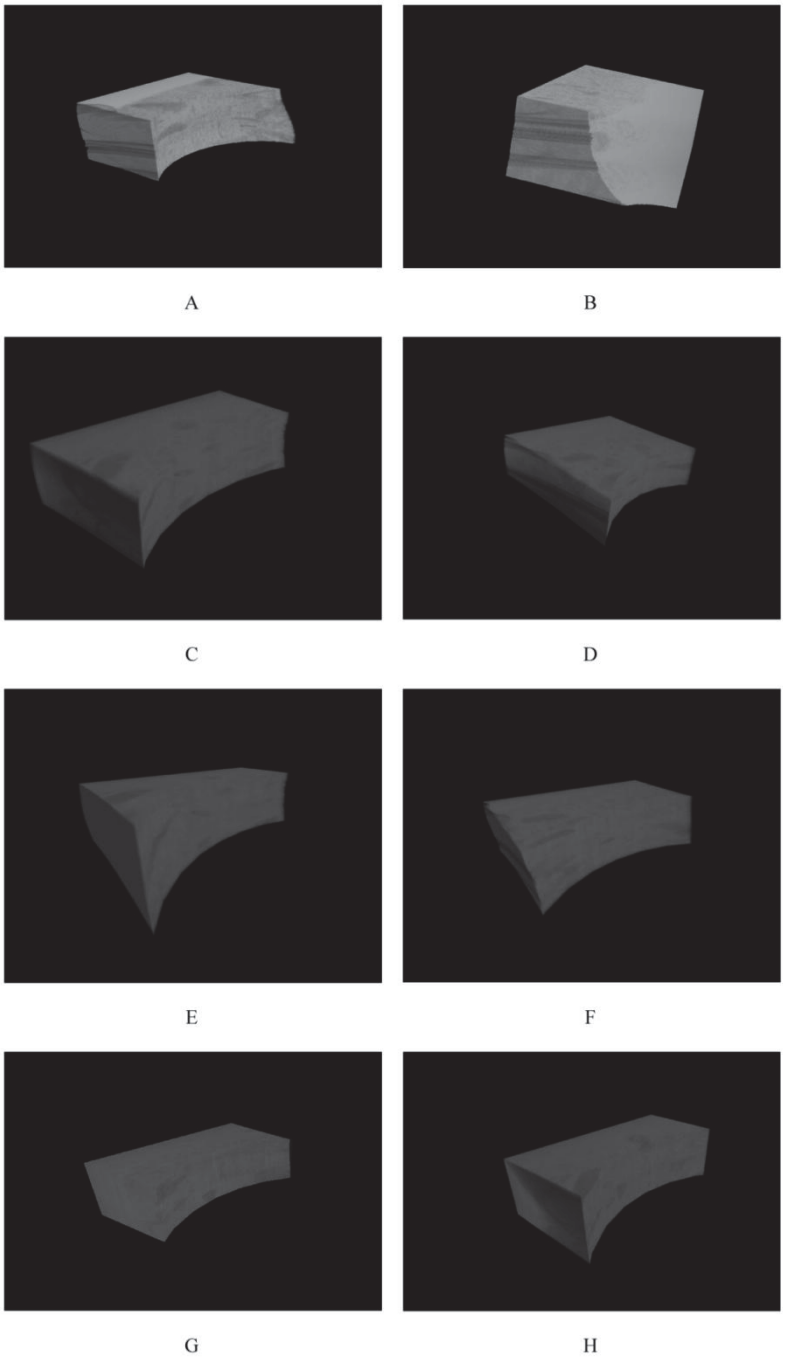


*Figure 2-11* Reconstructed and sectioned volume of $d_{i60}$ volume constraint foam expansion pure foam (A and B) and foam composites 5% (C, D), 10% (E, F), 15% (G, H) before and after compression test in microCT.

## 2.5 Conclusion

In this study we have examined kenaf core as a reinforcement. In contrast to prior efforts where kenaf core has never shown reinforcement, a new manufacturing approach of constraint during foaming enabled reinforcement to be obtained. The very low density of kenaf core 0.28 g/cc lead to the poor reinforcement when the foam was mixed and allowed to expand freely. The modulus and strength-concentration profiles show a large loss in mechanical performance in the free expansion foams in both compressive and bending modes. The nonlinear mechanical-concentration outcome correlates with the foam largely segregating and not reinforcing the foam till high concentrations of filler. Even then, the values are lower than the unreinforced rigid PU. In creating a constrained foaming environment, the kenaf core moved to the cell walls from non-reinforcement within the cell. Now gradual increase with concentration was obtained. More the constraint the better was the mechanical response. The compressive and flexural properties show increase with $d_{i60}$ foams with all kenaf core loading percentages due to dense packing of more number of smaller foam cells as seen from ESEM images. The foam densities show an increase for $d_{i60}$. The dense packing has given rise to smaller cell sizes and increased linear cell density in $d_{i60}$. This dense packing has contributed positively to the compressive and flexural properties. Further flexural response was better than compressive response relative to the unreinforced foam. This indicates that cell fracture under compression is the mode of failure.

## 2.6 References


[1] W.H. Tao, C.C. Chang and J.Y. Lin, Journal of Cellular Plastics, 36, 441(2000).

[2] M. Modesti, V. Adriani, F. Simoni, Polymer Engineering and Science, 40 2046(2000).

[3] M. Kapps and S. Buschkamp, The Production of Rigid Polyurethane Foam, Leverkusen-Germany, Bayer (2001).

[4] T.U. Patro, G. Harikrishnan, A. Misra, D.V. Khakhar, Polymer Engineering and Science, 48, 1778 (2008).

[5] H. Yeganeh, M. Razavi-Nouri, M. Ghaffari, Polymers for Advanced Technologies, 19, 1024 (2008).

[6] L.J. Lee, C. Zeng, X. Cao, X. Han, J. Shen, G. Xu, Composites Science Technology, 65, 2344 (2005).

[7] D. Yan, L. Xu, C. Chen, J. Tang, X. Ji, Z. Li, Polymer International, 61, 1107 (2012)

.

[8] V.B. Veronese, R.K. Menger, M.M. de C. Forte, C.L. Petzhold, Journal of Applied Polymer Science, 120, 530 (2011).

[9] S. Tan, T. Abraham, D. Ference, C.W. Macosko, Polymer, 52, 2840 (2011).

[10] J.C. Crane, Econ. Bot., 3, 334 (1947).

[11] M.S. Sreekala, S. Thomas, Compos Sci. Technol., 63, 861 (2003).

[12] P. Wambua, J. Ivens, I. Verpoest, Natural fibres: can they replace glass in fibre reinforced plastics?, Compos Sci Technol 63 (2003) 1259-1264.

[13] Y. Li, Y.W. Mai, Journal of Adhesion, 82, 527 (2006).

[14] M.R. Ishak, Z. Leman, S.M. Sapuan, M.Y. Salleh, S. Misri, International Journal of Mechanical and Material Engineering, 4, 316 (2009).

[15] S. Shibata, Y. Cao, I. Fukumoto, Polymer Testing, 25, 142 (2006).

[16] S.M. Ogbomo, K. Chapman, C. Webber, R. Bledsoe, N.A. D'Souza, J App Poly. Sci., 112, 1294 (2009).

[17] B. Yang, M. Nar, D.K. Visi, M. Allen, B. Ayre, C. L. Webber III, H. Lu, N.A. D'Souza, Journal of Composites Part B, 56, 926 (2013).

[18] M. Zampaloni, F. Pourboghrat, S.A. Yankovich, B.N. Rodgers, J. Moore, L.T. Drzal, A.K. Mohanty, M. Misra, Composites Part A: Applied Science and Manufacturing, 38, 1569 (2007).

[19] S. Fukuta, M. Nishizawa, Y. Ohta, Y. Takasu, T. Mori, M. Yamasaki, Y. Sasaki, Forest Products Journal, 60, 575 (2010).

[20] S. Terry,Jr, G.D. Miller, M.J. Fuller, Forest Products Journal, 43, 69 (1993).

[21] M.R. Ishak, Z. Leman, S.M. Sapuan, A.M.M. Edeerozey, I.S. Othman, 9th National Symposium on Polymeric Materials (NSPM 2009), IOP Conf. Series: Materials Science and Engineering , 11, 012006 (2010).

[22] H. Ismail, A.H. Abdullah, A.A. Bakar, Journal of Reinforced Plastics and Composites, 29, 2489 (2010).

[23] H.D. Rozman, L. Musa, A.A. Azniwati, A.R. Rozyanty, Journal of Applied Polymer Science, 119, 2549 (2011).

[24] M. Kuranska, A. Prociak, Composites Science and Technology, 72, 299 (2012).

[25] Jr. T. Sellers, N.A. Reichert, E. Columbus, M. Fuller, K. Williams, Kenaf properties, processing and products, Mississippi State University, MS (1999).

[26] A. Ashori, J. Harun, W. Raverty M. Yusoff, Polymer-Plastics Technology and Engineering, 45, 131 (2006).

[27] M.F. Juhaida, M.T. Paridah, M.M. Hilmi, Z. Sarani, H. Jalaluddin, A.R.M. Zaki, Bioresource Technology, 101, 1355 (2010).

[28] Z. Mitul, Absorbency characteristics of kenaf-core particles, Ph. D. thesis, North Carolina State University, USA (2004).

[29] H.M. Choi, R.M. Cloud, Environmental Science and Technology, 26, 772 (1992).

[30] K. Liang, S.Q. Shi, Journal of Applied Polymer Science, 119, 1857 (2011).

[31] V. Kumar, N.P. Suh, Polymer Engineering and Science, 30, 1323 (1990).

# CHAPTER 3

# ACOUSTICS OF POLYMER FOAMS

## 3.1 Introduction

Polymer foams are widely used in noise and vibration control. Amongst them polyurethane is the most versatile polymer family. The ability to tailor the desired properties by altering the molecular chain length, functionality etc. to make rigid, semi-rigid, or flexible polyurethane with control on open and closed cells has made polyurethane very much desirable for researchers [1]. Today increasing concern towards environmental and health hazard is expressed due to noise pollution [2,3]. Noisier environment which is closer to the highway or airport with a noise level above 60 dB has an adverse effect on children and their response to dealing with the stressful situations when compared to the children growing in the quiet neighbourhood [4]. Another study of subjects exposure to night time traffic with low frequency showed lower cortisol levels which is responsible for pleasantness after 30 min of waking up to mood swings [5]. This has led researchers worldwide to focus on acoustic properties [6,7].

Naturally occurring plant materials have shown good sound absorbing characteristics. These materials act as perfect alternate solutions to the presently used conventional material, such as glass fibres that pose additional environmental threat of disposal [8]. Substantial amount of research is directed towards natural materials those are recyclable, renewable, and sustainable [9]. As an example, the by-product of tea-leaf industry has shown superior sound absorption properties when compared to woven fabric [10]. Apart from the tea-leaf by-product, other efforts have been made to utilize waste such as corn stover, corncob [11], rice [12], wheat straws [13], and kenaf fibers

[14]. Polymer/natural composites from polypropylene/jute composites [15], polyethylene/wood flour composites [16], composites from bamboo [17], sisal [18], hemp [19] etc are studied.

Acoustics properties like sound absorption and transmission loss are important properties that have to be taken into consideration in many engineering applications [20, 21]. The phenomenon of sound absorption and transmission loss are fundamentally different. Sound absorption can be explained by two mechanisms, one is viscous losses between air and material, and other is due to thermal losses [22, 23].

## Objective of This Chapter

In this chapter polyurethane foam composites with kenaf core loadings of 5, 10, and 15 % are prepared with constrained expansion of 40 and 60 % and free foam expansion are used. This processing variation has led to foams with range of cell size distributions, void volume, and open porosities. These foam cell morphologies affect the acoustics properties. Therefore these were tested for sound absorption coefficient and transmission loss using the two and four microphone impedance tube method. The objective was to identify the higher sound absorption coefficient foam at wide range of frequencies. From the initial testing of 12 foam composites four foams were identified, two with approximately equal cell size however with different open porosity, and other two with equal open porosity and different cell size. Using these foam composites three combinations of design were created. In first one the foam were glued together using pure PU. In other one a slice was made at an angle to give maximum cross –sectional area thereby creating larger interface for sound absorption. A third design was made to enclose air inside the cavity to enhance the sound absorption. These combinations

gave a synergistic effect of both the foams to achieve higher sound absorption coefficient for wider range of frequencies.

## 3.2 Building of Acoustics System

### 3.2.1 Two-Microphone Impedance Tube Method

The test method for sound absorption coefficient (α) uses impedance tube with two microphones at normal incidence, which is 0º. The sound source is connected to one end and the sample to be tested is placed at other end. The plane waves are generated using broadband signal from the sound source. The tube had two slots for placing two microphones; these are the places where the sound pressures were measured of the decomposing stationary sound wave pattern into forward and backward-travelling components. From the measured transfer function calculations are done for normal-incidence absorption coefficient.

#### 3.2.1.1 Equipment

The impedance tube is a hollow brass cylinder with inner diameter of 34.82 mm and thickness of tube was 3.35 mm. The length of the tube that was used for sound absorption measurement was 910 mm. There are three holes on top of the tube of diameter 7.96 mm for the placement of microphones, these are called microphone ports. The first hole which is generally used as reference hole is at 127 mm from the sound source. The other two holes for microphones 1 and 2 are at 159, and 273 mm respectively. The outputs of these microphones are connected to multi-channel frequency analyzer that is directly connected to computer. A speaker is connected at the end of the tube as shown in Figure 3-1. The signal is generated directly from the

LabVIEW™ 2013 and fed to the amplifier and then to the speaker. This two microphone impedance tube is used to measure sound absorption coefficient and is accordance with ASTM E1050-12 [24].

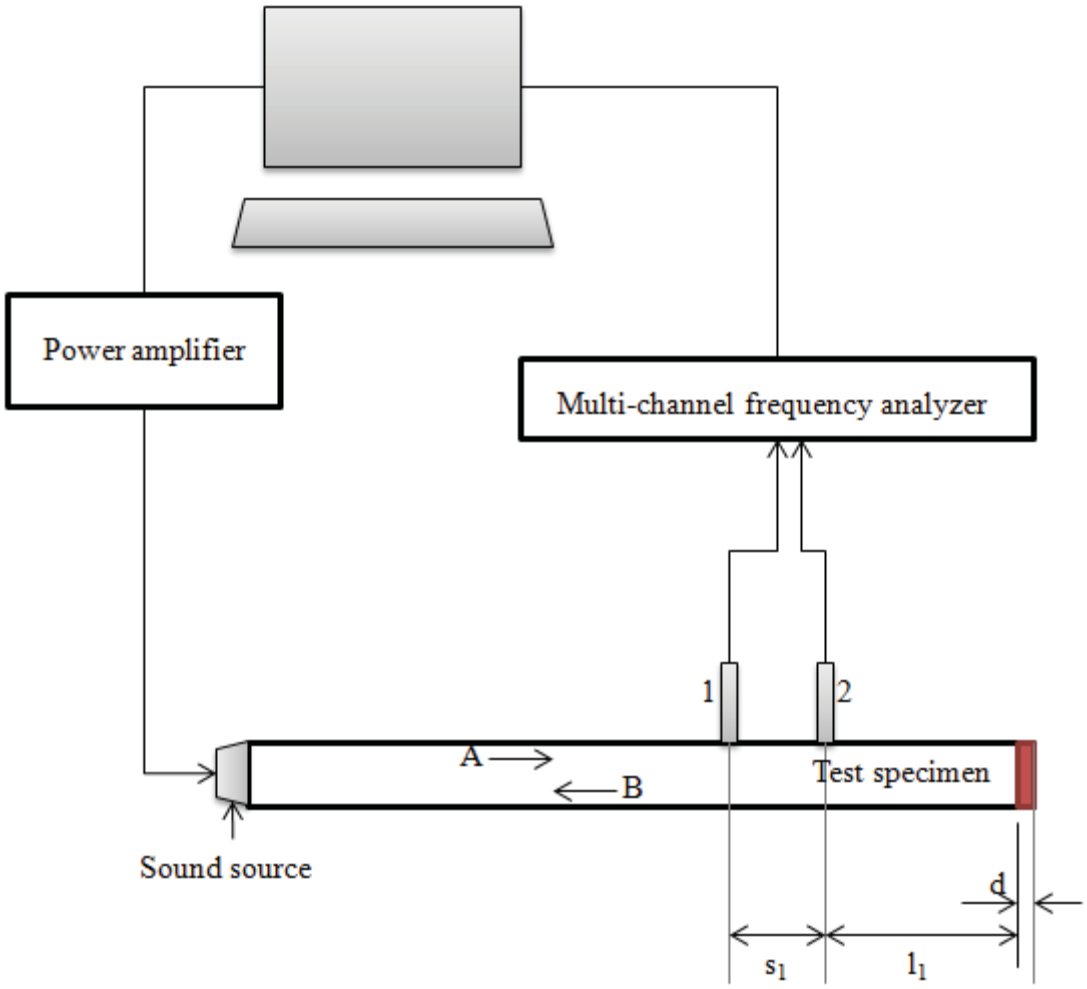


*Figure 3-1* Arrangement of components for sound absorption coefficient measurement with impedance tube method

3.2.1.2 Following Formulas Were Used

Working frequency range

$$f_l < f < f_u$$

Upper frequency limit

$$f_u < K(c/d)$$

Speed of sound

$$c = 20.047\sqrt{(273.15 + T)}$$

Air density

$$\rho = 1.290\left(\frac{P}{101.325}\right)\left(\frac{273.15}{273.15 + T}\right)$$

Where:

$f_1$ = lower working frequency of the tube (Hz)

f = operating frequency (Hz)

$f_u$ = upper working frequency of the tube (Hz)

K = 0.586

c = speed of sound in air (m/s)

d = diameter of the tube (m)

T = room temperature (ºC)

ρ = air density (gm/cc)

P = atmospheric pressure (kPa)

Using the above equations and taking parameters like diameter of tube as 0.03482 m, room temperature of 22 ºC, atmospheric pressure of 101.325 kPa, the working frequency range was calculated to be from 100 to 5000 Hz.

3.2.1.3 Calibration of Instrument

The signal-to-noise ratio was measured for two microphones with sound ON and OFF to make sure the test frequency band is 10dB greater than background noise. Vector averaging technique was used to average the transfer function. Hanning Window was used to measure transfer function spectra. This is employed because FFT analysis is made of data blocks recorded over finite length. The digital signal records the truncated spectra as against the continuous analogue spectra. Time weighting function (i.e. Hanning Window) was used to de-emphasize the truncated parts of time period.

Placing the microphones in standard configuration is shown in Figure 4-1

3.2.1.4 Measurements

Transfer function

$$\overline{H} = \frac{G_{12}}{G_{11}}$$

Complex reflection

$$R_r = \{2H_r \cos[\,k(2l+s)] - \cos(2kl) - (H_r^2 + H_i^2)\ \cos[2k(l+s)]\}/D$$

$$R_i = \{2H_r \sin.[\,k(2l+s)] - \quad \sin.(2kl) - (H_r^2 + H_i^2) \quad \sin.[2k(l+s)]\}/D$$

Normal incidence sound absorption coefficient

$$\alpha = 1 - R_r^2 - R_i^2$$

Where,

$G_{11}$, and $G_{12}$ = auto power spectra, and cross power spectra of acoustic pressure signal at microphone locations 1 and 2.

$\hat{H}$ = measured transfer function of two microphone signals.

k = wave number ($m^{-1}$)

l = distance from test sample to centre of the nearest microphone (m)

R = complex acoustic reflection coefficient.

s = centre-to-centre spacing between microphones (m)

### 3.2.2 Four-Microphone Impedance Tube Method

For transmission loss a four microphone impedance tube method was used in accordance with ASTM E2611-09 [25]. Referring toFigure 3-2, for transmission loss an extended tube is used which has two additional holes on top of the tube for placing two microphones. The length of this tube is 610 mm and has holes at 265 and 380 mm from the end which will be attached at the end of the other tube where sample is placed. The microphones 3 and 4 are connected to multi-channel frequency analyzer and then directly to computer.

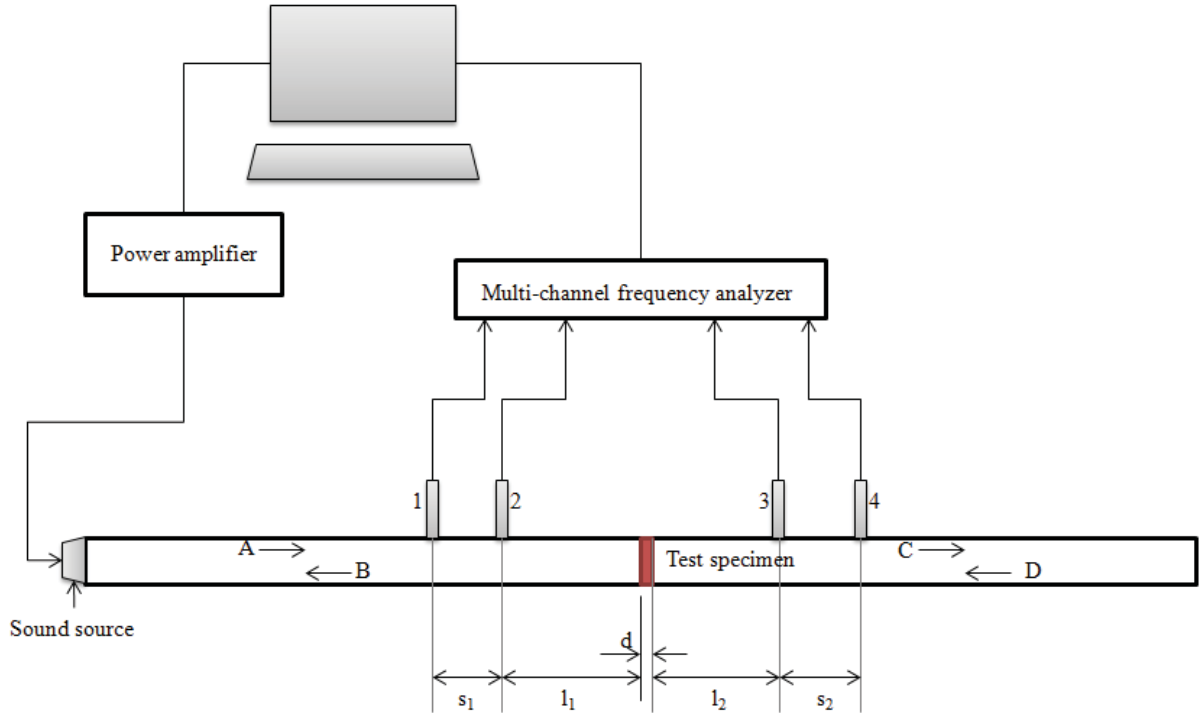


*Figure 3-2* Arrangement of components for transmission loss measurement with impedance tube method

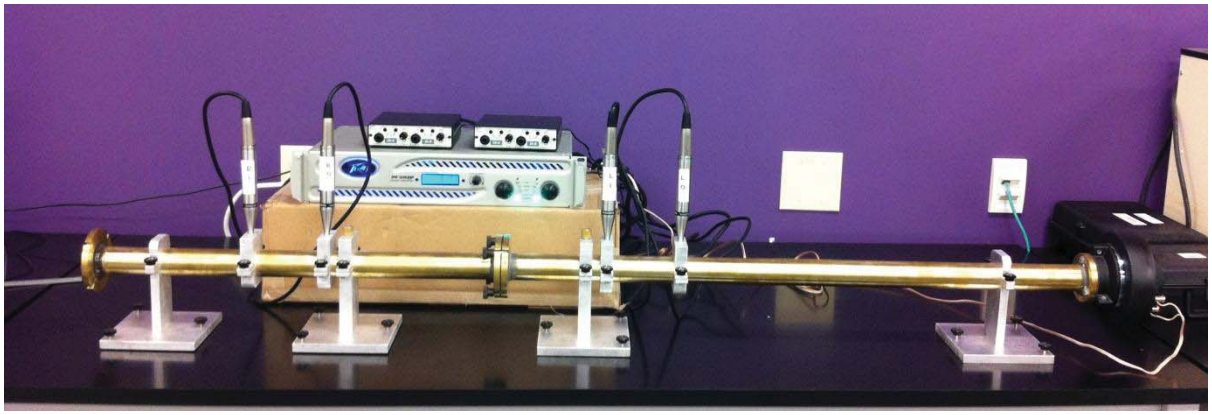

*Figure 3-3* Acoustics measurement system built in-lab with impedance tube and 4-microphone arrangement.

## 3.3 Experimental

### 3.3.1 Materials and Sample Preparation

The samples for foam composites were prepared as discussed in Chapter 2. They are named the same as before. The circular cut was made using a drill with internal diameter of 38.42 mm. The sample was cut to a thickness of 15 mm; the cut sample is shown in Figure 3-4 (A). This was used to measure the sound absorption coefficient and normal incident transmission loss. The sample placement inside the impedance tube is shown in Figure 3-4 (B).

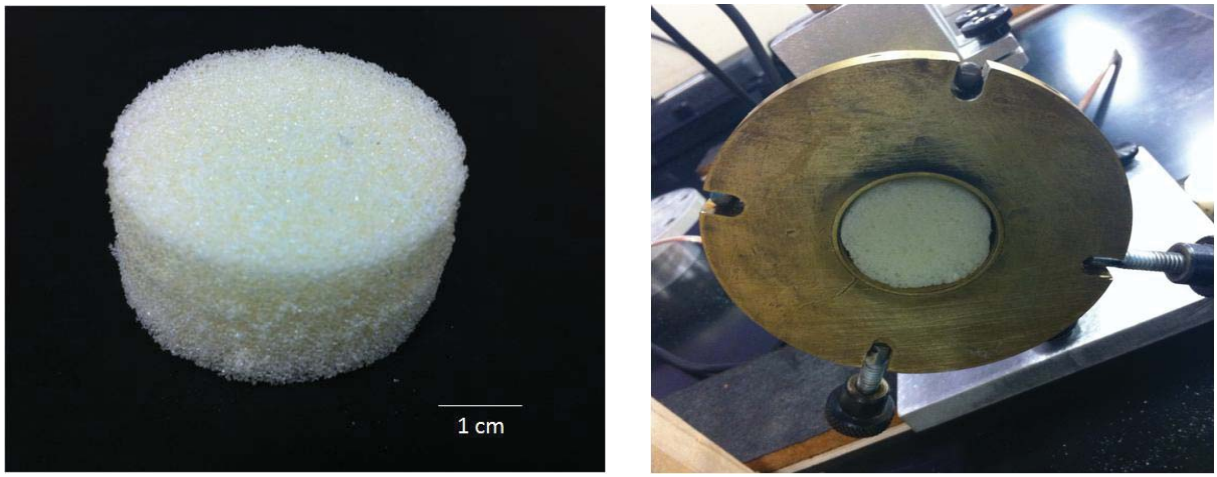


A B

*Figure 3-4* (A) Foam sample cut for acoustics measurements, and (B) placement of sample inside the impedance tube.

#### 3.3.1.1 CASE I

For combination foam composites with two layers the samples were cut with circular drill with internal diameter of 34.82 mm to a thickness of 7.5 mm. Later both the samples were glued together with the mixture of pure foam and a pressure was applied

until the foam is cured. These samples were used to measure the sound absorption coefficient and normal incident transmission loss.


A B

*Figure 3-5* Samples prepared for the Case I study for combination acoustics measurements

3.3.1.2 CASE II

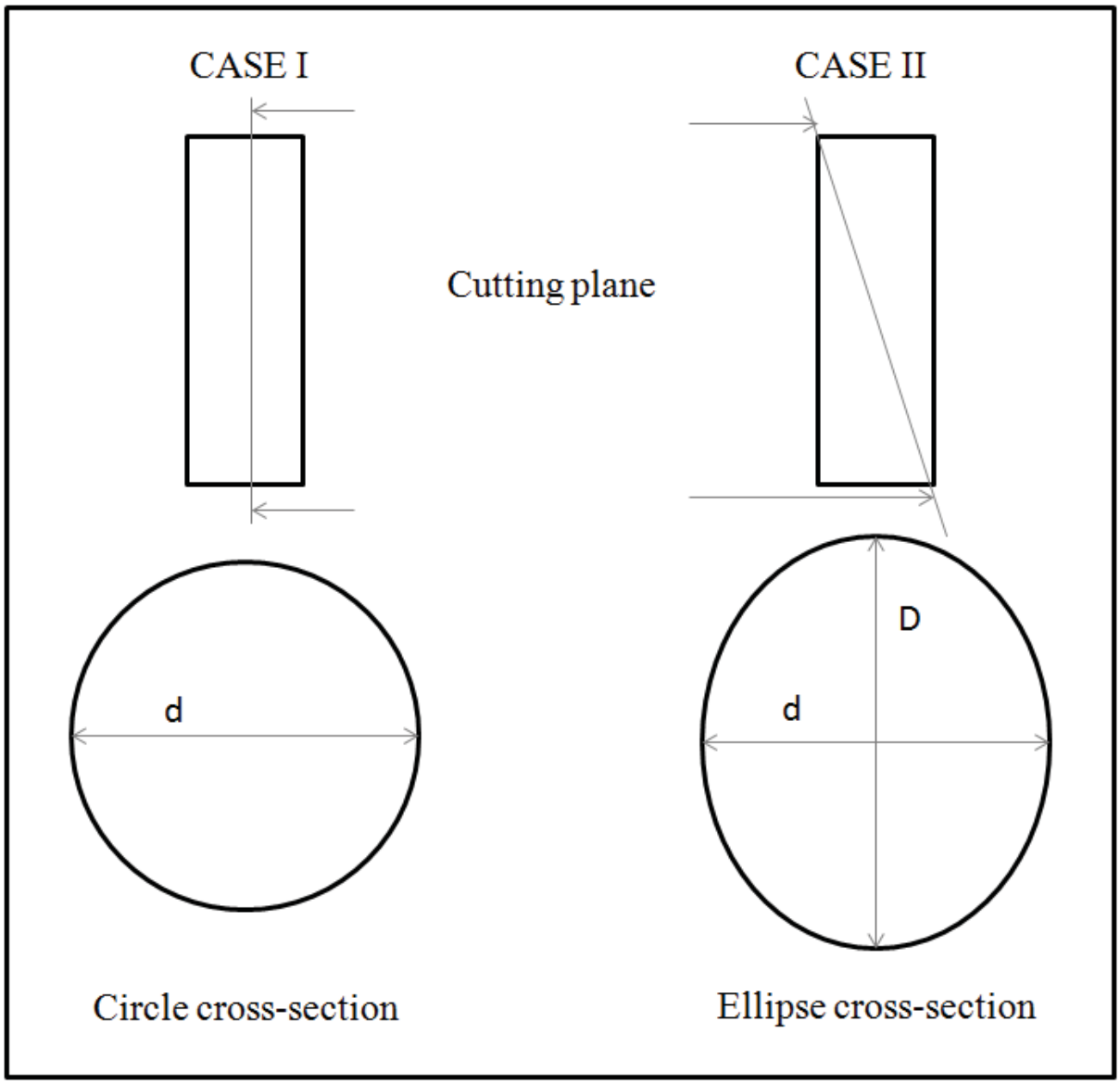


*Figure 3-6* Schematic showing the comparison of CASE I and CASE II for the influence of cutting plane with increase in cross-section.

For CASE I the area of the circle with diameter (d) of 38.42 mm was ~1160 $mm^2$, for CASE II the area of ellipse with major diameter (D) of 41.244 mm and with minor diameter (d) of 28.42 mm, area of ellipse comes to 1244.5 $mm^2$. Thus, providing an area increase of ~7.4 %, this means increase in interface area to ~7.4 %. This is shown in schematics outlined in Figure 3-6.

A sliced combination foam composites with two layers the samples were cut using saw and then polished with 800 grit size carbide paper to remove any unevenness that was introduced due to the saw cutting and cleaned with compressed air to remove loose material from the polished surface as shown in Figure 3-7 (A – D). The samples were glued together with the mixture of pure foam and a pressure was applied until the foam was cured (Figure 3-7 E and F). These samples were used to measure the sound absorption and transmission loss.

A

B

C

D

E

F

*Figure 3-7* Samples prepared for the Case II study for combination acoustics measurements (A), (B), (C), and (D) show the angled section of the foams and (E) and (F) showing the glued samples ready for testing.

3.3.1.3 CASE III

As a third design the foam F1 and F2 were cut and polished to a thickness of 5 mm. A second section was cut from F1 to thickness of 5 mm and a circular portion was cut with diameter 20 mm to give an annular middle section of the CASE III design as shown in Figure 3-8 (A) and (D). The annular middle section was glued to the F1 and F2 to the either side to create an air space in the sample, the glued specimen is shown in Figure 3-8 (B) and (E) where J is the glued pure PU joint. The microCT images in Figure 3-8 (C) and (F) clearly shows the joint J and also the difference in contrast of the glued foams.

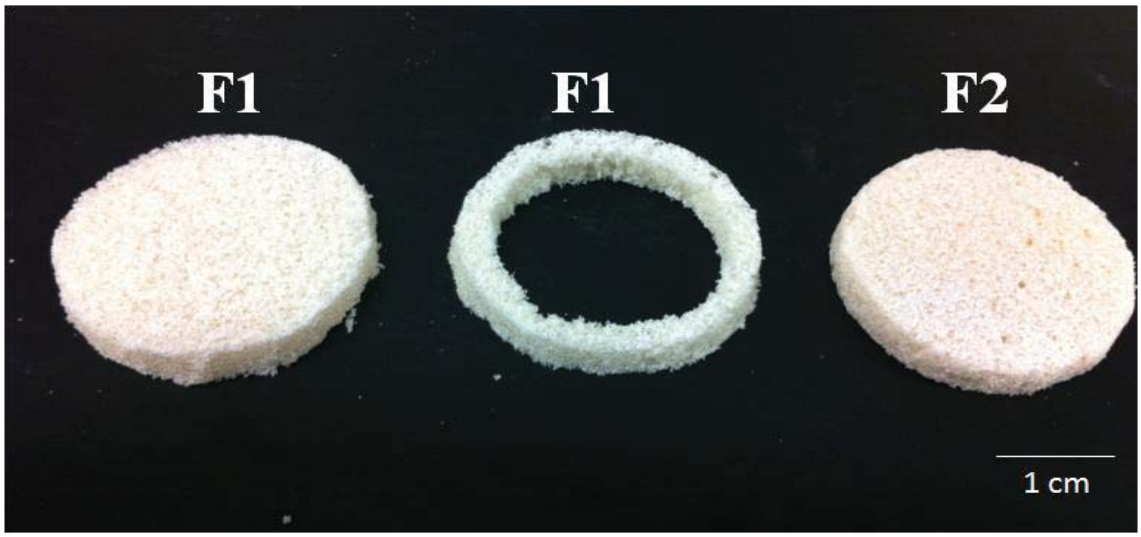


A

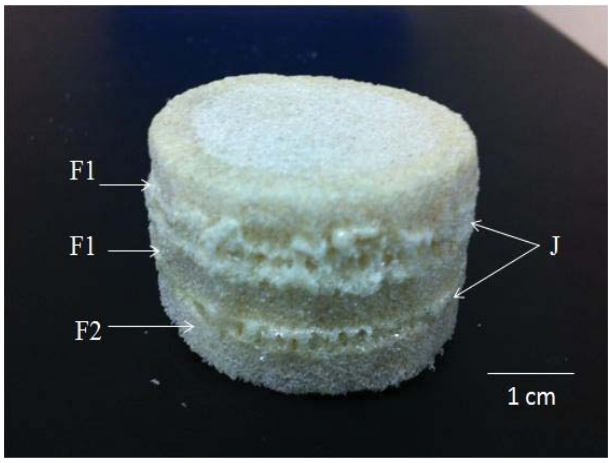


B

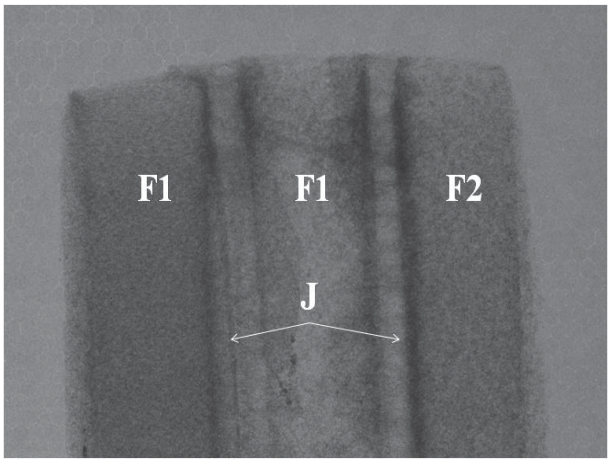


C

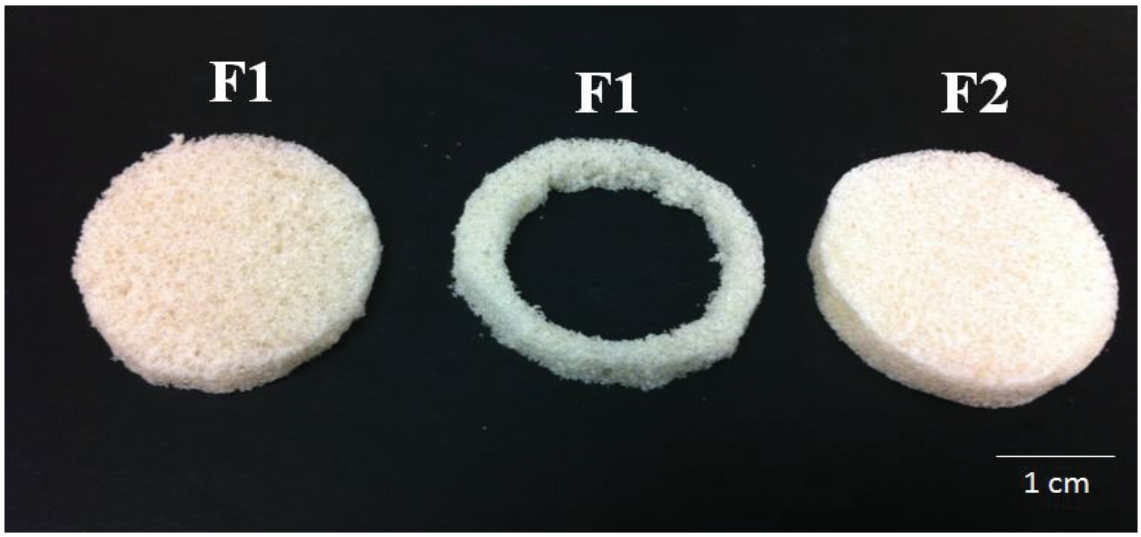


D

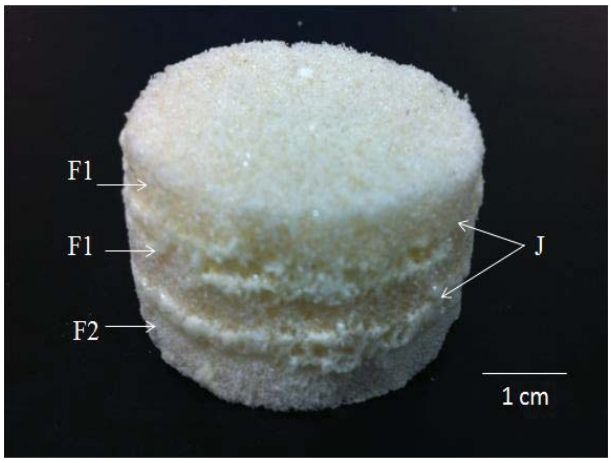


E

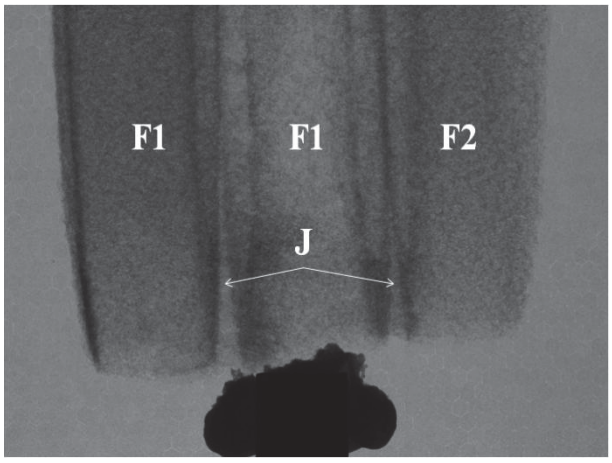


F

*Figure 3-8* CASE III samples (A) and (D) shows the 5 mm thickness cut foam sections, the inner section F1is cut in centre to create an air filled space, (B) and (E) shows the glued sample with sections F1, F2 either side of the annular F1, (C) and (F) shows the microCT image showing clearly the joints J in-between the glued foams.

### 3.3.2 Porosity and Open Porosity Measurement

The porosity was measured directly from microCT as void fraction. The open porosity was measured by identifying four structures forms in PU foams: open pore cell, half open pore cell, pin hole, and closed pore cell. Open porosity was calculated using following equation [26].

$$p = \frac{2N_{open} + N_{part}}{2(N_{open} + N_{part} + N_{pin} + N_{closed})}$$

Where p is open porosity of foams; $N_{open}$ is the number of open pore cells; $N_{part}$ is the number of half open pore cells; $N_{pin}$ is the number of pin holes; $N_{closed}$ is the number of closed pore cells.

### 3.3.5 Dynamic Mechanical Analysis

The foams were tested with the RSA 3 (TA Instruments, USA) for Dynamic Mechanical Analysis (DMA). A cylindrical test specimen of length 15 mm and diameter of 25 mm was used for the strain sweep and one for the temperature sweep. In phase storage modulus (E') and tan delta were measured at frequency of 1 Hz with strain amplitude of 0.2 % which was determined from the strain amplitude sweep test and the heating rate of 3 ºC/min. The temperature was ramped from -50 ºC to 200 ºC while testing.

### 3.3.6 Acoustics Properties

Sound absorption coefficient and transmission loss were studied using the acoustics system that was made as per ASTM and described in section 3.2. Sound absorption coefficient was obtained using two-microphone impedance tube method ASTM E1050. Frequency range of 80 to 5000 Hz was used. The incident sound was perpendicular to the surface of the foam rise direction. A four-microphone impedance tube method was used to measure transmission loss from 80 to 5000 Hz frequency range.

## 3.4 Results and Discussions

### 3.4.1 Effect of Cell Morphology on Sound Absorption Coefficient

The free foaming and constrained expansion of foam composites gave a range of cell sizes. The average cell sizes have been summarized in Table 3-1. Figure 3-9 shows the cell size distribution for the foam composites. The sound absorption coefficient as a function of frequency is shown in Figure 3-10 (A). At 500 Hz which is a low frequency range the sound absorption is higher for larger cell diameter foams. As the cell size reduces the sound absorption is seen to reduce. Thus constrained expansion of 60 % with no kenaf core and 5 % kenaf core loading with free foaming that gave higher cell sizes of around 583 and 650 μm have shown higher sound absorption coefficient of 0.889 and 0.881., Thus 60 % constrained expansion with 15 % kenaf core loading has a cell diameter of 150 μm and has the lowest sound absorption of 0.731. Apart from cell diameter, open pores have influenced the sound absorption of the foams. More the number of open pores, more is the interconnected cell structures that help absorption particularly at frequencies around 500 Hz (Figure 3-10 B).

It is interesting to note from Figure 3-10 A, that although the values for sound absorption decreases at higher frequencies, a general trend is that consistently improved sound absorption occur with higher cell diameter and open porosity. Sound is primarily dissipated due to viscous flow, thermal damping, and Helmholtz resonance effect. As the sound wave reaches the foam surface the gas inside the closed cells is set in motion thereby converting the sound energy into kinetic energy. Therefore, larger the cell diameter more is the air inside the closed cells to dissipate the sound energy giving higher sound absorption. The interconnectivity plays a role in dissipating sound

by converting sound energy into kinetic energy and heat. The air inside open pores flows due to the sound pressure generated. The friction of air flowing against the cell walls converts sound energy into heat thereby improving the sound absorption. Table 1 shows values of open porosity and confirms that higher open porosity better is sound absorption.

Other mechanisms that contribute to sound absorption at higher frequencies is deformations of cells walls such as stretching, bending, and buckling. When the higher frequency sound hits the foam, the air inside the closed cells gets higher kinetic energy. This high energy forces the cell wall to stretch, bend, and buckle. The larger cells contain more gas and hence show higher sound absorption.

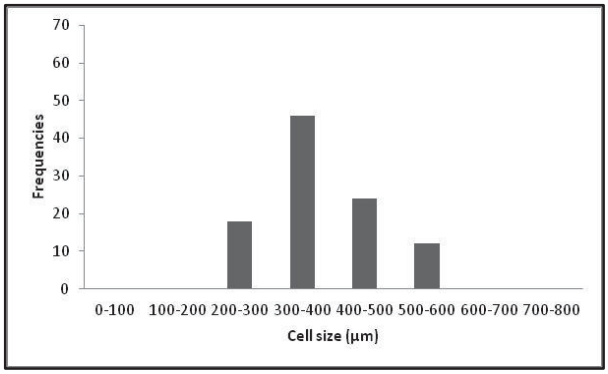


A

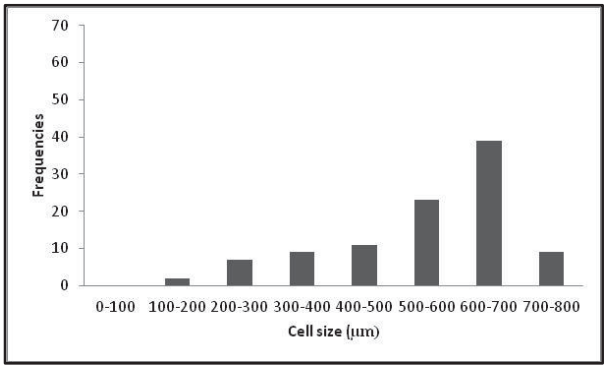


B

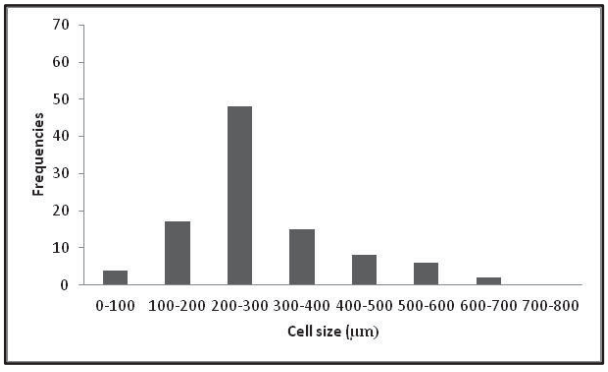


C

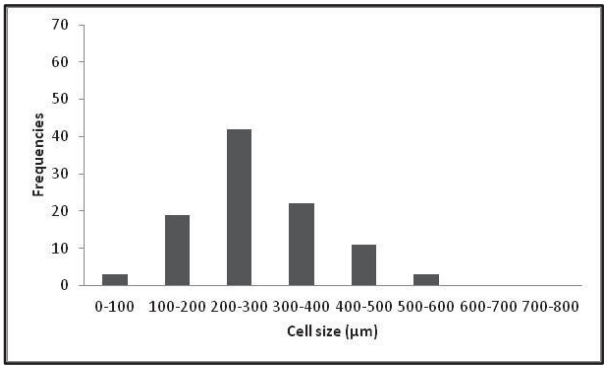


D

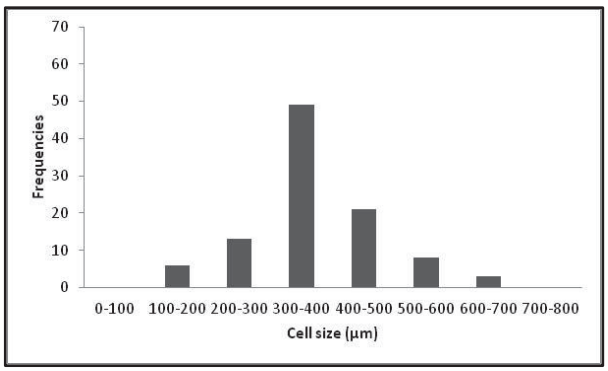
Frequencies
70
60
50
40
30
20
10
0
0-100 100-200 200-300 300-400 400-500 500-600 600-700 700-800
Cell size (µm)

E

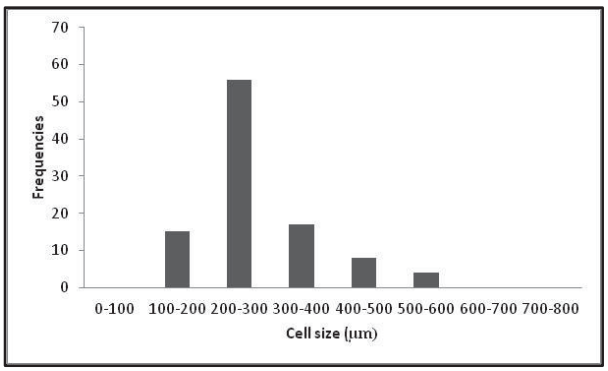
Frequencies
70
60
50
40
30
20
10
0
0-100 100-200 200-300 300-400 400-500 500-600 600-700 700-800
Cell size (µm)

F

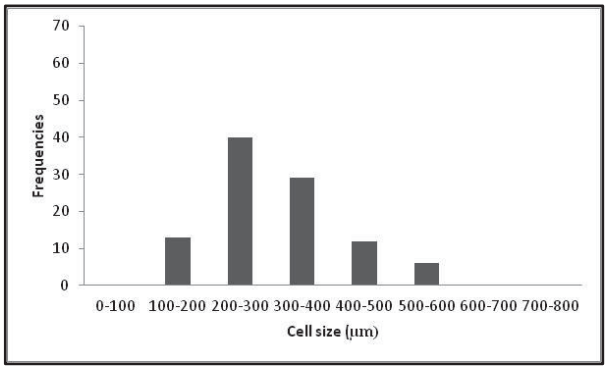
Frequencies
70
60
50
40
30
20
10
0
0-100 100-200 200-300 300-400 400-500 500-600 600-700 700-800
Cell size (µm)

G

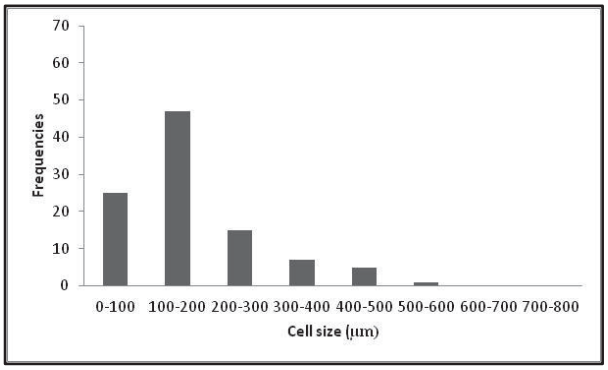
Frequencies
70
60
50
40
30
20
10
0
0-100 100-200 200-300 300-400 400-500 500-600 600-700 700-800
Cell size (µm)

H

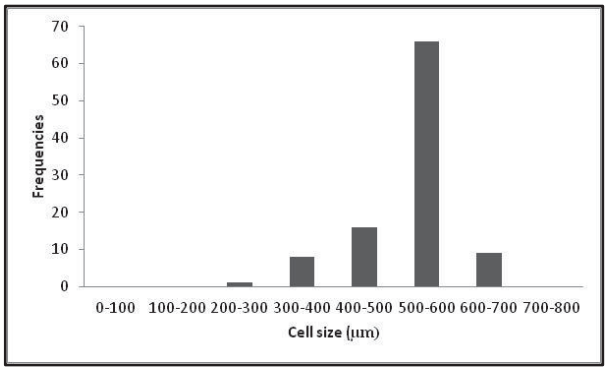
Frequencies
70
60
50
40
30
20
10
0
0-100 100-200 200-300 300-400 400-500 500-600 600-700 700-800
Cell size (µm)

I

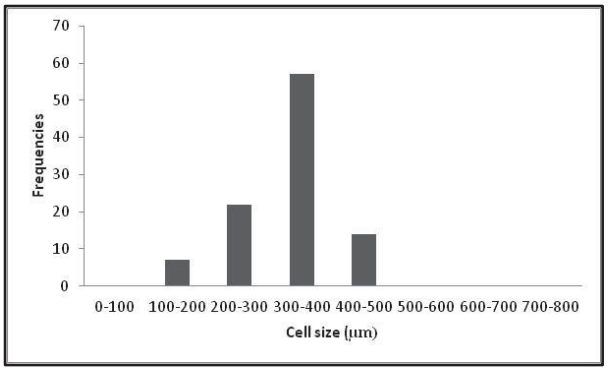
Frequencies
70
60
50
40
30
20
10
0
0-100 100-200 200-300 300-400 400-500 500-600 600-700 700-800
Cell size (µm)

J

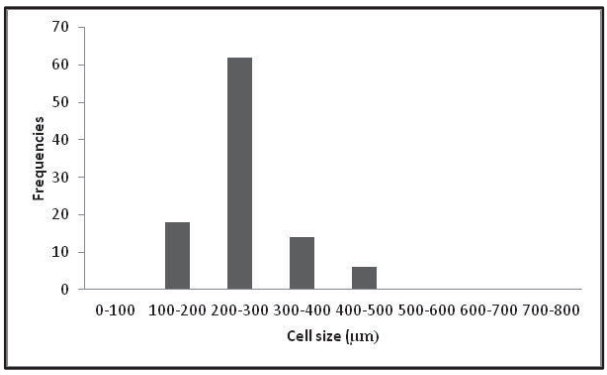


K

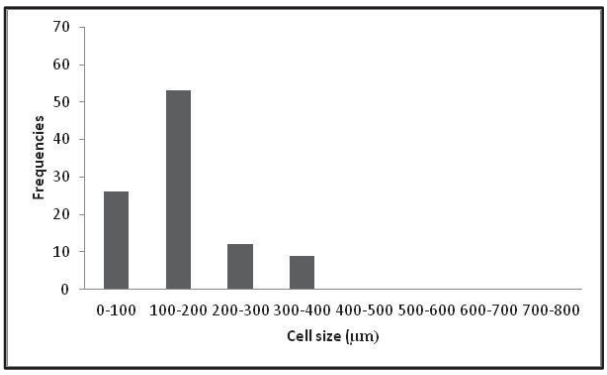


L

*Figure 3-9* Cell size distribution for rigid PU foam composites

Table 3-1

*PU foam composites properties including acoustical and dynamic mechanical compressive properties*

| | di | | | | di40 | | | | di60 | | | |
|---|---|---|---|---|---|---|---|---|---|---|---|---|
| | 0 | 5 | 10 | 15 | 0 | 5 | 10 | 15 | 0 | 5 | 10 | 15 |
| Average cell diameter (µm) | 316±28 | 650±50 | 250±132 | 293±158 | 350±50 | 300±70 | 283±76 | 168±23 | 583±76 | 300±86 | 250±50 | 150±50 |
| Foam density (g/cc) | 0.12 | 0.169 | 0.162 | 0.193 | 0.279 | 0.494 | 0.675 | 0.922 | 0.258 | 0.48 | 0.618 | 0.928 |
| Porosity (%) | 54.46 | 44.9 | 43.96 | 41.75 | 73.92 | 74.57 | 66.21 | 57.68 | 64.28 | 67.61 | 59.73 | 54.27 |
| Open porosity (%) | 15 | 18 | 21 | 23 | 19 | 13 | 17 | 10 | 26 | 19 | 8 | 13 |
| Sound absorption coefficient @ 500 Hz | 0.815 | 0.881 | 0.849 | 0.878 | 0.849 | 0.815 | 0.815 | 0.748 | 0.889 | 0.829 | 0.798 | 0.731 |
| Sound absorption coefficient @ 2000 Hz | 0.728 | 0.815 | 0.766 | 0.759 | 0.688 | 0.715 | 0.673 | 0.674 | 0.809 | 0.743 | 0.706 | 0.653 |
| Sound absorption coefficient @ 4000 Hz | 0.783 | 0.829 | 0.822 | 0.805 | 0.795 | 0.795 | 0.756 | 0.685 | 0.853 | 0.800 | 0.746 | 0.690 |
| Transmission loss (dB) | 21.27 | 22.26 | 20.35 | 21.05 | 22.84 | 23.25 | 21.12 | 20.78 | 20.96 | 20.37 | 22.11 | 21.22 |
| Log E' @ 22 °C (Pa) | 6.58 | 7.51 | 7.35 | 7.37 | 6.53 | 6.75 | 6.64 | 6.77 | 6.586 | 6.53 | 7.41 | 6.67 |
| Tan δ | 0.55 | 0.57 | 0.48 | 0.46 | 0.69 | 0.55 | 0.48 | 0.53 | 0.72 | 0.36 | 0.56 | 0.57 |

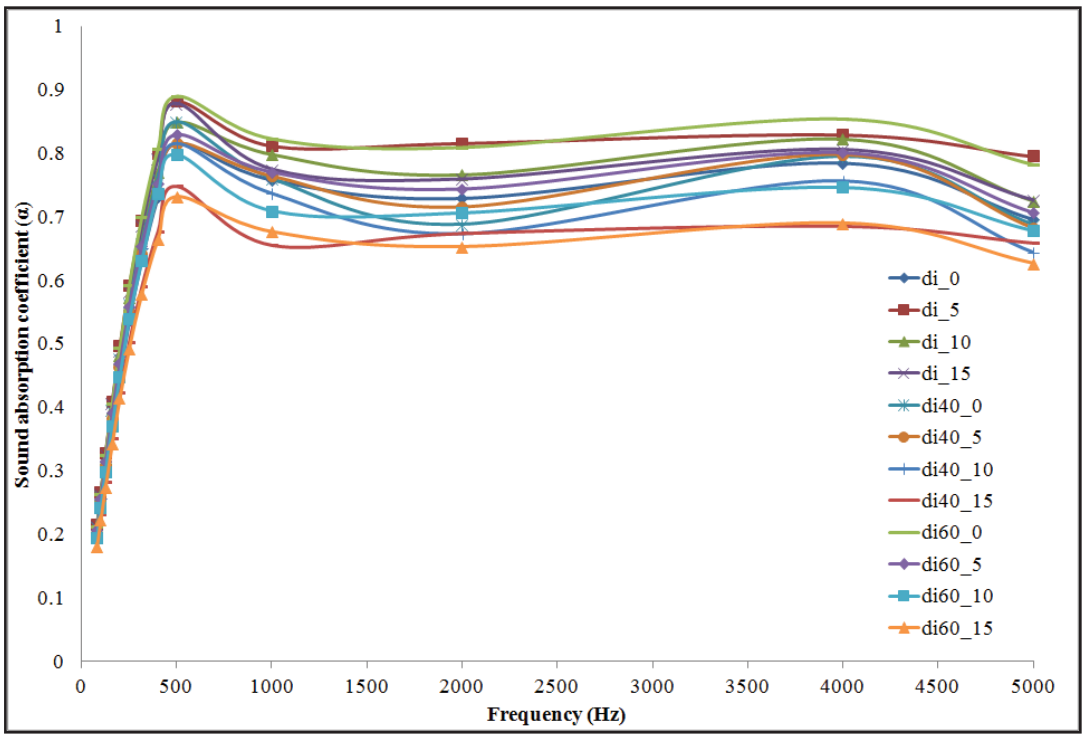


A

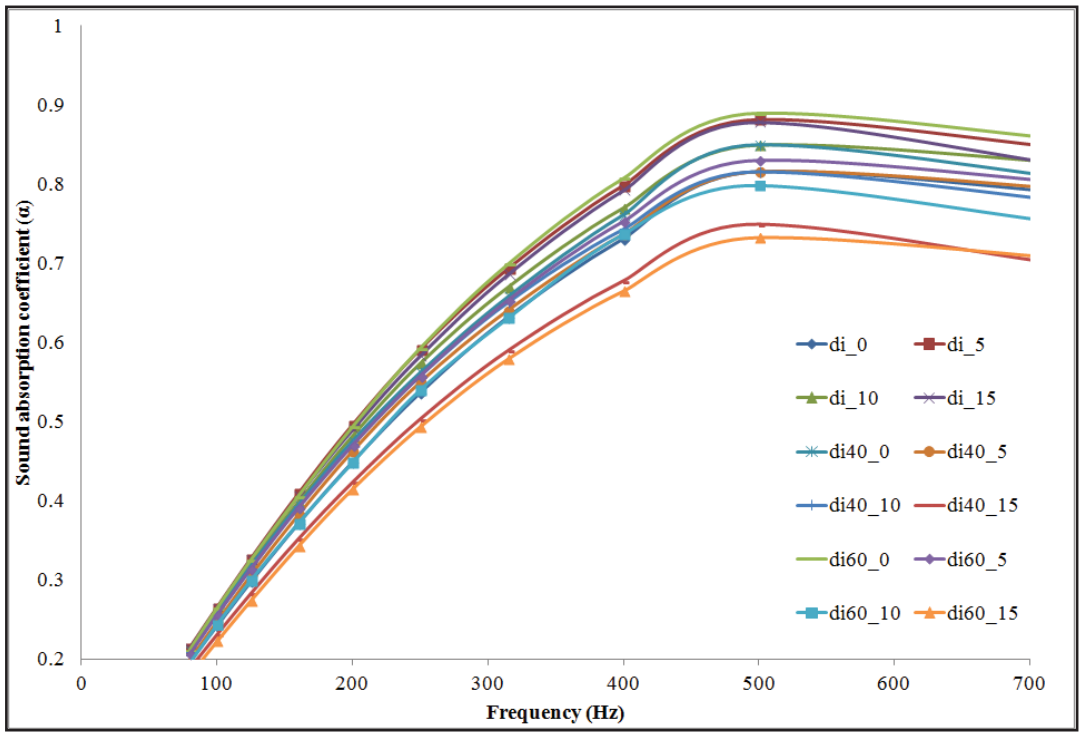


B

*Figure 3-10* Sound absorption coefficients as a function of frequency

### 3.4.2 Effect of Presence of Kenaf Core in Cells on Sound Absorption

Free expansion of foam with 10 and 15 % kenaf core loading had given rise to kenaf core reinforcements to settle in the cells and not in the material. Figure 3-11 shows the ESEM images that show the kenaf core in the cells Figure 3-11 (A), and also in the trapezoidal region of the intersection of cells Figure 3-11 (B).

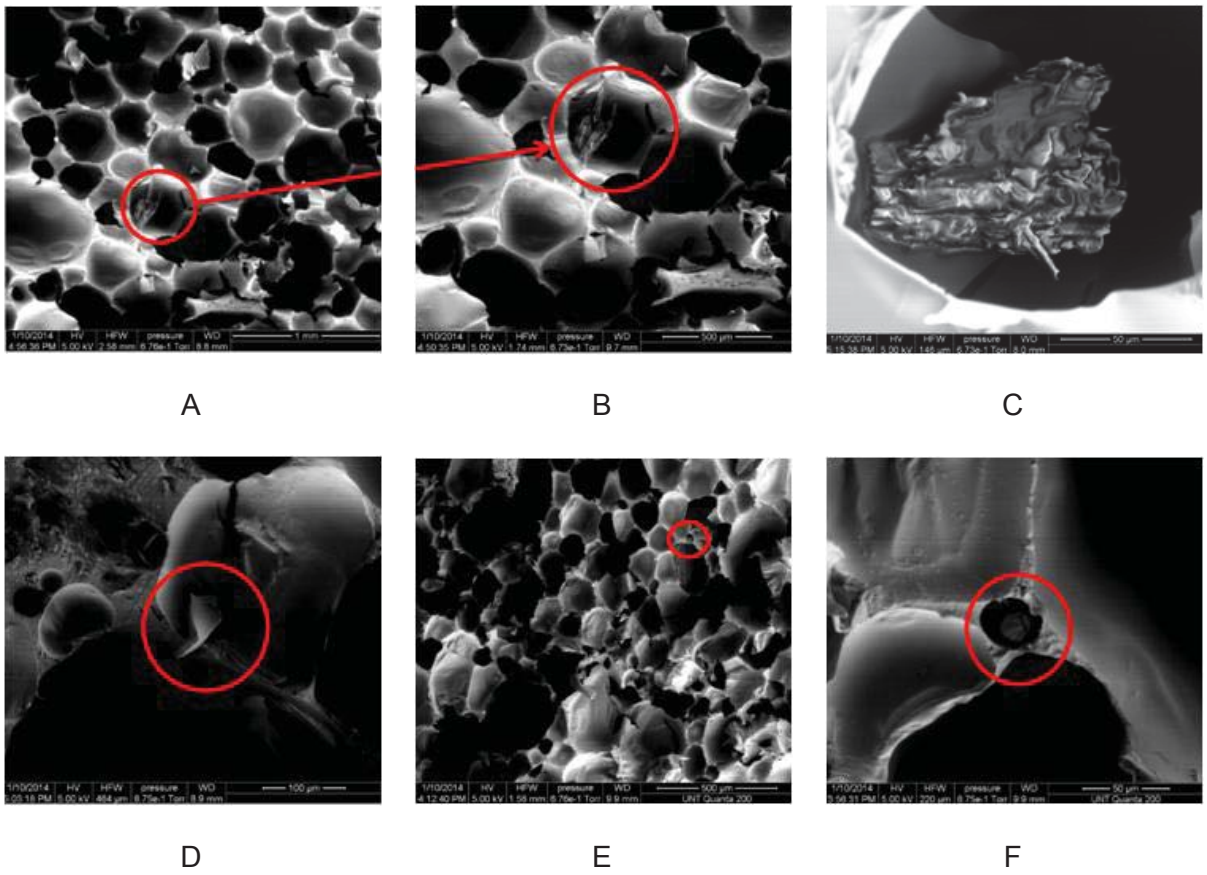

A B C

D E F

*Figure 3-11* ESEM images for 10 % kenaf core loaded foams (A), (B), and (C), and 15 % kenaf core loaded foams (C), (D), and (E) with kenaf core marked with open red circles.

These kenaf cores are loosely held and are free to the response of sound energy. Thus when the sound waves hit these foam surface the sound energy got converted into kinetic energy by setting these loosely held kenaf core in vibration. Thus, sound absorption of 0.849 and 0.878 for di_10 and di_15 respectively.

### 3.4.3 Effect of Design on Sound Absorption

Four foams were selected after the initial sound absorption tests. This selection was done on the basis of cell diameter and open porosity. di60_0 and di0_5 was selected due to almost equal and highest cell diameter of 583 and 650 μm and these both have different open porosity of 26 and 18 % respectively. So as shown in Figures 3-5, 3-7 and 3-8 F1 is di0_5 and F2 is di60_0.

For other two foams, selection was done on the basis of equal open porosity of 13 %, the foams were di40_5 and di60_15. The cell diameters were 300 and 150 μm respectively. So in this the F1 foam was taken as di40_5 and F2 foam was taken di60_15. These F1 and F2 were glued together by pure PU foam as adhesive. This made sure that the interface was foam that will allow the sound waves through to the other foam. The interface foam had cell diameter of ~100 μm.

CASE I: The interface between the foams are of smaller diameter than the foams itself, this makes Helmholtz resonance effect prominent in these cases. As the sound waves hit the surface of the foam the sound energy in the cells gets converted into kinetic energy, the interconnected cells that have variable cell sizes like in this case at the interface the sound waves creates a sound pressure, however this sound instead of propagating further due to partial pressure travels backward. This sets oscillations in the air flow further reducing the sound pressure. The open porosity allows the travel of air and again converts sound energy into frictional heat. When, the sound waves reach the cells that are of smaller diameter the air flow increases as the area becomes constricted and therefore the friction increases, hence giving high sound absorption.

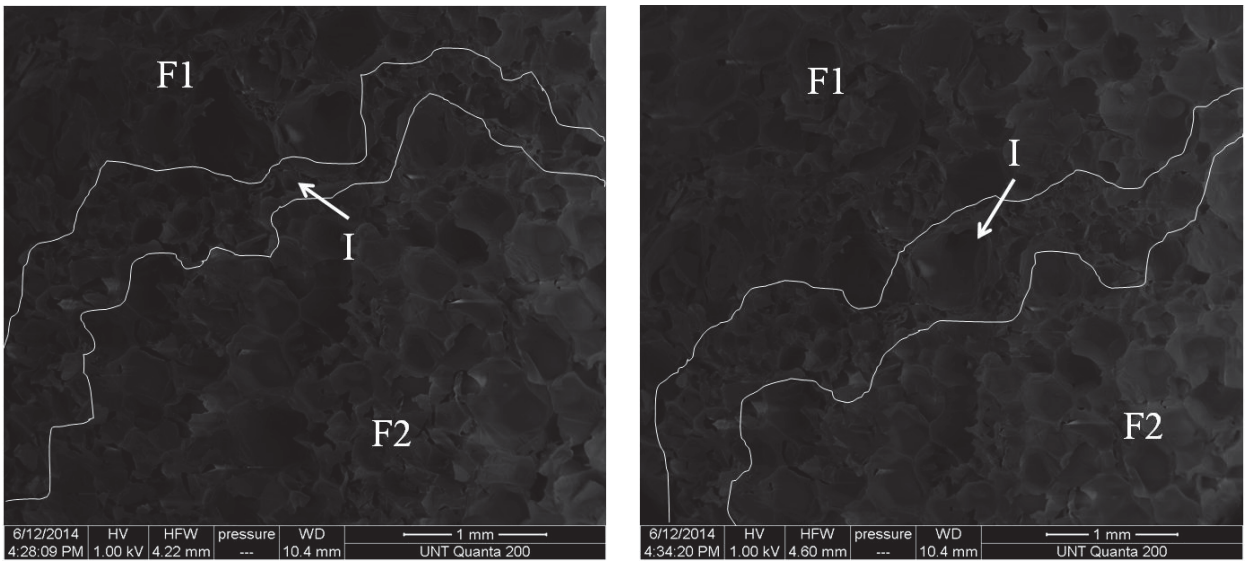


A B

*Figure 3-12* ESEM images showing the interface (I) which is within the marked white border on ESEM images of pure PU foam as glue between foams F1 and F2.

The foam with equal diameter cells Figure 4-13(A) shows lower improvement in sound absorption may be due to the less variation in cell diameters, on the contrary an increase in sound absorption is seen for the foams with different cell sizes and equal porosity Figure 4-13 (B). Hence, indicating that cell sizes play a major role in reducing sound absorption.

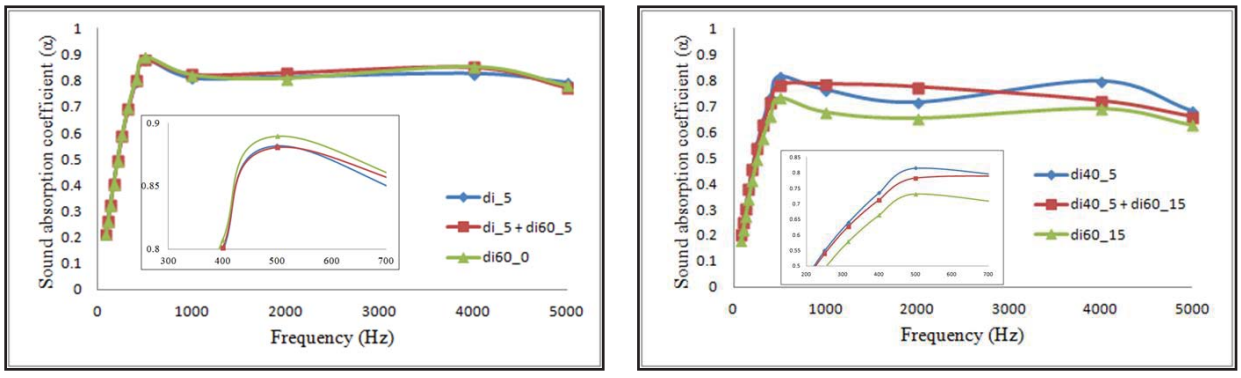


A B

*Figure 3-13* Sound absorption for CASE I.

CASE II:

The increase in area by 7 % (Figure 3-6) and therefore the increase in interfacial area have increased the sound absorption of the samples. Figure 3-14 (A) shows increase in sound absorption over the frequency range of 1000 – 2000 Hz. Whereas for Figure 4-14 (B) shows an increase in sound absorption in overall range.

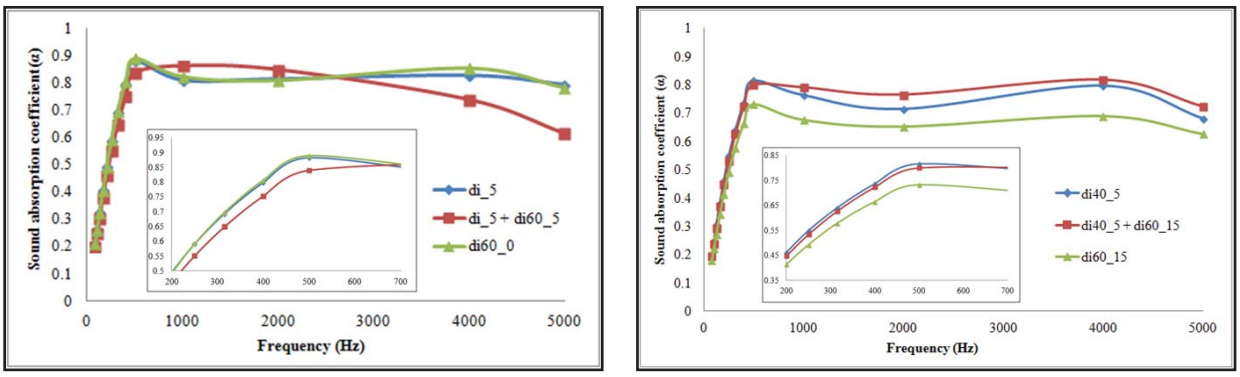


A B

*Figure 3-14* Sound absorption for CASE II.

CASE III:

The introduction of air space in the samples has shown to increase the sound absorption. This is due to the increase in kinetic energy generation from air flow. This, air flow within the centre space and the additional airflow from the space to the F2 foam samples in both cases has reduced the sound giving good sound absorption. When compared to cell sizes the one with higher difference in cell size that is from 300 to 150 µm cell diameters has given better sound absorption as compared to the one with 600 µm diameter cell sizes. This will be due to the Helmholtz resonance effect.

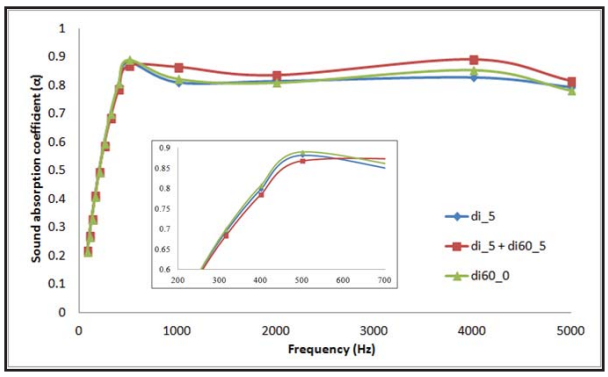


A

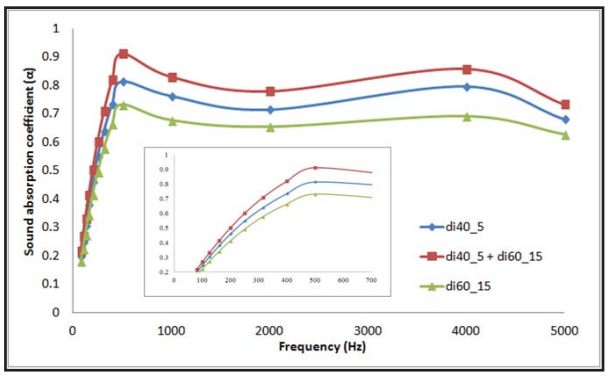


B

*Figure 3-15* Sound absorption for CASE III.

### 3.4.4 Viscoelasticity and Transmission Loss Correlation

Sound transmission loss for the foam composites show reverse trend as that of sound absorption. di40_5 showed a higher value of transmission loss and thus can be used as sound insulation material, followed by di40_0. Transmission loss results can be explained by understanding the definition; it is the ratio of sound wave transmitted at the rear surface to the incident sound wave. This lower sound intensity is due to the damping of sound waves when it travels through the material. The abrupt change in cross-section of the cells contributes to the transmission loss. The cell size distribution from Figure 3-9 suggests that the co-existence of large cells and small cells give higher transmission loss. For example di40_5, di40_0 have large cells with smaller cells with no smooth transition of cell sizes.

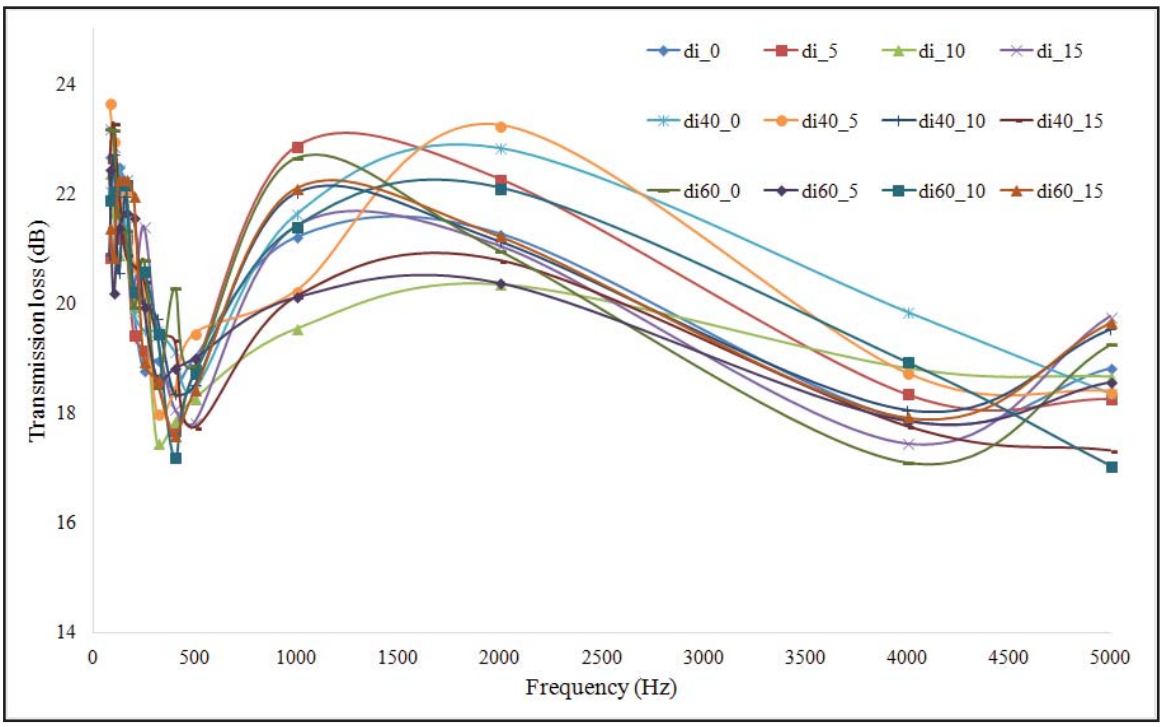


A

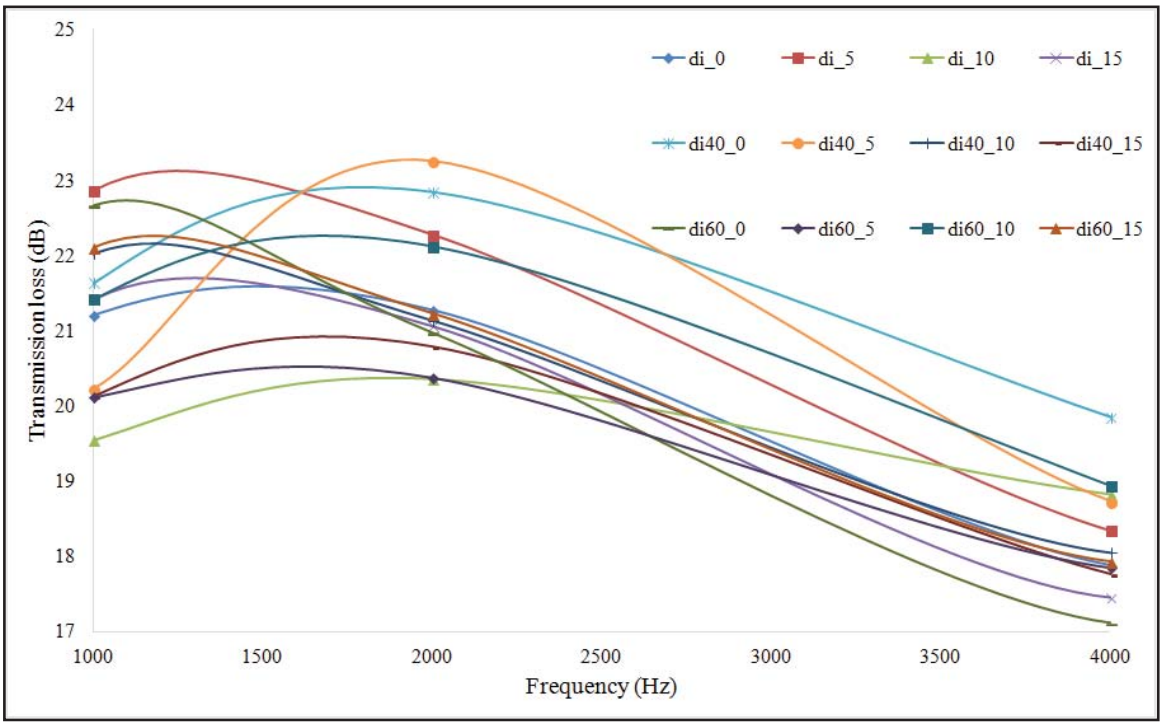


B

*Figure 3-16* Sound transmission loss as a function of frequency

Viscoelastic behaviour of the material can be correlated to the transmission loss of the materials. The storage modulus of the material is the measure of elastic property whereas tan δ is the indication of the loss in a material. Higher value of tan δ shows higher damping behaviour and therefore higher sound insulation. Figure 3-13 (B) shows tan δ values for the foam composites. Di40_0 showing higher tan δ value and hence shows higher transmission loss of 23.25. Hence decreasing trends in the tan δ values have shown to have decreasing transmission loss.

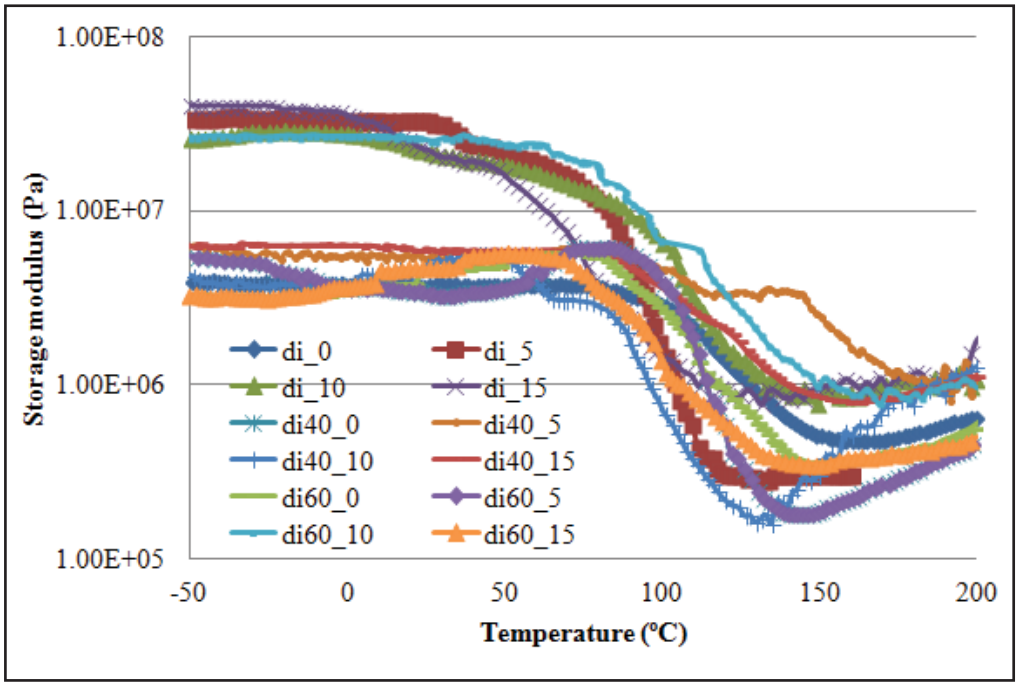


A

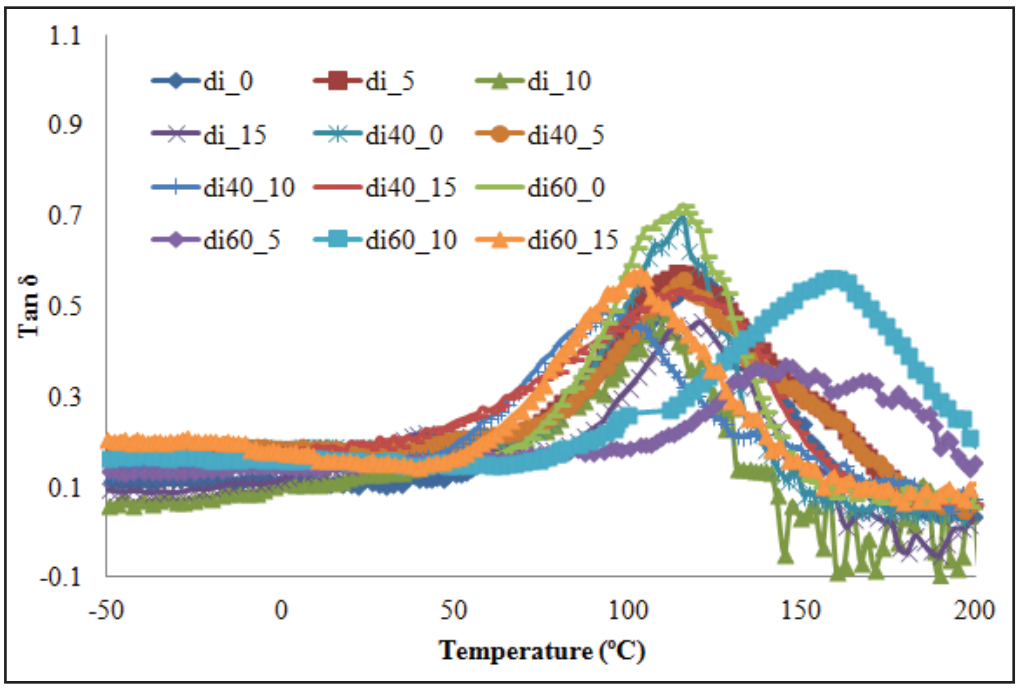


B

*Figure 3-17* Storage moduli (A), and tan δ (B)

For CASE I, II, and III a decrease in transmission loss has been observed for all the designs. Therefore a trade-off between both the properties can be seen. Indicating; that the designed materials are good as sound absorbers than sound insulators.

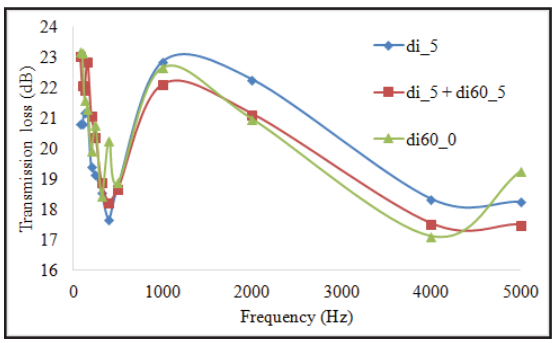


A

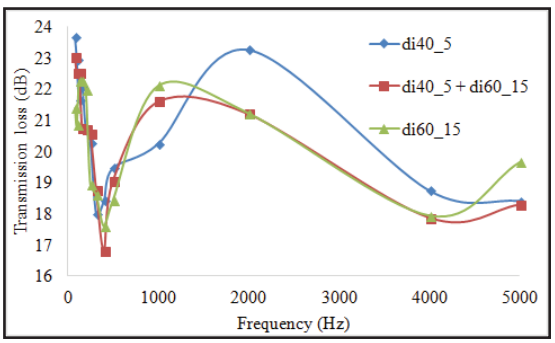


B

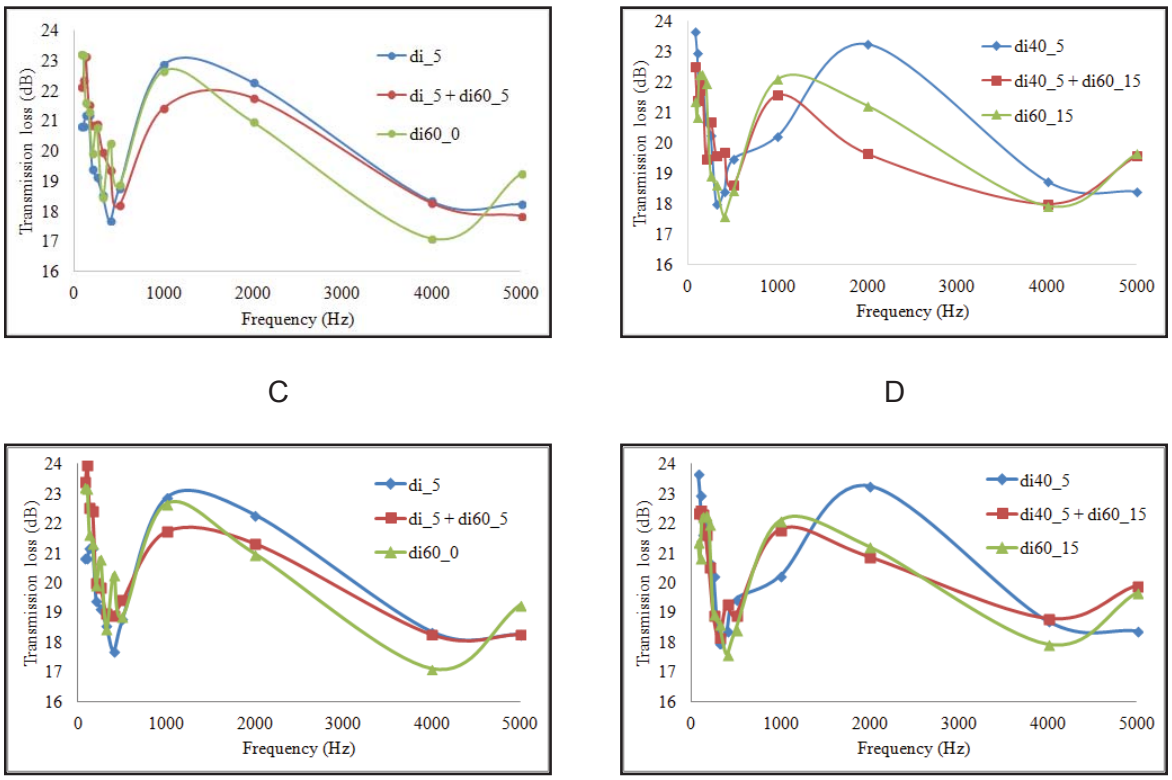


*Figure 3-18* Sound transmission loss as a function of frequency (A) and (B) CASE I, (C) and (D) CASE II, and (E) and (F) CASE III.

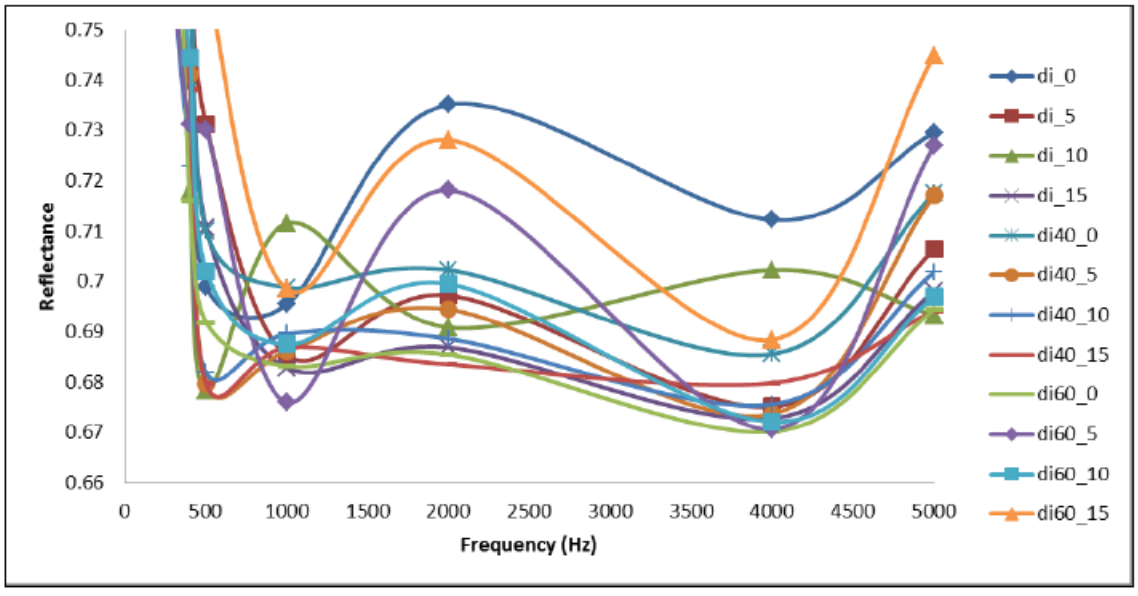

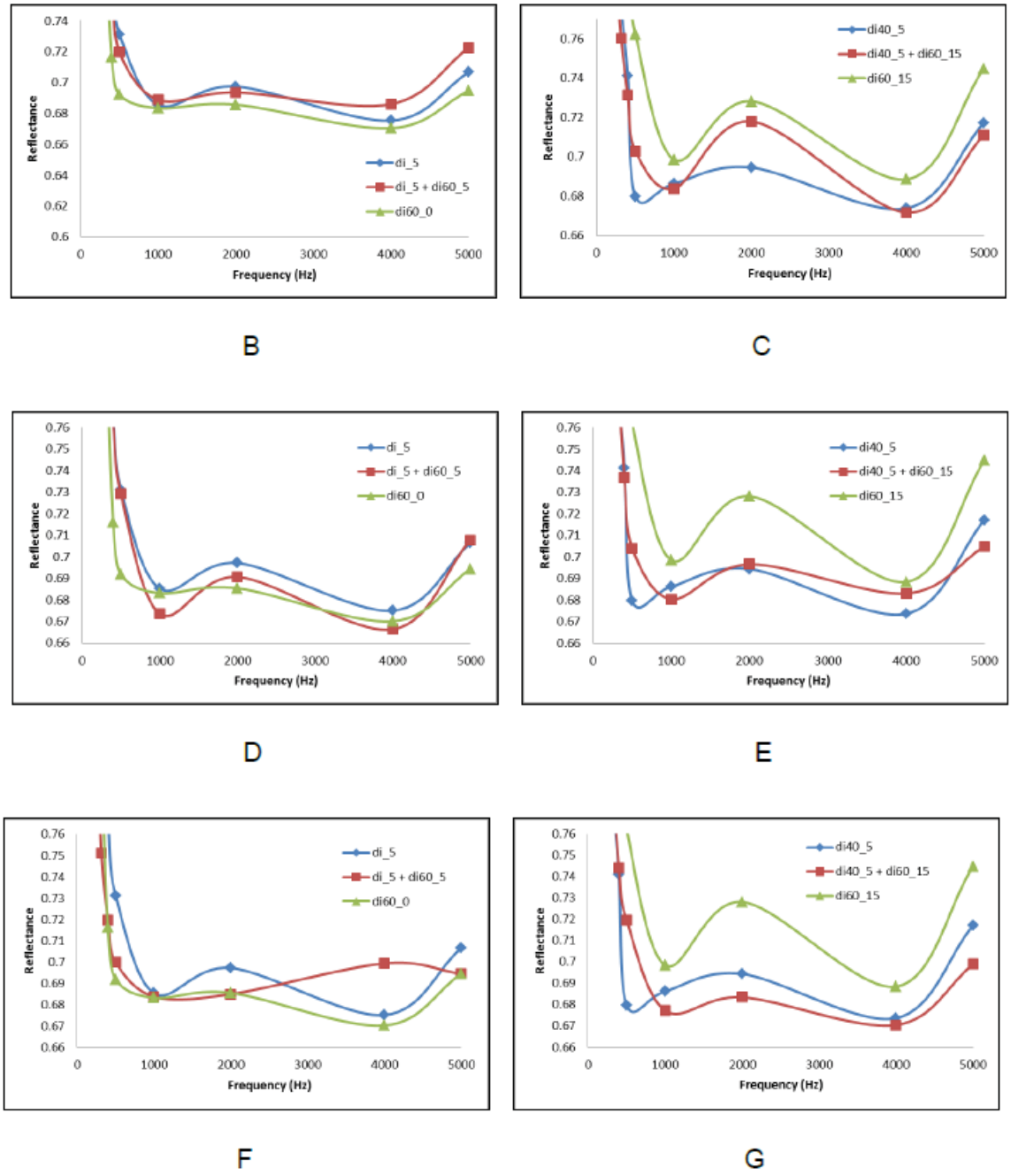


*Figure 3-19* Reflectance as a function of frequency (A) for foam composites, (B) and (C) CASE I, (D) and (E) CASE II, and (F) and (G) CASE III.

## 3.5 Conclusion:

In this work foam composites that were made by free foaming and constrained expansion technique with kenaf core loading of 5, 10 and 15 % were tested for

acoustical properties, such as sound absorption and transmission loss. Cell morphologies such as cell size and open porosity influenced the sound absorption of the foams. Larger cell size and higher open porosity has led to foams with higher sound absorption. Transmission loss was fairly co-related by the viscoelastic response of the material. Higher tan δ values showed higher transmission loss and therefore good sound insulation. Further two foams with cell diameter of 650 and 583 μm (these foams were chosen as they had highest cell size: initial test showed high sound absorption) that had open porosity of 26 and 18 % was chosen for fashioning three types of composite samples. And other two foams were chosen such that they had 13 % porosity and 300 and 150 μm cell diameter. The later samples showed improved sound absorption than former foam samples. A further improvement in design with increase in interface area by 7 % showed an increase in sound absorption in both the cases. A third design with air space showed further improved sound absorption over a wide range of frequencies. All the three designs showed lower transmission loss.

## 3.6 References


[1] Klempner, Daniel, and Kurt Charles Frisch, eds. Handbook of polymeric foams and foam technology. Munich etc.: Hanser, 1991.

[2] Tiwari T, Shukla A, and B and se A. Acoustic properties of cenosphere reinforced cement and asphalt concrete. Appl. Acoust 2004; 65(3): 263–275.

[3] Zannin PH and Ferreira JA. In situ acoustic performance of materials used in Bazilian building construction. Constr Build Mater 2007; 21(8): 1820–1824.

[4] Evans GW, Lercher P, Meis M, Ising H and Kofler WW. Community noise exposure and stress in children. J Aoust Soc Am 2001; 109(3): 1023–1027.

[5] Waye, Kerstin Persson, Angela Clow, Sue Edwards, Frank Hucklebridge, and Ragnar Rylander. "Effects of nighttime low frequency noise on the cortisol response to awakening and subjective sleep quality." Life sciences 72, no. 8 (2003): 863-875.

[6] H. Zhou, G.S Huang, X.R. Chen, et al., Advances in sound absorption polymer, Progress in Chemistry 16 (3) (2004)

[7] H. Zhou, B. Li, G.S. Huang, Sound absorption characteristics of polymer micro-particles, PolymericMaterials Science and Engineering 20 (3) (2004).

[8] Wassilieff C. Sound absorption of wood-based materials. Appl Acoust 1996; 48: 339–356.

[9] Kru¨ ger EL and Zannin PH. Acoustic and thermal field investigation of low-cost dwellings, a case study in Brazil. Appl Acoust 2007; 68: 1213–1223.

[10] Ersoy S and Ku¨ cu¨ k H. Investigation of industrial tealeaf- fibre waste material for its sound absorption properties. Appl Acoust 2009; 70: 215–220.

[11] Tsai, W. T., C. Y. Chang, and S. L. Lee. "A low cost adsorbent from agricultural waste corn cob by zinc chloride activation." Bioresource technology 64, no. 3 (1998): 211-217.

[12] Yang, Han-Seung, Dae-Jun Kim, and Hyun-Joong Kim. "Rice straw–wood particle composite for sound absorbing wooden construction materials." Bioresource Technology 86, no. 2 (2003): 117-121.

[13] D.H. Wang and X.S. Sun, Ind Crops Prod., 15, 43 (2002).

[14] Xue JY, Widyorini R and Suichi K. Properties of kenaf core binderless particleboard reinforced with kenaf bast fiber-woven sheets. J Wwood Sci 2005; 51(4): 415–420.

[15] C.K. Honga, I. Hwangb, N. Kimb, D.H. Parkc, B.S. Hwangd, and C. Nahb, J. Ind. Eng. Chem., 14(1), 71 (2008).

[16] M. Bengtsson, P. Gatenholm, and K. Oksman, Compos. Sci. Technol., 65, 1468 (2005).

[17] X.Y. Chen, Q.P. Guo, and X.L. Mi, J. Appl. Polym. Sci., 69, 1891 (1998).

[18] Y. Li, Y.W. Mai, and L. Ye, Compos. Sci. Technol., 60, 2037 (2000).

[19] B.M. Prasad and M.M. Sain, Mater. Res. Innovations, 7, 231 (2003).

[20] Jaouen, Luc, Amélie Renault, and Mickael Deverge. "Elastic and damping characterizations of acoustical porous materials: Available experimental methods and applications to a melamine foam." Applied acoustics 69, no. 12 (2008): 1129-1140.

[21] Lee, C-M., and Y. S. Wang. "A prediction method of the acoustical properties of multilayered noise control materials in standing wave-duct systems." Journal of sound and vibration 298, no. 1 (2006): 350-365.

[22] Sagartzazu, X., L. Hervella-Nieto, and J. M. Pagalday. "Review in sound absorbing materials." Archives of Computational Methods in Engineering 15, no. 3 (2008): 311-342.

[23] Han, Fusheng, Gary Seiffert, Yuyuan Zhao, and Barry Gibbs. "Acoustic absorption behaviour of an open-celled aluminium foam." Journal of Physics D: Applied Physics 36, no. 3 (2003): 294.

[24] ASTM E1050-12 Standard Test Method for Impedance and Absorption of Acoustical Materials Using a Tube, Two Microphones and a Digital Frequency Analysis System

[25] ASTM E2611-09 Standard Test Method for Measurement of Normal Incidence Sound Transmission of Acoustical Materials Based on the Transfer Matrix Method

[26] Zhang, Chunhua, Junqing Li, Zhen Hu, Fenglei Zhu, and Yudong Huang. "Correlation between the acoustic and porous cell morphology of polyurethane foam: Effect of interconnected porosity." Materials & Design 41 (2012): 319-325.

# CHAPTER 4

# MODELING DEFORMATION IN RIGID POLYURETHANE FOAM

## 4.1 Introduction

Low density open and closed cells polymeric foam materials such as low density polyethylene (LDPE), polystyrene (PS), expanded polystyrene (EPS), expanded polypropylene (EPP) are used in various packaging, personal protective equipments (PPE), sports, medical, structural applications etc. Closed bead EPS foams have variable densities and hence difficult to model the foam geometry [1]. Polyurethane (PU) foams can be fabricated for wide range of mechanical properties like low density, low stiffness etc. [2]. PU can be categorized into open cell foam and closed cell foam. The foam which allows fluid to pass through is open cell [3] and is also termed as dry Kelvin foam. An attempt was made by Kraynik et al. to model the variable size closed-cell dry foam with 3D Voronoi model and same foam when annealed, these foams were dodecahedron geometry that showed anisotropy effects [4]. An open foam cell model was created with 3D Voronoi by Roberts and Garboczi [5].

In an essay to study the foam microstructure and model it, initially model was designed with pentagon dodecahedrons which were a regular lattice [6]. Later tetrakaidecahedron model was developed which satisfied most of the rules [7] which comprised of 8 hexagonal non-planar faces with 6 quadrilateral surfaces with edges angle of 109.5º. Further modified tetrakaidecahedron model with 2 square faces, 8 pentagonal faces and 4 hexagonal faces was termed as β-tetrakaidecahedron that was seldom used [8]. Today widely used model for foam is called Kelvin foam whose design

was originally proposed by Lord Kelvin and further modified by Kraynik and Warren [9]. This model had inner edge angles of 120º or 90º.

Development of foam cells were studied using wet foams, a thin cell membrane is formed when the wet bubbles meet to form the face of the wet foam. These wet foams retained liquid at the edges and vertices of the foam [10]. When this liquid face membranes collapse the open cell foam is formed [11]. Syntactic foams were studied to generate model with controlled bubble distribution as a method to develop foams [12]. Some PU foams are syntactic foams and S. Youssef et al. studied this type of foam by microCT and later modeling for the obtained volume, but the model overestimated the modulus and underestimated the plateau border indicating that improvements to the technique had to be made [13]. Gas-filled closed cells modeling was studied by Mills and found that the gas-filled cells caused post yield hardening [14].

Study of failure modes in foam have been investigated by experimental methods; however micromechanical details of foam responses to the loading are yet to be fully understood. High resolution microCT techniques were used to study the deformation of the open cells where the buckling of foam struts was seen to be the major foam deformation mechanism [15].

The efforts in this article are made to improve the foam design in following ways. First, design includes combinations of bulk, open, and closed cell foams. These foams encompass the porosity, and void volume generally seen in all possible foam structures. Second, compare the deformation for bulk, open, and closed cell foams as improvisations have been done in models taking into account the inner edges of the cells. The thickness of the inner edges has increased as seen from scanning electron

microscopy. The edge thickness have increased for open cell foams considering the extra material flowing to the edges which in case of closed cell would have been seen as a membrane, the membrane thickness is uniform in core of the faces. Third, it predicts deformation initiation and stress localization points in the foam during compression. Fourth, cell gas contribution to the compressive stress has been investigated for the foams that have closed cells. This article does not take into consideration the irregularity in foam cells and the anisotropic effects.

## 4.2 FEA Modeling

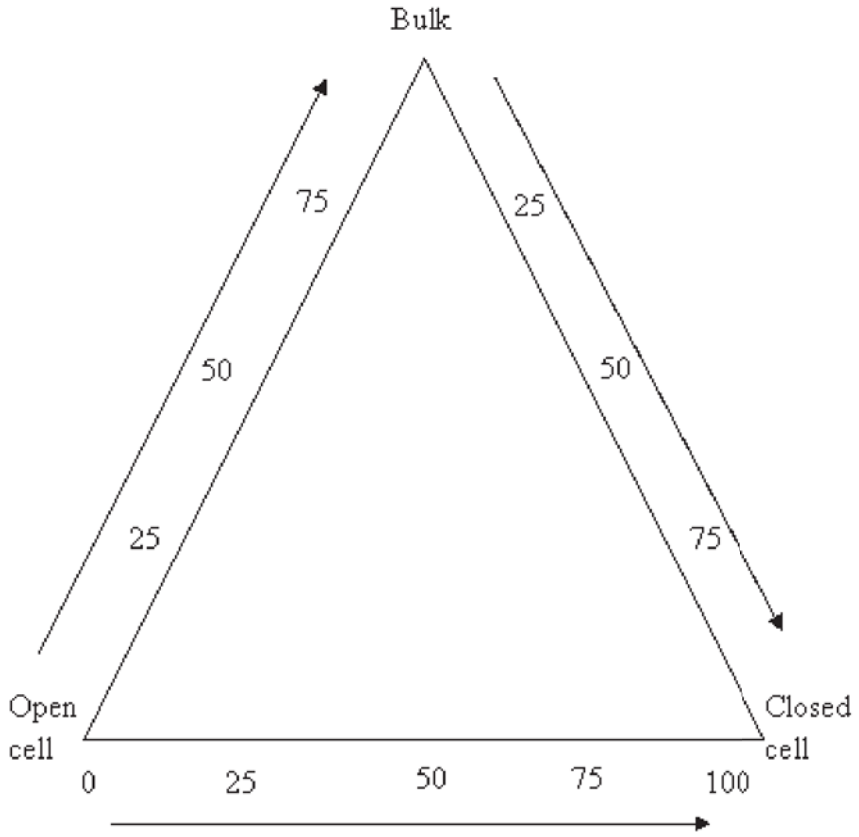


*Figure 4-1* Schematic of the foam models being studied.

Figure 4-1 summarizes the foam models that have been studied in this paper. The three vertices of the triangle show the extreme of open, closed, and bulk foam into

consideration. The horizontal triangle side takes into account the porosity of the foam. From left to right the porosity decreases, which are along the axis to the extreme right the foam is 100 % closed cell foam. The intervals are taken to be at 25 % increment. The top vertex for the triangle is the bulk material; however the simulation for 100 % bulk material is not performed as it does not affect the analysis. The material on the open cell and bulk material side of the triangle shows increase in bulk foam cells that are randomly distributed across the open cell foam. Similarly, bulk foam cells are randomly distributed across the closed cell foam. Therefore, across the triangle it can be seen that the complete combinations of existing foam are designed for this study. Open cell to closed cells takes into account the porosity of the foams, open cell to bulk, and closed cell to bulk shows the void volume of the foams with change in type of foam cell. From here on following nomenclature will be used for the foam types based on bulk, open, and closed cell structure throughout the paper. The foams with all the cells are closed is 100 % closed (C100), similarly the foam with the cells that are open is 100 % open (O100), 25% closed cells (C25), 50% closed cells (C50), 75% closed cell is (C75). The combination of open and bulk will be B25O75, B50O50, and B75O25, similarly combination of closed and bulk will be B25C75, B50C50, and B75C25. Where; B, O, and C represent bulk, open, and closed cell with 25, 50, and 75 being the percentage of the respective material.

Figure 4-2 (A) shows the SEM image of the foam cross-section showing the intersection of three adjoining foam cells that make the edge thicker than the cell faces. The thicker region in the figure that is depicted by A is termed as solid plateau border, B is the plateau border shell and C is the foam cell face that remains uniform in thickness

for these foams showing plateau border geometry [16]. Figure 4-2 (B) shows the designed model of closed cell foam that shows a similar intersection of three adjoining cells with the triangular thicker section with uniform cell wall thickness. Further the inner radius for edge spread factor for the closed cell foam is taken to be 30 μm, whereas for open cell foam it was taken as 50 μm.

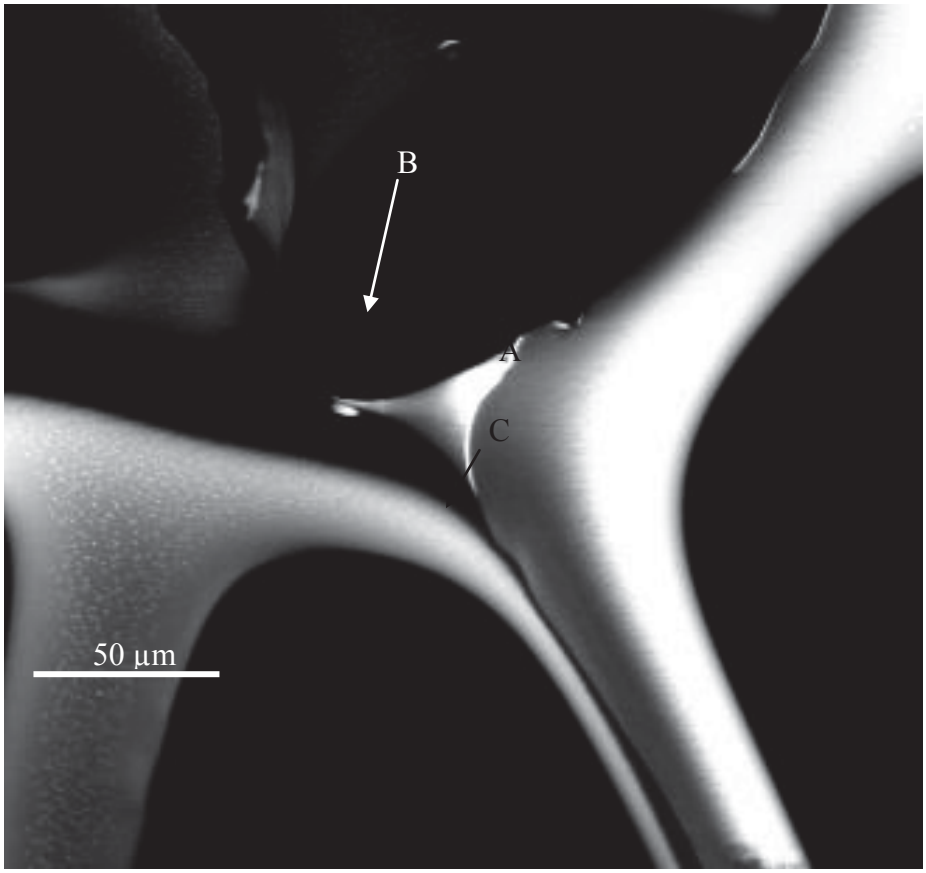


A

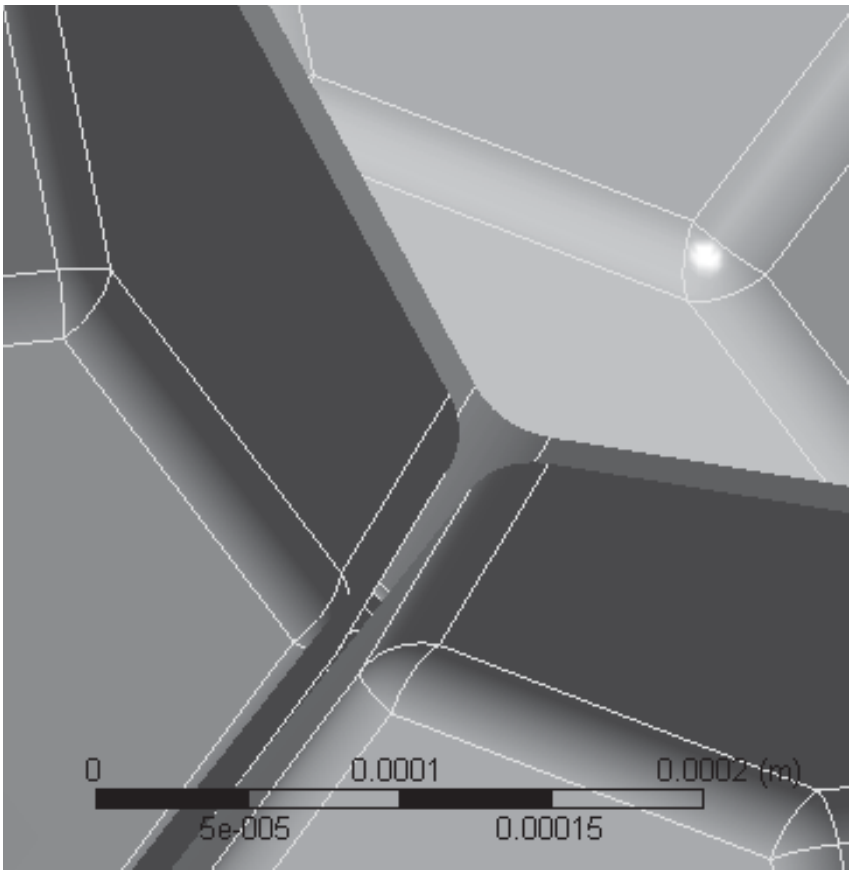


B

*Figure 4-2* Scanning electron microscope image of (A) cross-section of an edge in rigid polyurethane foam, in the figure the different parts of the merged cells are indicated with the arrows A: solid plateau border, B; shell on plateau border surfaces, and C: foam cell face (in this image the adjoining three foam cells have merged to give a triangular foam edge), and (B) shows modeled closed cell in Autodesk Inventor.

## 4.3 Modeling

### 4.3.1 Modeling of Single Closed Cell

Autodesk Inventor was used to create foam geometries. A modified version of Kelvin model of dry foam was designed with cell diameter (D) of 600 μm between two square faces, the edge length being 200 μm. The geometry of single foam is said to

be tetrakaidecahedron, this includes 6 square faces and 8 hexagonal faces; a total of 14. A foam structure of 22 single foams was glued together with intersection of glued faces by thickness of the face (10 μm) in order to keep the uniform thickness. The edges in foam are thicker and hence a fillet tool was used to give an inner radius of 30 μm. This geometry was then exported to ANSYS workbench 14.5 to boolean the 22 single foams to make it as one single solid body.

### 4.3.2 Modeling of Open Cell Foam

The single closed cell explained in pervious section was used to make open cell foam. The circular hole was fabricated on each face with diameter of 175 μm for square face and 236 μm for hexagonal face. The total volume that was removed from the holes was accounted in the fillet of the inner edges of the cell. Thus, adding a radius of 50 μm as compared to the 30 μm radius for the closed cell.

### 4.3.3 Modeling of Porosity and Void Volume in Foams

A range from 0, 25, 50, 75, and 100 % porosity, and void volumes were designed for foams. A combination of closed cells and open cells were used to make the 5 models of foams.

### 4.3.4 Material Properties from Experiments

Rigid polyurethane foam was tested for compression properties [17]. A sample with 25 mm in length and 27 mm in diameter was used with strain rate of 0.5 mm/min. The compressive modulus of 21 MPa and compressive strength of 1 MPa was recorded for pure PU foam. Density measured for the same was 107.54 kg $m^{-3}$.

### 4.3.5 Periodic Boundary Conditions

Periodic boundary condition was applied for the foam model. The experiment

was conducted in compressive mode with the base of the sample fixed and in displacement control mode the top surface of the sample was moved. The finite element somewhere in the middle of the sample experiences the compression forces. Therefore periodic condition applied was a origin of the model was fixed, the faces XY, XZ, YZ was applied with frictionless motion, and the top face was applied with the displacement.

## 4.4 Results and Discussions

### 4.4.1 Compression Result from Experiment

The compressive modulus has been seen to increase with increase in constrained expansion when compared to free foaming. Figure 4-3 shows compressive modulus (A) and compressive strength (B). Free foaming shows compressive modulus of 21 ±2.31 MPa, which increased to 22.59±2.48 and 24±2.61 MPa for 40 and 60 % constrained expansion. Similarly compression strength increased to 1.07±0.12 and 1.2±0.17 MPa for 40 and 60 % constrained expansion from 0.97±0.09 MPa for free expansion. The open porosity has increased as the constrained expansion increased. For free foaming the open porosity was 15 %, it increased to 19 and 26 % for 40 and 60 % constrained expansion. The increase in open porosity can be attributed to the increase pressure inside the mold during foaming. As a result the neighbouring cells fuse together to give a larger cells with open walls. These open walls provide the interconnectivity to the foam, however in the process of fusing the cells the excess material that would have been formed into the cell walls, now move towards the edges providing extra strength. The extra material makes the joining edges (struts) wider as can be seen from the Figure 4-2 (A). The more open porosity in foam gives rise to

wider edges and therefore more resistant to deformation and hence more compressive strength and modulus.

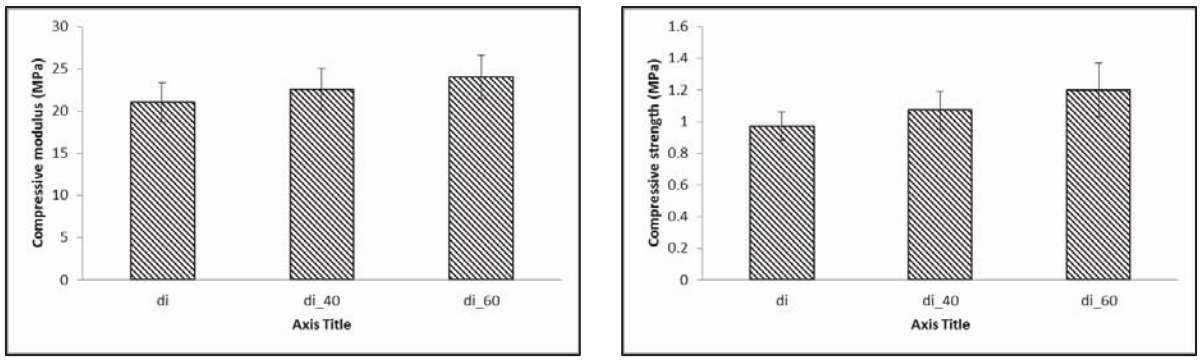


A B

*Figure 4-3* Compression modulus (A) and compressive strength (B) for free foaming, 40 and 60 % constrained expansion method.

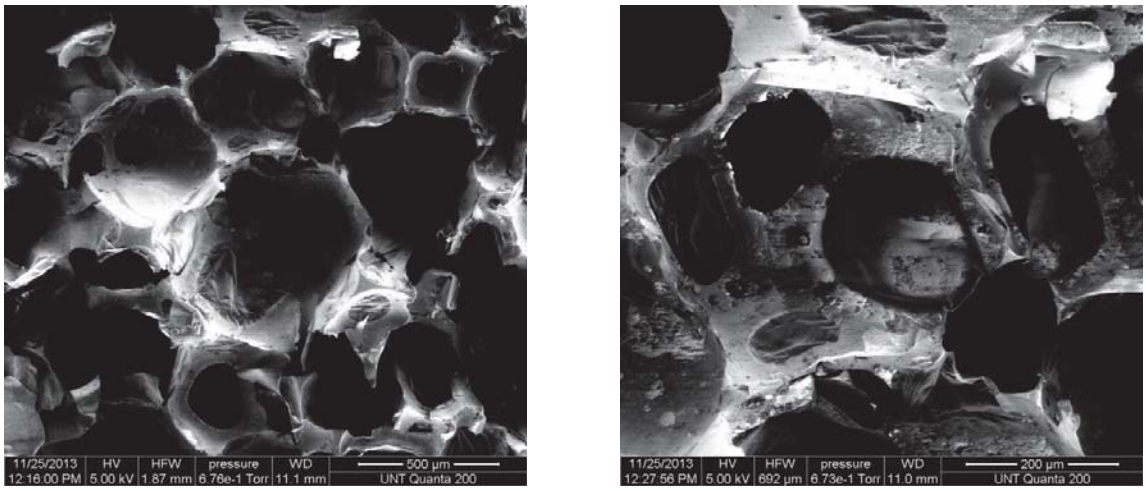


A B

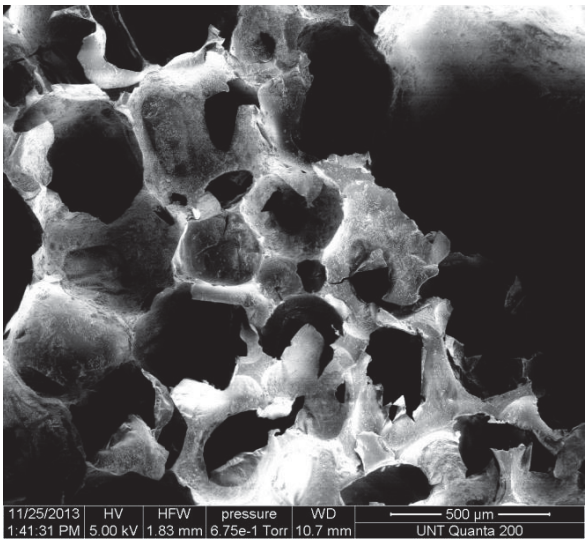


C

*Figure 4-4* ESEM images showing partial porosity of the foam samples, membranes that make up the closed pores, completely open cells, and partially open cells.

### 4.4.2 Deformation of Closed and Open Cells Foam Models

The initial stress responses for the tetrakaidecahedron models with strain were compared for five types of foams. Figure 4-5 compares the open cell and closed cell foams. The compressive load was applied along the [001] direction, this direction is the foam rise direction along z-axis. Figure 4-5 A1 shows C100 at 1.42% strain, the initiation of the plastic deformation can be seen generating along the top corners and the centre of the hexagonal faces which are along the compressive direction. At 2.5% strain (Figure 3 A2) the hexagonal faces start to buckle, at this strain the square faces start to deform. In Figure 3 A3 the cell has deformed by forming plastic hinge along the edges of square and hexagon, compaction of lower cells can be seen. For C25 the initial deformation can be observed along the hexagonal faces around the square face, this is because the open cells that have inner edge radius of 50 µm give resistance to deformation and transfers the stress along the sides of the open cell. At strain of 2.04% the above observation is true as seen in Figure 3 B1, but the open cells that are at an

angle from the compressive direction show the plastic deformation and the face tends to buckle inward the cell. The cells that are on the edge of the foam tend to deform the same way. But the cell along compressive direction doesn't deform as seen in Figure 3 B2. At 3% strain the hexagonal faces buckles as well as the open cell along the compressive direction buckles. C50 on the other hand deforms for as low as 1% strain (Figure 3 C1) this is seen due to more number of open cells that are at an angle of applied load. The open face that are along compressive direction start showing deformation at strain of 2% (Figure 3 C2) where the tendency of the faces that are on top side to buckle upward rather than inward, and the bottom side is seen to have hexagonal faces deformed inward. This is because as strain increases the plastic hinges are created along square and hexagon face, the top side plastic hinge is the first to form and hence deforms more than the bottom one thereby creating a funnel like shape with the vertical faces. This forces the hexagonal faces to buckle upward. The bottom faces are thereby forced to buckle inward as seen in Figure 3C3 for strain of 6.13%. C75 with 75% open cells shows the initial deformation at strain at 3.2% (Figure 3 D1). The deformation can be seen concentrated on the open faces rather than the uniform thickness closed faces. This is due to open cells acting as load bearing members of the foam when the open cells are increased to 75% of total foam cells (Figure 3 D2). The similar deformation as C50 is seen in C75 at strain of 7%, of that of the funnel shape forcing the upper faces to bulge outside and lower faces to buckle inwards (Figure 3 D3). O100 with all open faces shows the initial deformation along the hexagonal open cell faces at initial strain of 3.5% (Figure 3 E1). Even at strains of 4.7% the square face doesn't show any deformation (Figure 3 E2). At 8% strain (Figure 3 E3)

the prime deformation mechanism remains the buckling of the faces rather than the development of plastic hinges along the edges of square and hexagon.

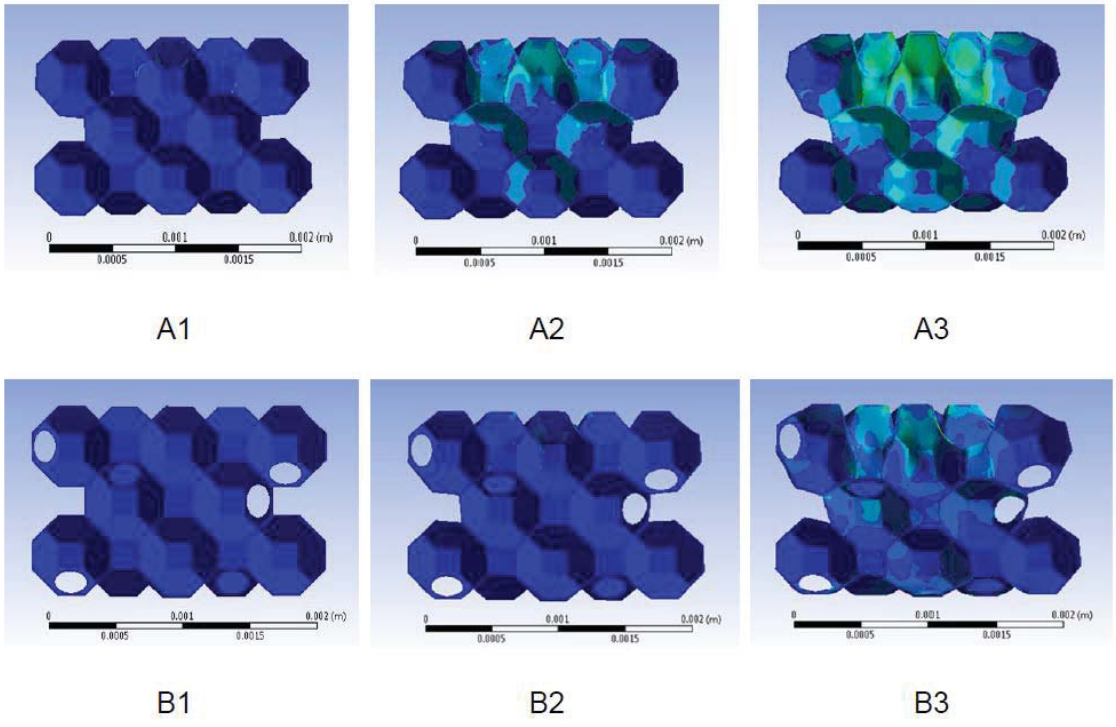

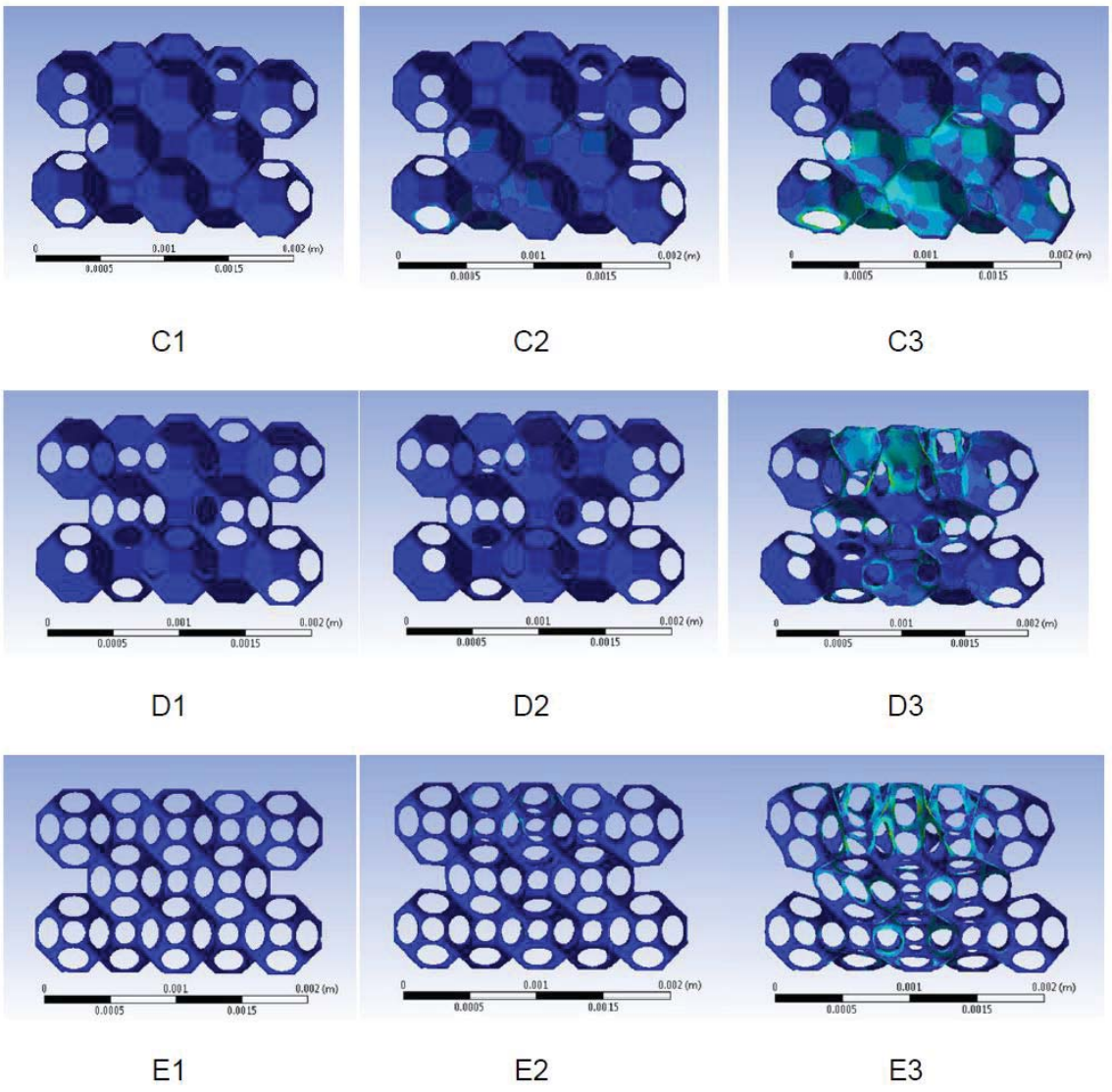


*Figure 4-5* Deformation of foams to visualize the initial plastic deformation at different strains for (A) C100, (B) C25, (C) C50, (D) C75, and (E) O100.

## 4.5 Conclusion

The models designed for foams represented low density foam with possible combinations of foam geometry for open and closed cell combinations. They were compared with the compression tested samples from experiments. The experiments showed the influence of constrained expansion on compression modulus and strength. Open porosity influenced with the increased constrained expansion. The

hypothesis of increased open porosity which makes the edges wider have influenced the resistance for deformation can be seen from the models. The 100 % open cells show low deformation due to the wider edges of the foams that bear the compressive loads during deformation. Whereas the 100 % closed foams cell model show higher deformation.

## 4.6 References


[1] Viot P, Plougonven E, Bernard D (2008) Compos Part A 39:1266

[2] Jmal H., Dupuis R., Aubry E., Journal of Cellular Plastics, 47 (2011) 447- 465.

[3] Romero P.A., Zheng S.F., Cuitino A.M., Journal of the Mechanics and Physics of Solids, 56 (2008) 1916-1943.

[4] Kraynik A.D., Reinelt D.A. & van Swol F. (2003) Structure of monodisperse foam, Phys. Rev. E 67, 031403.

[5] Roberts A.P. & Garboczi E.J. (2002) Elastic properties of model random 3-D open-cell solids, J. Mech. Phys. Solid. 50, 33–55.

[6] Kraynik A.D. & Warren W.E. (1994) The elastic behaviour of lowdensity cellular plastics, Chapter 7 in Low Density Cellular Plastics, Eds. Hilyard N.C. & Cunningham A., Chapman and Hall, London.

[7] Ko W.L. (1965) Deformation of foamed elastomers, J. Cell. Plast. 1, 45–50.

[8] Williams R.E. (1968) Space-filling polyhedron: its relation to aggregates of soap bubbles, plant cells, and metal crystallites, Science 161, 276–277.

[9] Kraynik A.D. & Warren W.E. (1994) The elastic behaviour of lowdensity cellular plastics, Chapter 7 in Low Density Cellular Plastics, Eds. Hilyard N.C. & Cunningham A., Chapman and Hall, London.

[10] Kraynik A.M., Neilsen M.K. et al. (1999) Foam micromechanics, in Foams and Emulsions, Eds. Sadoc J.F. & Rivier N., Nato ASI Series E, Vol. 354, Kluwer, Dordrecht.

[11] Weaire D., Phelan R. & Verbist G. (1999) The structure and geometry of foams, in Foams and Emulsions, Eds. Sadoc J.F. & Rivier N., Nato ASI Series E, Vol. 354, Kluwer, Dordrecht

[12] Lorenzo Bardella, Alessandro Sfreddo, Carlo Ventura, Maurizio Porfiri, Nikhil Gupta, A critical evaluation of micromechanical models for syntactic foams, Mechanics of Materials, Volume 50, July 2012, Pages 53-69

[13] S. Youssef et al. Acta Materialia 53 (2005) 719–730

[14] Mills, Nigel J. "Modeling the dynamic crushing of closed-cell polyethylene and polystyrene foams." Journal of Cellular Plastics 47, no. 2 (2011): 173-197.

[15] N. P. Daphalapurkar, J. C. Hanan, N. B. Phelps, H. Bale, and H. Lu, Tomography and Simulation of Microstructure Evolution of a Closed-Cell Polymer Foam in Compression, Mechanics of Advanced Materials and Structures, 15:594–611, 2008

[16] Miller RE (2000) A continuum plasticity model for the constitutive and indentation behaviour of foamed metals. Int J Mech Sci 42:729–754.

[17] Rigid polyurethane and kenaf core composite foams, M Nar, C Webber, N Anne D'Souza - Polymer Engineering & Science, 2014

[18] Tu, Z.H; Shim, V.P.W; Lim, C.T, Plastic deformation modes in rigid polyurethane foam under static loading, 2001, Volume 38, Issue 50, pp. 9267 – 9279.

[19] Menges G, Knipschild F (1975) Estimation of mechanical properties for rigid polyurethane foams. Polym Eng Sci 15:623–627.

# CHAPTER 5

# ENERGY CONSUMPTION OF ZERO NET ENERGY BUILDING

## 5.1 Introduction

In USA residential energy consumption is 25% when compared internationally [1]. Building sector alone consumed 50.1 % of total energy which accounted for 50.6 Quadrillion Btu (QBtu) in 2008 as compared to industry and transportation sector contributing 22.3 and 27.6 % respectively [2]. The projected energy consumption for 2030 is 60 QBtu for building sector which shows an increase of 19.76 % in 22 years. Commercial buildings in USA; accounts for 18 % of annual energy consumption [3] as reported by National Research Energy Laboratory (NREL) in 2010. This energy consumes up to 30% just for lighting. The US Department of Energy (DOE) has a goal to develop market viable ZEBs by 2025.

Research has been carried out inorder to study properties of rigid polyurethane by many means, such as change in % of water as blowing agent. This has affected the density and thereby affecting mechanical properties and thermal conductivity [4]. Attempts have been made to reinforce PU foams with nanoparticles, that will aid improve mechanical and thermal properties, by increasing nucleation sites and reducing cell size [5]. Instead Cao et.al observed a reverse trend of reduction in compressive properties by addition of montmorillonite (MMT). Further reaction temperature affected the clay dispersion [6]. It is also shown that the increasing amount of water and catalyst have increased mechanical properties [7]. Reinforcing PU foams with clays, fibers etc are being considered too [8,9].

Foaming with different blowing agents affects the properties of foam. Water has been widely used as blowing agent for rigid polyurethane foams. The reaction of polyol and isocyanate gives polyurethane linkages, the reaction of isocyanate and water gives carbamic acid which is unstable and that quickly decomposes into amine and carbon dioxide [10,11]. Physical, chemical, or a combination of both can be used for blowing agents. Chemical blowing agents such as monofluorotrichloromethane and difluorodichloromethane are widely used but pose environmental hazards for ozone depletion. A need to develop and use more environmental friendly blowing agents is looked into [12]. Plant based synthesis routes have been investigated such as soy based [13], rape seed oil [14], vegetable oils [15] polyols for preparing polyurethane foams that can be the substitutes for petroleum based precursors. Natural fibers such as jute, hemp, sisal etc have been used to reinforce polyurethane foams [16]. Also a possibility of natural fibers as reinforcing agents in microfoams made from polypropylene (PP), and rigid polyvinyl chloride (PVC) [17,18].

Insulating materials in a building envelope is not independent energy conservation technique but forms one of the important one from the complex components of the building envelopes. Less information is known when it comes to residential housing for energy consumption mainly because of no documentation from the occupant, who sometimes can consume 100 % of supplied energy. From the total energy consumption, around 50 – 70 % of the energy is consumed in maintaining the indoor temperature while heating and cooling the space [19]. Insulation even today is one of the most effective ways to reduce energy consumption of any building, for reasons such as city restrictions on building orientation [20]. Incorporation of design

methods like building envelope design [21] to utilize energy efficient materials can reduce the energy consumption of a building to a large extent; for example, windows with double low E in this case reduced the energy consumption by 40 %.. Thickness of insulation [22], window area and window type [23] are other design strategies that architects take into consideration in order to reduce the energy consumption.

The objective of this study was to compare polyurethane foams with different cell sizes with kenaf core loading of 5, 10, and 15% to the sandwich panels made of kenaf fibers, bacterial retted kenaf fibers, fiberglass, and sugarcane fibers. Time-temperature characteristics suggests that the higher constrain has shown more rise in temperature and therefore more hard domains of polyurea. This was confirmed from Raman spectroscopy with urea-to-urethane ratio. These hard domains gave better resistance to $CO_2$ diffusion and thereby better aged thermal conductivity. Commercially available foams have been tested in combination with panels made from kenaf fibers, bacterial retted kenaf fibers, fiberglass, and sugarcane fibers to compare with the conventional structural insulated panel (SIP) made from polystyrene bead foam and steel panel. Thermal conductivities were measured for the foams as well as for the sandwich foam composites. These thermal conductivity values were then used in the Energyplus software to get energy consumption based on the insulation in the walls.

## 5.2 Experimental Method

### 5.2.1 Materials and Sample Preparation

#### 5.2.1.1 Polyurethane Foams

4,4’-Methylenebis (phenyl isocyanate) and polyester-block-polyether α, ω-diol were procured from Fiber Glast Developments. The average molecular weight for

polyester-block-polyether α, ω-diol was 468. Kenaf-core that was obtained from USDA was powdered using cryo-milling for 30 min under liquid $NO_2$ bath. Kenaf-core had density of 0.28 g/cc and particle size of 150 ± 20 μm.

5.2.1.2 Composite Panels

The unsaturated polyester AROPOL Q 6585 resin was obtained from Ashland Chemicals, Ashland, KY. The hardener 1,1-Di(tert-butylperoxy)cyclohexane, 50% solution in mineral oil was obtained from Acros Orgaincs, Pittsburgh, PA. The proportion of polyester and hardener is 1:0.015. Mechanically retted kenaf fibers (called mechanical kenaf below) were supplied by Kengro Incorporation, Charleston, MS. Bacterially retted kenaf fibers (called bacterial kenaf below) were supplied by David Visi, UNT. Sugarcane fibers were supplied by Chuck Webber, USDA, LA. All fibers were dried at 50 $^{o}$C for 24 hours before using.

The process of fabrication is detailed for polyurethane foams [21], kenaf fibers panels, and sugarcane fiber panels [22].

5.2.1.3 Commercial Foams

Divinycell H35 foam was supplied by Diab Incorporated and HyPUR-cel GT® T0503 foam were supplied by Rubberlite™ Incorporated. From here on we have termed these foams as Diab™ and Rubberlite™ respectively for simplicity.

5.2.2 Average Cell Diameter

FEI Quanta Environmental Scanning Electron Microscope (ESEM; FEI Company, Oregon, USA) was used. The foam was cryo-fractured using liquid nitrogen; to ensure no surface yielding; this cryo-fracturing kept the micro-structure intact for analysis. The

average cell diameter was determined using ImageJ, and counting on an average 50 cells.

### 5.2.3 Foam Density

Macro-foam densities were measured using Archimedes principle of water-displacement. Densities were calculated using volume of water displaced by sample divided by weight of sample. Measurements were done in triplicate using AEA/AAA Density kit from Adam Engineering.

### 5.2.4 Thermal Conductivity

Thermal conductivity is defined as the rate of heat transfer through unit thickness, across unit area for unit difference in temperature. Thermal conductivity is defined by following equation:

$$K = \left(\frac{Q \times S}{A \times \Delta T}\right)$$

Where: K, Q, S, A, and ΔT are thermal conductivity, Q is heat flow, S is thickness of specimen, A is area of specimen, and ΔT is temperature difference across the sample.

Thermal conductivities and specific heats were measured at 22 ºC using HotDisk from Therm Test Inc. Canada. The samples used for this test measured 50 mm by 50 mm with a slight variation on thickness. Depending on the thickness the probe depth was adjusted. The 5505 sensor was used at 1 W power which is shown in Figure 5-1A. A typical measuring arrangement is shown in Figure 5-1B with placement of sensor between the sample and tightening the clamp to make sure the samples are not loosely held together.


*Figure 5-1* The images of Kapton insulated sensor (A) and an arrangement for the testing of foams (B)

5.2.5 Time-Temperature Characteristics

Time-temperature characteristics were recorded for each type of foam by measuring time taken for the raw materials mixture to start gelling, foaming, and curing to attain dimensional stability, Figure 5-2 shows the setup used for the measurement. OMEGA Type CN63100 closed loop-relay output temperature controller from Omega Company, was used to control temperature and PRTF Type 3-wire general purpose RTD probes with fiberglass insulated cable was used as temperature measuring unit. A thermocouple was placed in the pot where the mixture was poured and allowed to foam freely in case of free foaming and with an airtight lid in case of constrained expansion. Temperature was recorded and plotted against time.

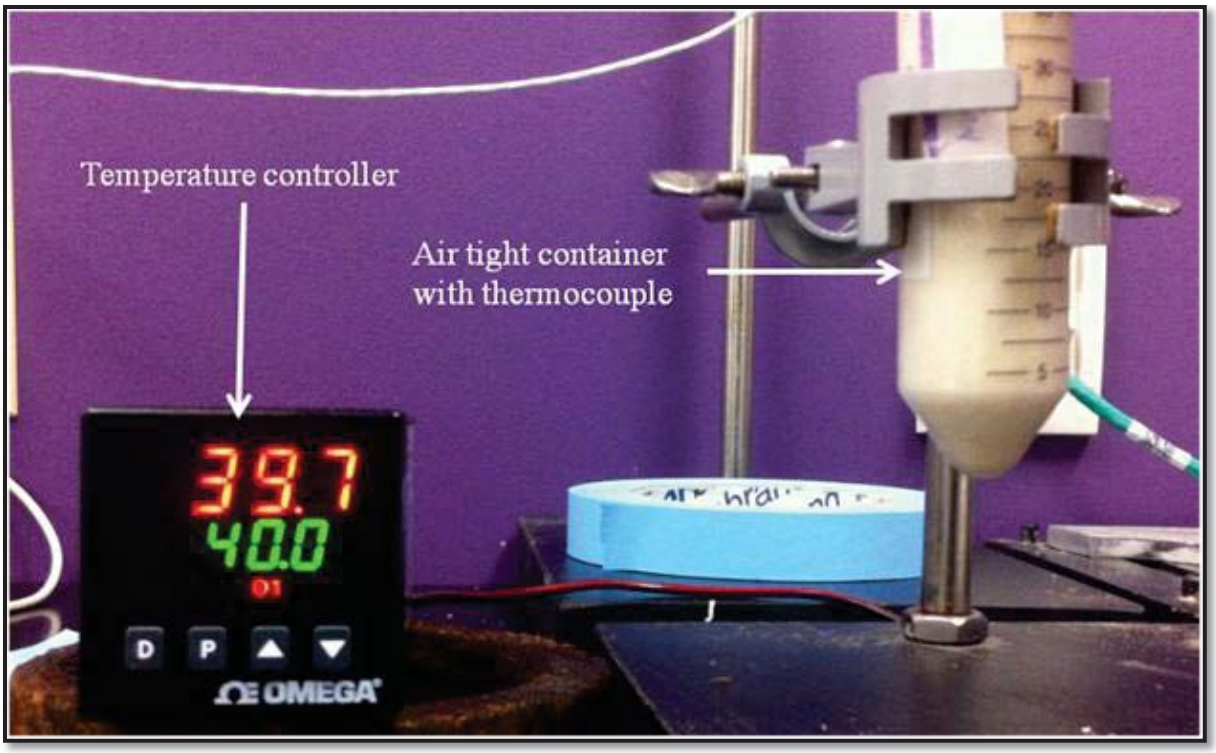


*Figure 5-2* Setup used for recording the temperature rise during the process of foaming reaction, gelling, and cure.

5.2.6 Raman Spectroscopy

A 532 nm intensity laser was used at 1 % power with aperture of 10 μm slit and objective lens with 10X zoom; this gave a spot size of 2.1 μm. The scan was done from 500 to 2000 $cm^{-1}$. The exposure time was 15 sec and background and sample exposure was performed five times. Background was collected before every sample. This background was subtracted from the Raman spectroscopy results and a baseline correction was performed. Later the spectra were analyzed for peaks listed in Table 5-3 for urea and urethane linkages at 1650 and 1710 $cm^{-1}$. Areas for these peaks were measured and a ratio of urea-to-urethane was calculated.

Table 5-1

*Assignments of Raman spectra signals for polyurethane foams, u: urethane, ua: urea, a.r.: aromatic ring, υ: stretching, δ: bending*

| Signal | Frequency $cm^{-1}$ |
|---|---|
| υ(C=O) u(broad) | 1710 |
| υ(C=O) ua | 1650 |
| δ(NH), υ(CN) | 1521, 1535, 1540 |
| υ(C-N), υ(C-O) | 1303-1312 |
| υ(C-O-C) sym. U, δ(CH) a.r. | 1181 |
| δ(C-O-C), δ(C-C-C) | 860-865 |

5.2.7 Atomic Force Microscopy

Digital instruments multimode NanoScope® III was used to image all the PU foam samples that was equipped with nanoscope® IIIa controller. Silicon AFM probes from Ted Pella. Inc. was used in tapping mode. The single beam cantilevers that had tip radii of <10 nm were used. The resonating frequencies ranged from 200-300 kHz with force constant of 20-75 N/m, with length of 125 μm, width of 30 μm, thickness of 4 μm, tip height of 17 μm, Phase images were collected which showed the contrast based on the hardness and softness of the phases.

The sample for the AFM was prepared by embedding the foams in cold mounting epoxy. An embedding PP mold cup supplied by Electron Microscopy Sciences was used. EpoFix™ epoxy and EpoFix™ hardener was mixed in ratio 15:2 by volume in a separate cup, procured from Electron Microscopy Sciences. The mixture was mixed thoroughly and kept aside to remove bubbles. The epoxy was then poured in the mold where the foam was stuck to the base of the cup with a double sided tape (this was

done to ensure that the foam does not rise due to the buoyancy) and kept for 24 h to cure. After curing the mold was cut open and the sample was then polished with series of 400, 600, 800, 1200 silicon carbide paper and finally polished with 0.05 micron alumina suspension at 60 rpm. The polished sample was sonicated for 30 min in distilled water and then dried before the AFM imaging. Care was taken to image the sample at the trapezoidal junction of the pores.

## 5.3 Energy Simulation

### 5.3.1 Building Description

Figure 1 A is a photo of Zero Energy Research Laboratory at Discovery Park, University of North Texas. The building is located at 32.9 deg latitude and -97.04 deg longitude, with elevation of 182 m. The floor construction is made of heavyweight concrete with 3” thick rigid insulation and has 1200 $ft^2$. Total building area is 2671.3 $ft^2$ with net conditioned area of 1848 $ft^2$. There are two types of windows, one being operable window with metal frame and the other being with fixed metal frame. Window area is 620.32 $ft^2$, window to wall ratio is 33.56. Main roof is made of 4” SIP and mechanical roof is made of single ply roofing with 5” thick rigid insulation. Masonry wall is made of 100 mm brick with air gap and 6” full batt insulation sandwich between 1/2” thick sheathing and 5/8” thick Gyp BC. Metal panel wall is made of three layers 1/2" thick sheathing, 3 5/8” full batt insulation and 5/8” thick Gyp BC. Partition wall has three layers with 5/8” thick Gyp BC, 3 5/8” full batt insulation and 5/8” thick Gyp BC. In this the standard SIP was replaced by foams and sandwich foam composites to perform the simulation.

A

B

*Figure 5-3* (A) Photo of Zero Energy Research Lab, and (B) is the model in OpenStudio

Renewable energy generation is from sun and wind. It's heating, ventilation and air conditioning system (HVAC) utilizes the ground as its heat source in heating season, and its heat sink in cooling season. Heating and cooling system for the building is from

a water-to-water heat pump (WWHP) with radiant floor and water-to-air heat pump (WAHP) with air ducts respectively. Six vertical ground heat exchangers each of 225 feet into the ground transfers heat to WWHP and WAHP. There are around 150 sensors network connected to data acquisition system managed by TAC Vista building management system.

### 5.3.2 System Design

OpenStudio is used to create model of building, the model is shown in Fig. 1 B. and EnergyPlus is used to perform simulation. The building is divided into three zones.

1. Conditioned zone,
2. Mechanical zone, and
3. Electrical zone

A dual set point thermostat control system is employed for heating and cooling the conditioned zone. Heating set point of 18.3 °C and cooling set point of 21.1 °C. Denton weather data file for a year was downloaded from OpenStudio to be used for simulation. Weather data includes outside air temperature, relative humidity, wind speed, etc.

## 5.4 System Modeling

### 5.4.1 Model Calibration

The building has three electric meters monitoring HVAC, lighting, and appliance energy consumption. TAC Vista data recording software designed and installed by Schneider Electrics is used. By creating a log in the system, the software automatically records his data.

Total electricity consumption by the HVAC systems of the building which includes WAHP and WWHP compressor electric power consumption, fan electric power consumption, and heating and cooling water circulation pump. Recorded real data is matched with simulated data for total electricity power consumption; it was made sure that both the heat pumps were working during the measurement of data recording. Indoor air temperatures that were recorded by TAC Vista were also equated with simulated mean air temperatures of the zones. Dual set point thermostat was used to control heating and cooling simultaneously to maintain the set temperature (Cooling set point was 21.1°C & heating set point was 18.3°C).

### 5.4.2 Energy Simulation

EnergyPlus from Department of Energy (DOE) was used to create envelopes for the building giving details of building materials in input data files (IDF) editor. Weather file for Dallas Fortworth TX in weather data format (EPW) was downloaded from http://www.energyplus.gov. The material details were created for wall envelopes as shown below:

Table 5-2

*Specifications of wall created in IDF editor*

| | Masonry Wall | Metal Panel Wall | S.I.P. Wall |
|---|---|---|---|
| Layer 1 | Masonry | Corrugated metal panel | Textured coating |
| Layer 2 | Building wrap | Building wrap | Structural insulated panel |
| Layer 3 | ½" Thick sheathing | ½''Thick sheathing | 30 mil metal studs at 16'' OC |
| Layer 4 | 43 mil metal studs at 16'' | 43 mil metal studs at 16'' OC | 5/8''Thick gypsum BD |

| | | | |
|---|---|---|---|
| Layer 5 | Full batt insulation | J-Trim, Type-finish to match panel | Connector per S.I.P |
| Layer 6 | 5/8'' Thick gypsum BD | - | Sealant |

The materials for SIP wall were changed to as per Tables 2, 3, 4, 5, 6, and 7 with properties such as density, thermal conductivity, specific heat measured for the foam, foam composites, and sandwich foam composites as detailed in section foam density and thermal conductivity. The annual energy consumption for the each SIP wall material change was estimated by running simulation.

## 5.5 Results and Discussions

### 5.5.1 Influence of Cell Size on Thermal Conductivity

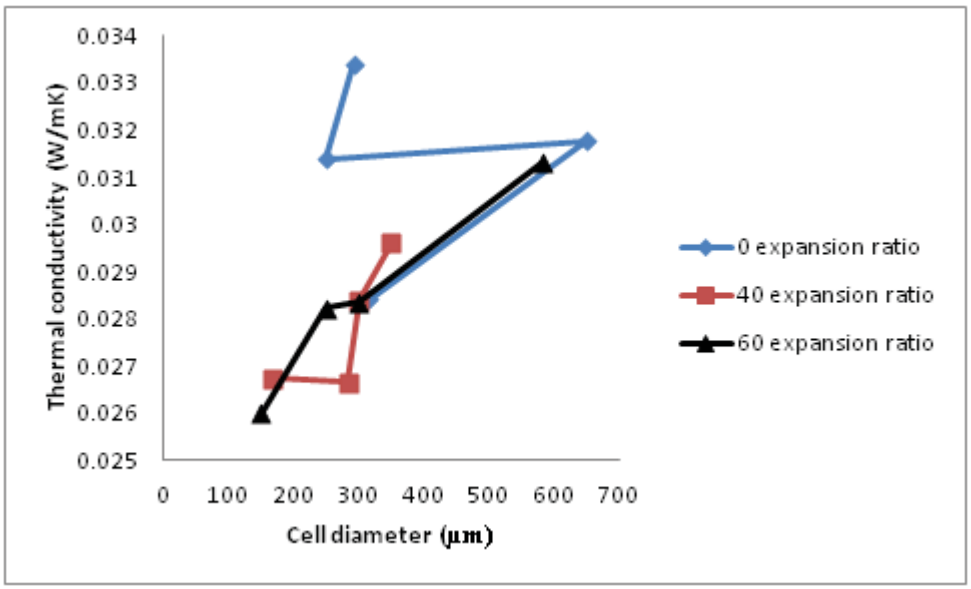


*Figure 5-4* Thermal conductivity as a function of cell diameter

As can be seen from Fig. 2, an interesting trend for cell size and its influence on thermal conductivity is seen. As the cell size of the foams decreases, the thermal conductivity decreases (Table 1). A 650 micron cell diameter shows the highest thermal conductivity of 0.0317 W/mK and 300 micron shows the conductivity of 0.0314 for 0 expansion ratio. This indicates that the smaller the cell size, the smaller the pockets of airs that hinder the heat flow through the material. Thus 60 expansion ratio with 15% kenaf core loading has given a higher number of smaller volume air pockets, which have increased the thermal insulation by 18 % when compared to the largest cell size of 650 microns of 0 expansion ratio with the lowest number of air pockets. Moreover the processing with constrained volume expansion of 40 and 60 has given a control on the cell size which indirectly gives a control on thermal conductivity. The 60 expansion gives a steady cell decrease with increase in kenaf core loading with minimum deviation. The 0 expansion ratio gives the least control on the cell size and therefore on thermal conductivity.

### 5.5.2 Influence of Urea-to-Urethane Ratio on Thermal Conductivity of Aged Foams

During foaming reaction, the first step is of hydroxyl group with the isocyanate group to form urethane linkages. This reaction is characterized by increase in viscosity and generally the term “gel” is used. Later during second step one part of water is reacted with two parts of isocyanate. Water reacts with isocyanate to form an intermediate unstable carbamic acid and then this carbamic acid decomposes into amine and $CO_2$.

$$\text{R-N=C=O} + H_2O \rightarrow \text{R-NH}_2 + CO_2\uparrow$$

$$\text{R'-N=C=O} + \text{R-NH}_2 \rightarrow \text{R'-NH-CO-NH-R}$$

Table 5-3 shows rate 1 and rate 2 which and maximum temperature reached during the reaction. Rate 1 is the characteristics for urea formation and rate 2 is for urethane formation. Initial rate for urea formation is always more than that for urethane formation, indicating predominance of urea formations at early stages of foaming. Figure 5-4 shows time-temperature plot for the reactions. It can be consistently seen that the maximum temperature reached during the reaction for constrained expansion of 60 reaches a maximum temperature when compared to both free foaming and 40% constrained method. This will be due to the higher pressure built-up during reaction. Aging of foams in general has shown to increase thermal conductivity over a period of 20 days and showing the improvement in thermal insulation by addition of nanofiller [24].

This aging effect of reducing thermal insulation properties is due to the diffusion of gas from inside of the cells. This diffusion driving force comes from classical sorption/desorption process. Table 5-2 shows measured thermal conductivity values for the foams it can be seen that over the period of 90 days there has been no observation of significant change in thermal conductivity. This implies that there has been negligible $CO_2$ diffusion, which would have otherwise increased the thermal conductivity. This can be attributed to the formation of polyurea during the curing reaction. Figure 5-3 shows Raman spectra for the foams, the peaks observed in the spectra are listed in Table 5-3. Polyurea formed during the reaction are the hard domains in the matrix. Table 5-4 shows the computed areas for urethane and urea with the ratios of urea-to-urethane. The ratio shows an increase of urea-to-urethane from free expansion to di60 expansion. It is noted that as the constrained volume expansion is carried out the urea-to-urethane

ratio is increased, suggesting that the urea hard domains are formed which hinders in the diffusion of gas. Thus improve the thermal insulation even after aging to 90 days. Figure 5-4 shows the plot of % change in thermal conductivity with respect to urea-to-urethane ratio. It can be seen that as the urea content increases, the change in thermal conductivity is negligible. This indicates that the hard domains due to urea formation have increased that hinders the diffusion of $CO_2$ gas from expelled out of the foam thereby keeping the thermal conductivity almost the same after aging to 90 days.

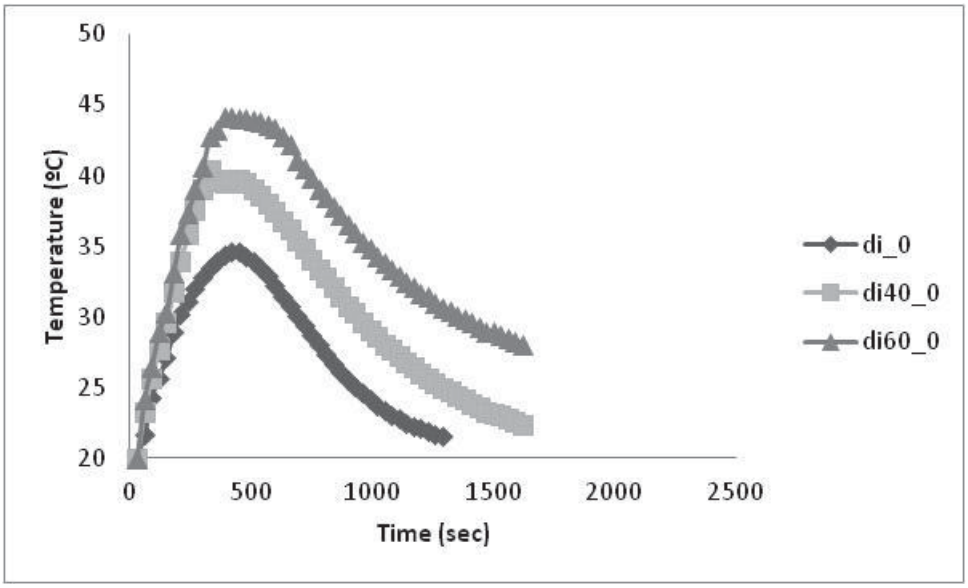


A

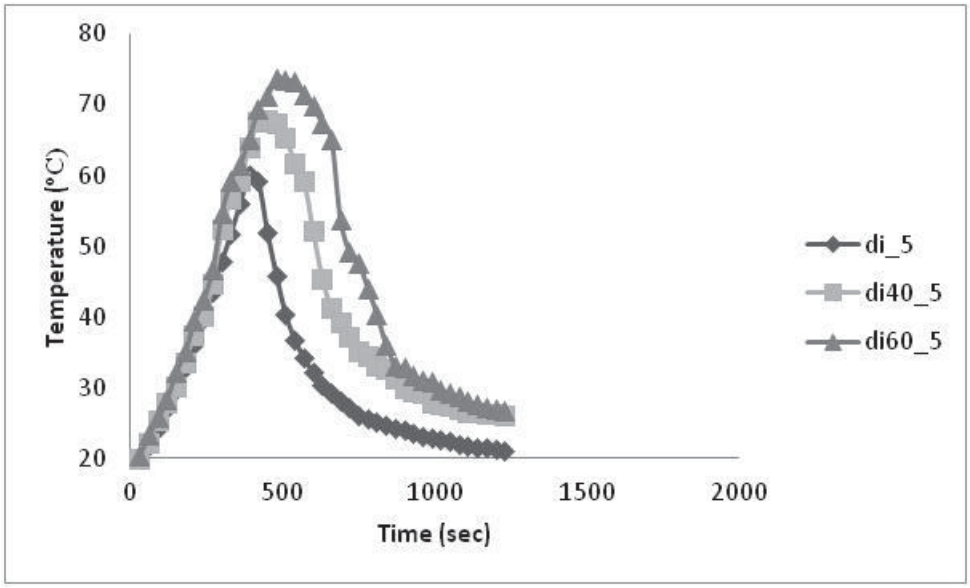
80
70
60
50
40
30
20
Temperature (°C)
0
500
1000
1500
2000
Time (sec)
di_5
di40_5
di60_5

B

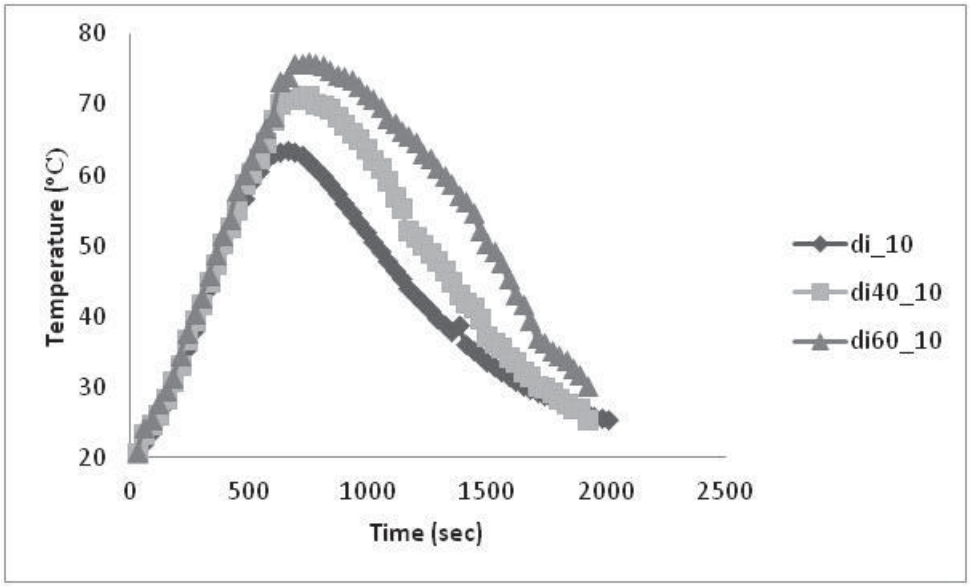
80
70
60
50
40
30
20
Temperature (°C)
0
500
1000
1500
2000
2500
Time (sec)
di_10
di40_10
di60_10

C

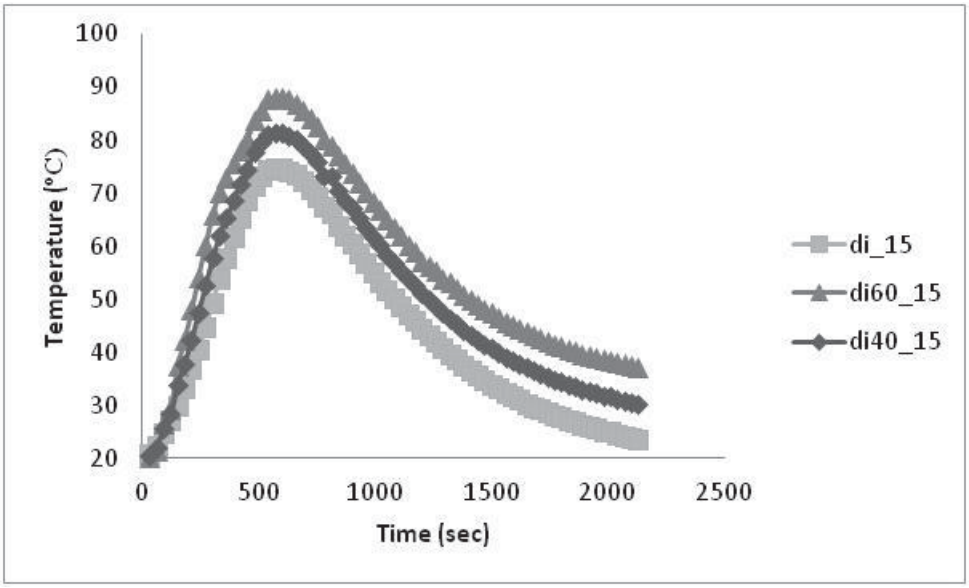


D

*Figure 5-5* Time-temperature characteristics for foams

Table 5-3

*Initial rate, final rate of heating, and maximum temperature reached during the foaming reaction*

| | Rate 1 | Rate 2 | Max. temp |
|---|---|---|---|
| di_0 | 9.63 | 1.52 | 34.6 |
| di_5 | 13.5 | 8.1 | 60.2 |
| di_10 | 12.7 | 5.45 | 63.5 |
| di_15 | 12.04 | 8.3 | 74.8 |
| di40_0 | 17.1 | 3.86 | 39.7 |
| di40_5 | 11.23 | 9.65 | 67.9 |
| di40_10 | 9.46 | 5.02 | 71.2 |
| di40_15 | 14.15 | 8.05 | 81.5 |
| di60_0 | 14.45 | 3.45 | 44.2 |
| di60_5 | 12.88 | 6.73 | 73.7 |
| di60_10 | 11.84 | 5.38 | 76 |
| di60_15 | 13.4 | 5.52 | 88.2 |

Table 5-4

*Thermal conductivity without and with aging of 90 days at 20 ºC for free volume, di40, and di60 volume expansion rigid polyurethane foams with kenaf core loadings of 0, 5, 10, and 15 %*

| | di | | di40 | | di60 | |
|---|---|---|---|---|---|---|
| Kenaf core | Thermal conductivity | Thermal conductivity after aging (90 days) | Thermal conductivity | Thermal conductivity after aging (90 days) | Thermal conductivity | Thermal conductivity after aging (90 days) |
| (%) | (W/m-K) | (W/m-K) | (W/m-K) | (W/m-K) | (W/m-K) | (W/m-K) |
| 0 | 0.0473 | 0.0495 | 0.0296 | 0.0307 | 0.0313 | 0.0316 |
| 5 | 0.0317 | 0.0326 | 0.0284 | 0.0291 | 0.0283 | 0.0287 |
| 10 | 0.0314 | 0.0324 | 0.0266 | 0.0273 | 0.0282 | 0.0285 |
| 15 | 0.0334 | 0.0346 | 0.0266 | 0.0272 | 0.0259 | 0.0263 |

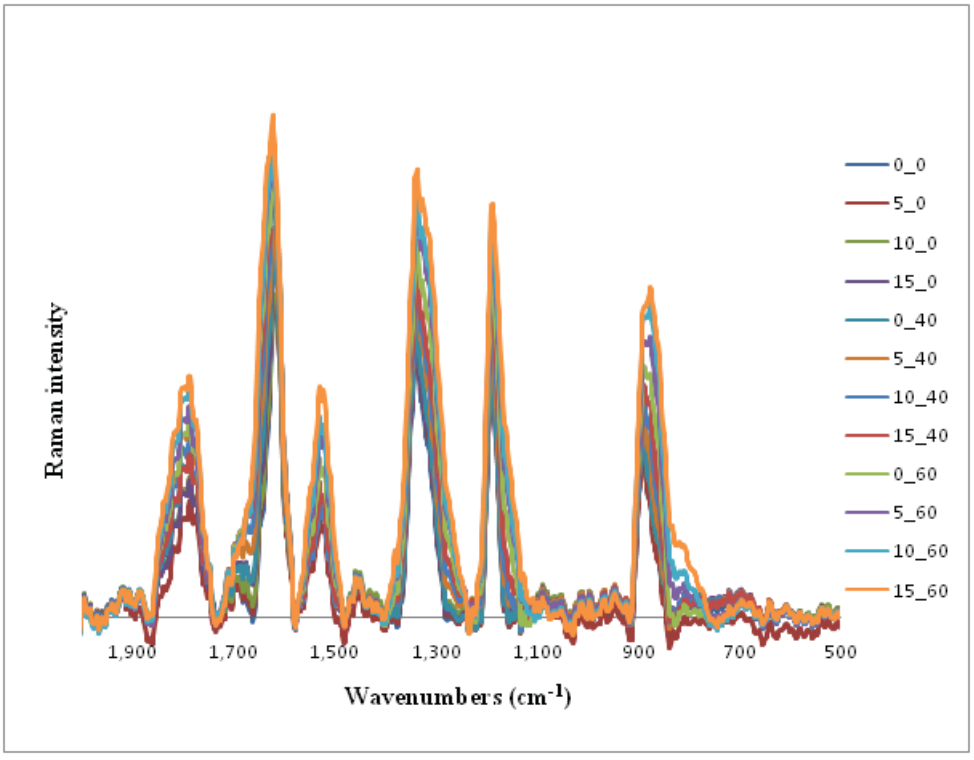


*Figure 5-6* Raman spectroscopy of free volume, di40, and di60 volume expansion rigid polyurethane foams with kenaf core loadings of 0, 5, 10, and 15 %.

Table 5-5

*Areas of urethane and urea peaks with ratio of urea to urethane peaks for free volume, di40, and di60 volume expansion rigid polyurethane foams with kenaf core loadings of 0, 5, 10, and 15 %.*

| | di | | | di40 | | | di60 | | |
|---|---|---|---|---|---|---|---|---|---|
| Kenaf core % | Area of urethane peak 1710 | Area of urea peak 1650 | Ratio of urea to urethane peak 1650/1710 | Area of urethane peak 1710 | Area of urea peak 1650 | Ratio of urea to urethane peak 1650/1710 | Area of urethane peak 1710 | Area of urea peak 1650 | Ratio of urea to urethane peak 1650/1710 |
| 0 | 1348 | 1225 | 0.91 | 1056 | 1423 | 1.34 | 2023 | 3391 | 1.68 |
| 5 | 1350 | 1653 | 1.23 | 1025 | 1449 | 1.41 | 1451 | 2547 | 1.76 |
| 10 | 1113 | 1378 | 1.24 | 1050 | 1531 | 1.46 | 1615 | 3011 | 1.86 |
| 15 | 1147 | 1467 | 1.28 | 1541 | 2319 | 1.50 | 1370 | 2837 | 2.07 |

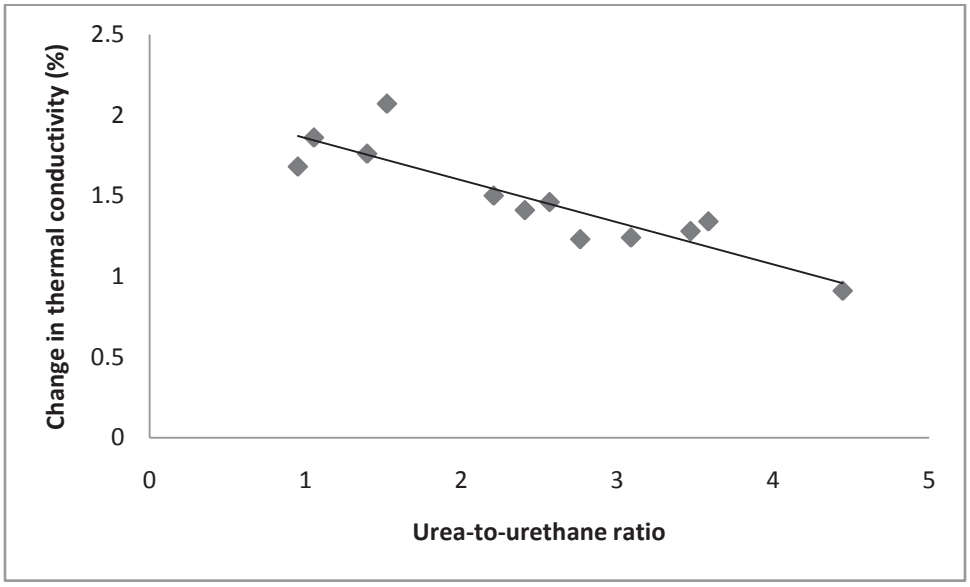


*Figure 5-7* Influence of urea-to-urethane content on change in thermal conductivity on foam aging ($R^2$=0.7936)

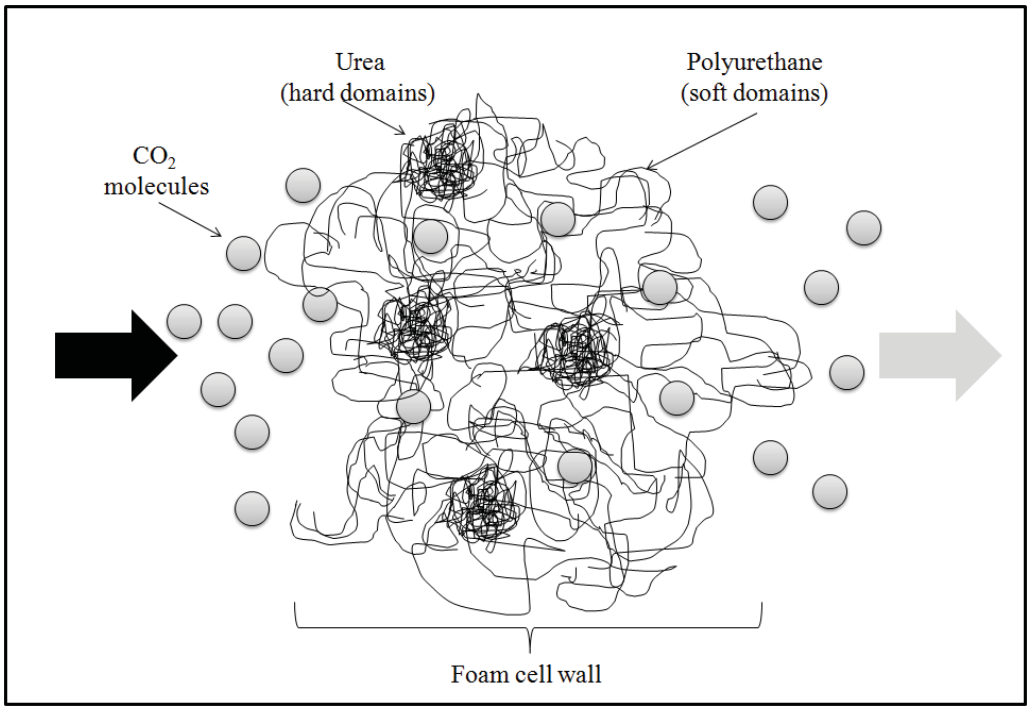
Urea
(hard domains)
Polyurethane
(soft domains)
$CO_2$
molecules
Foam cell wall

A

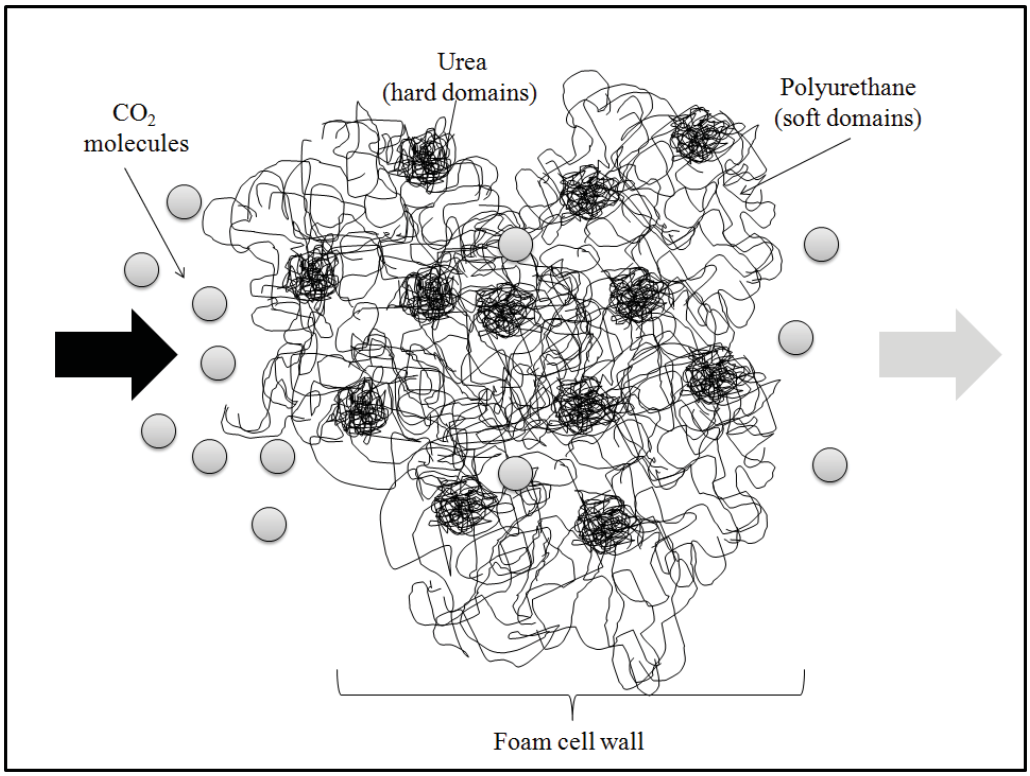
Urea
(hard domains)
Polyurethane
(soft domains)
$CO_2$
molecules
Foam cell wall

B

*Figure 5-8* Schematics showing the hard domains of urea dispersed in polyurethane, the black arrow represents the inside of the pores and the lighter arrow is the atmosphere, gray solid circles represent $CO_2$ gas molecules (A) fewer hard urea domains in the polyurethane matrix and (B) more number of hard urea domains in polyurethane matrix that influences the $CO_2$ gas diffusion to the atmosphere.

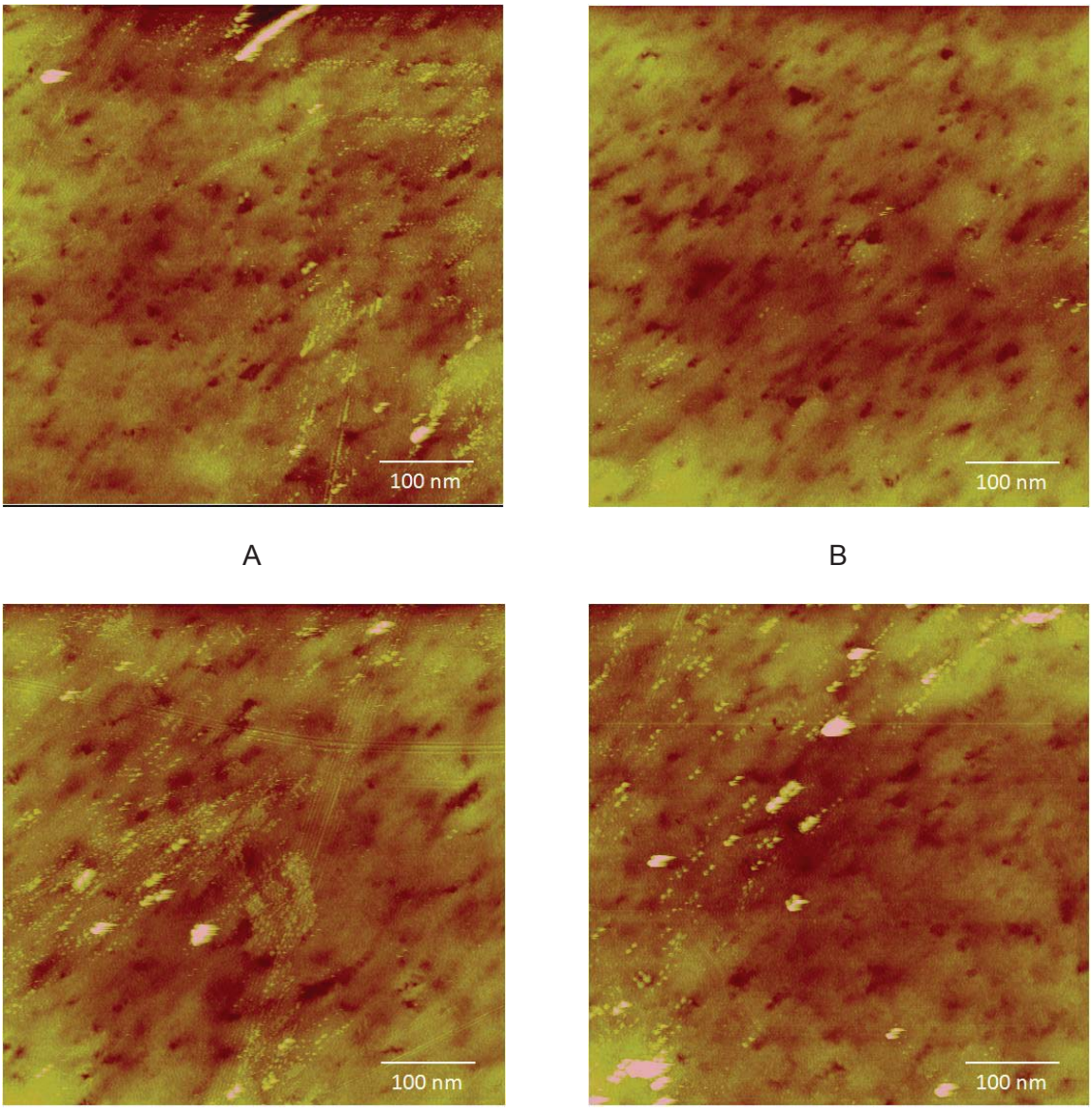


A B

C D

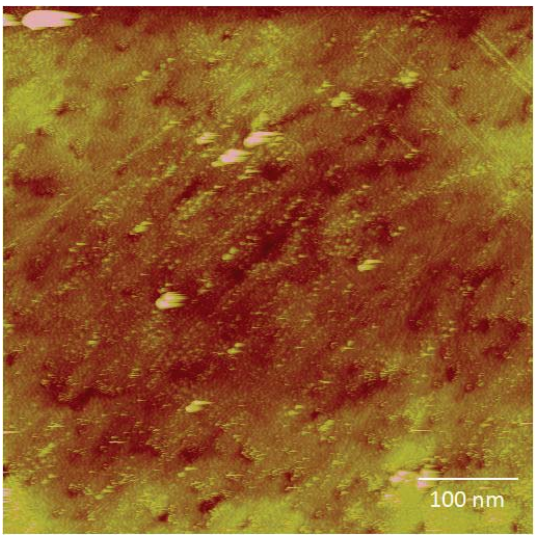


E

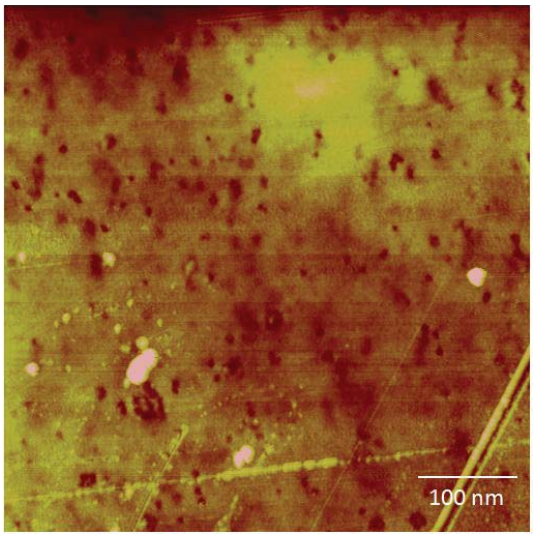


F

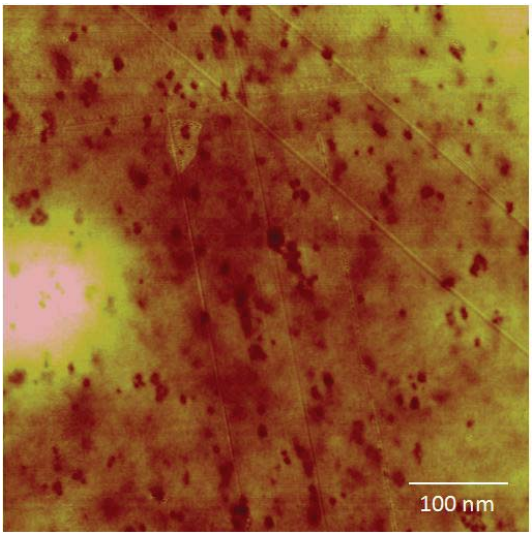


G

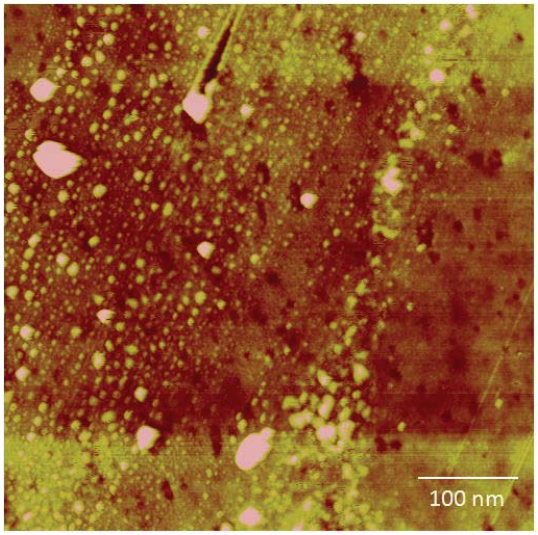


H

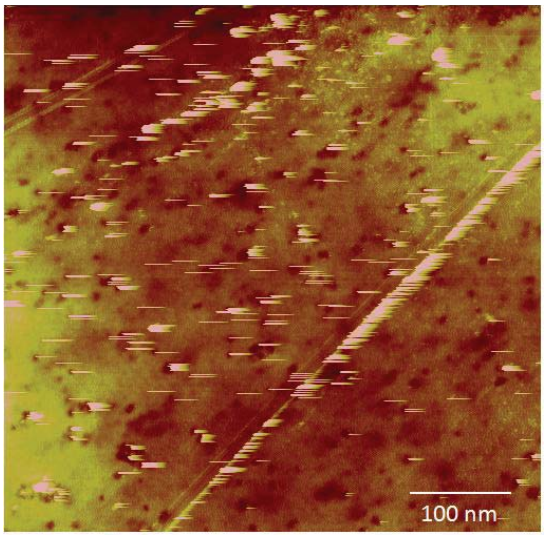


I

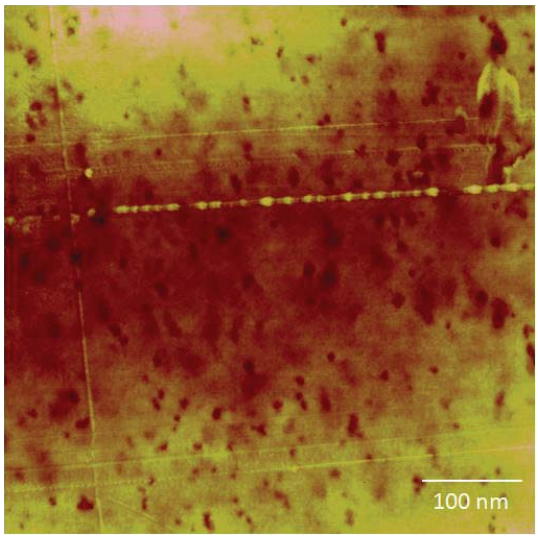


J

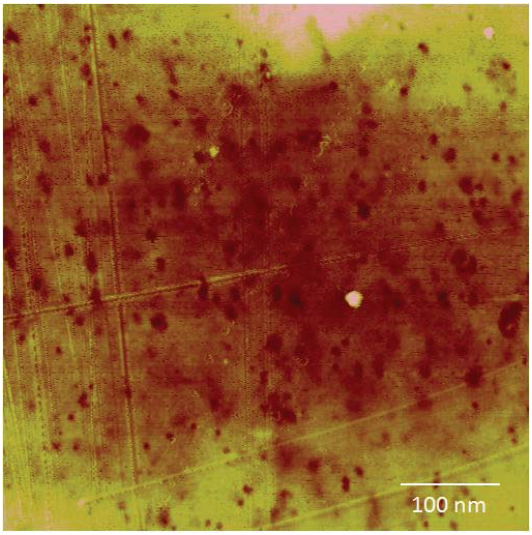


K

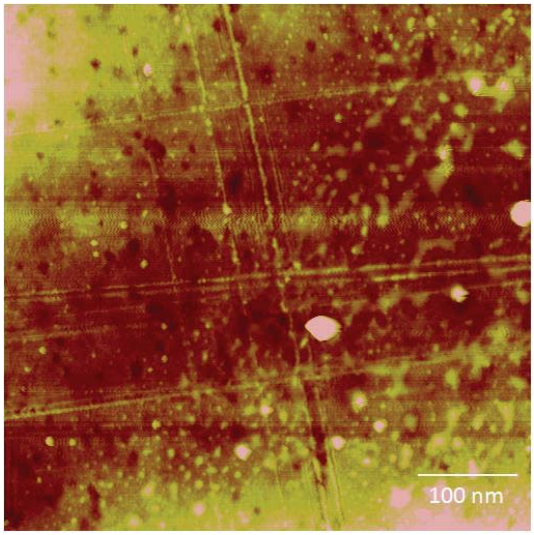


L

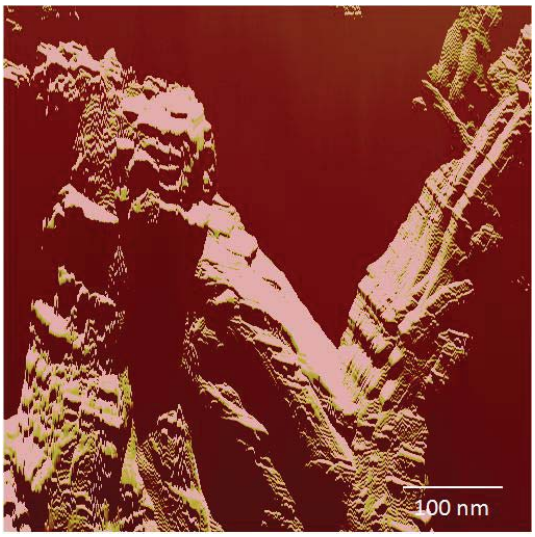


M

*Figure 5-9* AFM phase images in tapping mode, light contrast showing softer polyurethane phase, and darker circles that are harder urea phase.

Figure 5-8 shows the schematics of the dispersion of hard domains in the matrix of polyurethane. The reaction of isocyanate and water gives a thermally unstable carbamic acid, which dissociates into an amine and $CO_2$ gas [25]. Later the amine reacts with isocyanate to give urea. The diol present simultaneously reacts with isocyanate to give polyurethane. The result of these series of reaction is the dispersion of urea in polyurethane matrix. A study showed that during the course of reaction the urea is formed first showing phase separation, the in-situ FTIR showed that the polyurethane is a slower reaction than urea reaction [26]. The AFM images show a lighter region that is softer polyurethane matrix and dark spots that corresponds to the urea phase separation. Also it is shown that as the distilled water content increased the urea formation increased, that gave higher blown foams with lesser density and improved mechanical strength [27].

Figure 5-9 shows AFM images for free foaming, 40, and 60 % volume expansion with 5, 10, and 15% kenaf core loading. It can be seen that there is increasing number urea hard domains dispersed in the matrix of soft polyurethane as we go from free foaming to 40 and then 60 % volume expansion. Although the distilled water content remained equal in all the foam samples we can see that the urea hard domains have increased, this might be due to the effect of increasing volume expansion. From time temperature plots we can also see that the temperature rise for the 15 % is more than the 10, 5, and 0 % kenaf core loading, that has influenced the urea formation. The less darker phase around the hard urea domains will be microdomains of urea, these are the mixture of urea and polyurethane. That might give intermediate properties of PU and urea.

These urea hard domains have given barrier properties to the foams. They act as resistant for the diffusion of CO2 gas molecules thereby keeping the gas inside the foam pores for longer time. Figure 5-9(M) shows kenaf core AFM, this proved that the topography of kenaf core and other images are not matched hence can be said that the area scanned were PU and not of kenaf core.

### 5.5.3 Thermal Conductivity

Thermal conductivity in foam is from three heat transfer mechanisms: polymer conduction, gas conduction, and radiation. And the thermal conductivity measured as described in 5.3.4 gives the total thermal conductivity of the samples. An increase in density has shown to reduce thermal conductivity. This is because as the density increases the number of cells per unit volume increases. There are larger number of

smaller cells that isolate the gas and reduce the thermal conductivity, by reducing gas conduction and effects of internal radiation.

Table 5-6

*PU foam properties*

| | PU foam | | | | | | | | | | | |
|---|---|---|---|---|---|---|---|---|---|---|---|---|
| Volume expansion | 0 | | | | 40 | | | | 60 | | | |
| Kenaf core (%) | 0 | 5 | 10 | 15 | 0 | 5 | 10 | 15 | 0 | 5 | 10 | 15 |
| Density (kg/m3) | 57 | 77 | 77 | 86 | 271 | 484 | 658 | 899 | 197 | 394 | 514 | 797 |
| Cell diameter (μm) | 316 | 650 | 250 | 293 | 350 | 300 | 283 | 168 | 583 | 300 | 250 | 150 |
| Thermal conductivity (W/m-K) | 0.0473 | 0.0317 | 0.0314 | 0.0334 | 0.0296 | 0.0284 | 0.0266 | 0.0266 | 0.0313 | 0.0283 | 0.0282 | 0.0259 |
| Specific heat (J/kg-K) | 334 | 718 | 600 | 617 | 890 | 834 | 867 | 841 | 725 | 932 | 904 | 824 |

Table 5-7

*Properties of sandwiched foam composites with kengro kenaf fiber panels*

| | Sandwiched foam composite (kengro Kenaf fiber) | | | | | | | | | | | |
|---|---|---|---|---|---|---|---|---|---|---|---|---|
| Volume expansion | 0 | | | | 40 | | | | 60 | | | |
| Kenaf core (%) | 0 | 5 | 10 | 15 | 0 | 5 | 10 | 15 | 0 | 5 | 10 | 15 |
| Density (kg/m3) | 70 | 90 | 90 | 99 | 284 | 497 | 671 | 912 | 210 | 407 | 527 | 810 |
| Thermal conductivity (W/m-K) | 0.0426 | 0.0271 | 0.0269 | 0.0276 | 0.0263 | 0.0259 | 0.0253 | 0.0254 | 0.026 | 0.0259 | 0.0259 | 0.0249 |
| Specific heat (J/kg-K) | 368 | 496 | 457 | 463 | 554 | 535 | 546 | 537 | 499 | 568 | 558 | 532 |

Table 5-8

*Properties of sandwiched foam composites with bacterial kenaf fiber panels*

| | Sandwiched foam composite (bacterial Kenaf fiber) | | | | | | | | | | | |
|---|---|---|---|---|---|---|---|---|---|---|---|---|
| Volume expansion | 0 | | | | 40 | | | | 60 | | | |
| Kenaf core (%) | 0 | 5 | 10 | 15 | 0 | 5 | 10 | 15 | 0 | 5 | 10 | 15 |
| Density (kg/m3) | 68 | 88 | 88 | 97 | 282 | 495 | 669 | 910 | 208 | 405 | 525 | 808 |
| Thermal conductivity (W/m-K) | 0.0115 | 0.0066 | 0.0056 | 0.0060 | 0.0047 | 0.0045 | 0.0042 | 0.0043 | 0.0052 | 0.0043 | 0.0045 | 0.0042 |
| Specific heat (J/kg-K) | 328 | 681 | 579 | 591 | 863 | 814 | 859 | 826 | 717 | 914 | 883 | 821 |

Table 5-9

*Properties of sandwiched foam composites with sugarcane fiber panels*

| | Sandwiched foam composite (Sugarcane fiber) | | | | | | | | | | | |
|---|---|---|---|---|---|---|---|---|---|---|---|---|
| Volume expansion | 0 | | | | 40 | | | | 60 | | | |
| Kenaf core (%) | 0 | 5 | 10 | 15 | 0 | 5 | 10 | 15 | 0 | 5 | 10 | 15 |
| Density (kg/m3) | 76 | 96 | 96 | 105 | 290 | 503 | 677 | 917 | 216 | 413 | 533 | 816 |
| Thermal conductivity (W/m-K) | 0.0095 | 0.0068 | 0.0040 | 0.0041 | 0.0036 | 0.0033 | 0.0033 | 0.0028 | 0.0026 | 0.0017 | 0.0016 | 0.0015 |
| Specific heat (J/kg-K) | 351 | 479 | 439 | 445 | 536 | 517 | 528 | 520 | 481 | 550 | 541 | 514 |

Table 5-10

*Properties of sandwiched foam composites with fiberglass panels*

| | Sandwiched foam composite (fiberglass) | | | | | | | | | | | |
|---|---|---|---|---|---|---|---|---|---|---|---|---|
| Volume expansion | 0 | | | | 40 | | | | 60 | | | |
| Kenaf core (%) | 0 | 5 | 10 | 15 | 0 | 5 | 10 | 15 | 0 | 5 | 10 | 15 |
| Density (kg/m3) | 75 | 95 | 95 | 104 | 289 | 502 | 676 | 916 | 215 | 412 | 532 | 815 |
| Thermal conductivity (W/m-K) | 0.0220 | 0.0156 | 0.0132 | 0.0137 | 0.0114 | 0.0112 | 0.0110 | 0.0112 | 0.0123 | 0.0108 | 0.0112 | 0.0110 |
| Specific heat (J/kg-K) | 348 | 732 | 614 | 631 | 904 | 848 | 881 | 855 | 740 | 946 | 918 | 839 |

Table 5-11

*Properties of Diab™ and Rubberlite™ foam sandwich composites*

| | Diab™ and Rubberlite™ foam sandwich composites | | | | | | | | | | |
|---|---|---|---|---|---|---|---|---|---|---|---|
| Foams | Diab | Diab and Kenaf fiber | Diab and Bacterial kenaf fiber | Diab and Sugarcane fiber | Diab and Fiberglass | Rubberlite | Rubberlite and kenaf fiber | Rubberlite and bacterial kenaf fiber | Rubberlite and sugarcane fiber | Rubberlite and fiberglass | SIP |
| Density (kg/m3) | 51 | 204 | 194 | 182 | 168 | 150 | 303 | 293 | 281 | 69 | 90 |
| Thermal conductivity (W/m-K) | 0.0133 | 0.0141 | 0.0134 | 0.0142 | 0.0230 | 0.0058 | 0.0066 | 0.0062 | 0.0068 | 0.0116 | 0.086 |
| Specific heat (J/kg-K) | 362 | 396 | 362 | 379 | 376 | 377 | 411 | 377 | 394 | 391 | 904 |

### 5.5.4 Energy Consumption and Energy Savings

Sandwich foam composites show lower energy consumption as compared to the foam by itself. Tables 1, 2, 3, 4, 5, and 6 show thermal conductivity values for the foams and sandwich foam composites. For foams the conductivity has decreased by 54 % from free expansion with 0 % kenaf core loading to 15 % kenaf core loading for 60 volume expansion. These two foams are compared, as the free expansion with 0 % kenaf core is taken as reference foam to compare with all other foams that are discussed. For the kenaf fiber panel sandwich foam composites, thermal conductivity reduced to 58 % and for sugarcane fiber panel sandwich foam composites thermal conductivity reduced to 23 %. Sandwich foam composites with fiberglass panels have the highest energy consumption. Although a similar trend with 15 % kenaf core loading has provided lowest energy consumption by 5.2 % within fiberglass composites, when compared to free expansion. Thus sugarcane fiber panel provides lowest thermal conductivity, thereby giving lowest energy consumption. It can also be seen that the

higher the foam or sandwich foam composite density, lower is the thermal conductivity. The density in these samples is a function of pore size. Thus, while foaming volume expansion was restricted as described in our previous work, the pore sizes decreased. This has led to reduced thermal conductivity. The pores that are filled with air acts as pockets of thermal resistance. Even when the material has high thermal conductivity when compared to air, the combined foam structure lowers this value. Thus when these air pockets are smaller as in the case of 60 volume expansion, they provide more resistance for the heat to pass through. For sandwich foam composites, the panels are solid that are placed on both sides of the foam which makes the composites more thermally resistant. Thermal conductivity by adding sugarcane panels has drastically reduced when compared to kenaf fiber panels.

Considering high energy consumption for free foamed pure PU and its sandwich panels with kenaf fiber, bacterial kenaf fiber, sugarcane fiber, glass fiber, and SIP; they are taken here as a reference for calculating energy savings. Figure 5-8 shows the annual energy savings for foams and sandwich foam composites with panels. It can be seen form Figure 5-8A that as the kenaf core loading has increased a 3% energy savings can be seen when compared to free foamed pure PU. A further increase by 4% can be seen with constrained foaming process. Adding panels of polyester with fibres have improved the thermal resistance thereby increasing energy savings. Bacterial retted kenaf fibres have shown to increase savings by 13% as compared to SIP, followed by kenaf fibers and sugarcane fibers. Diab foam with panels composites with kenaf fiber, bacterial kenaf fiber, and sugarcane fiber gives savings of 8% but reduces for glass fiber. And a similar trend is seen with Rubberlite™ foam and its composite

panels giving savings of 11.5% and seen to give lower savings with glass fiber. Natural fibers have shown superior thermal resistance because of the naturally occurring pores in the fibers, which reduce the thermal conductivity. Glass fiber being more solid and free of defects shows less thermally resistant giving less energy savings.

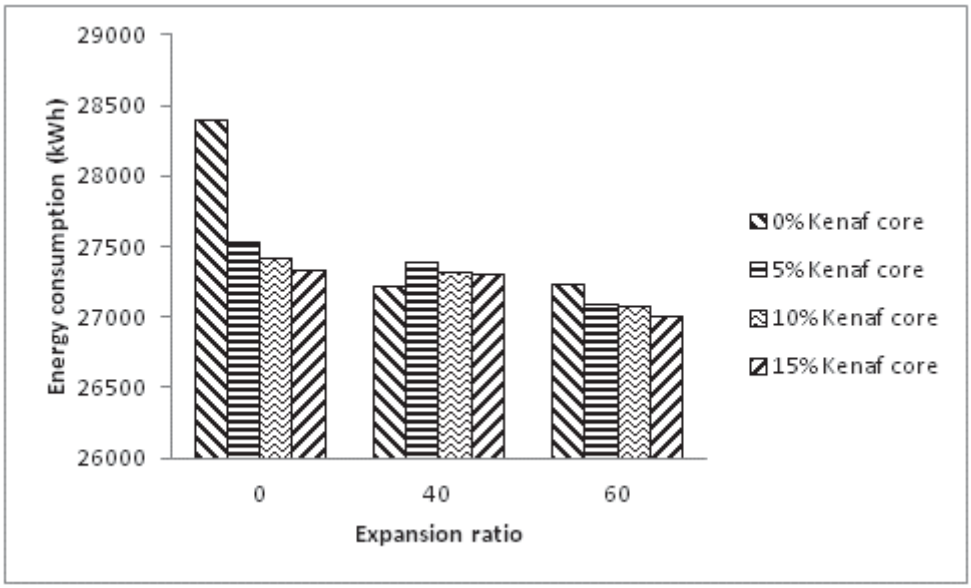


A

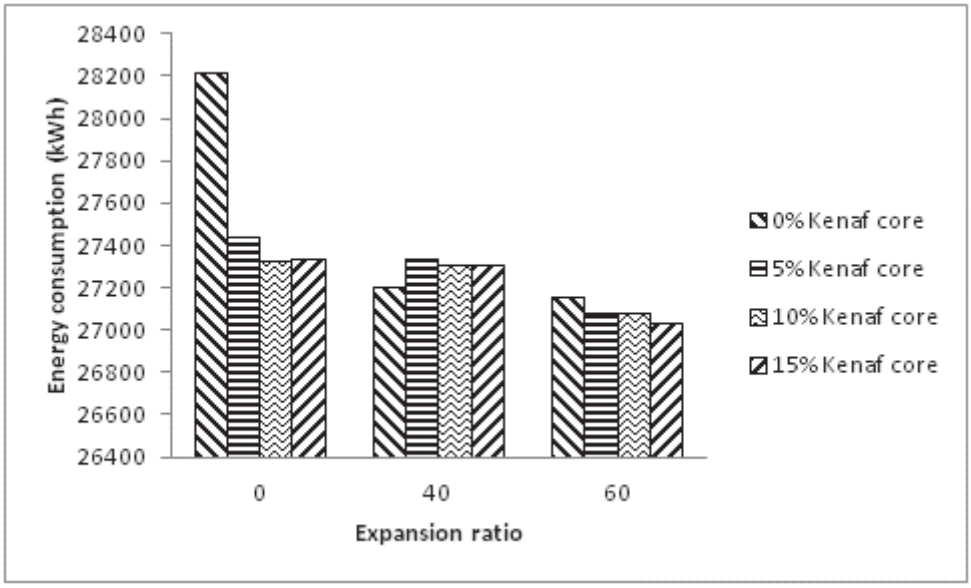


B

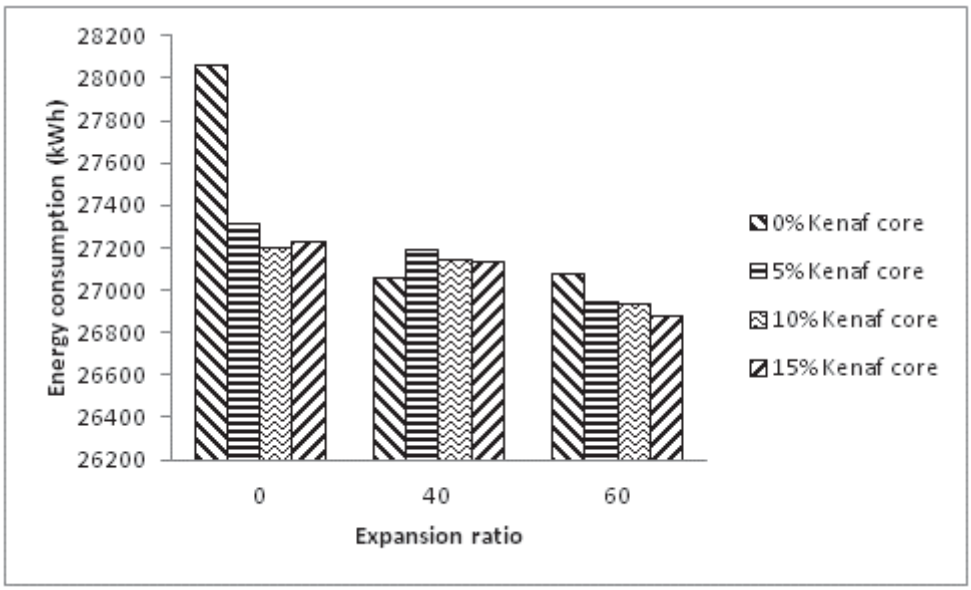
28200
28000
27800
27600
27400
27200
27000
26800
26600
26400
26200
Energy consumption (kWh)
0
40
60
Expansion ratio
0% Kenaf core
5% Kenaf core
10% Kenaf core
15% Kenaf core

C

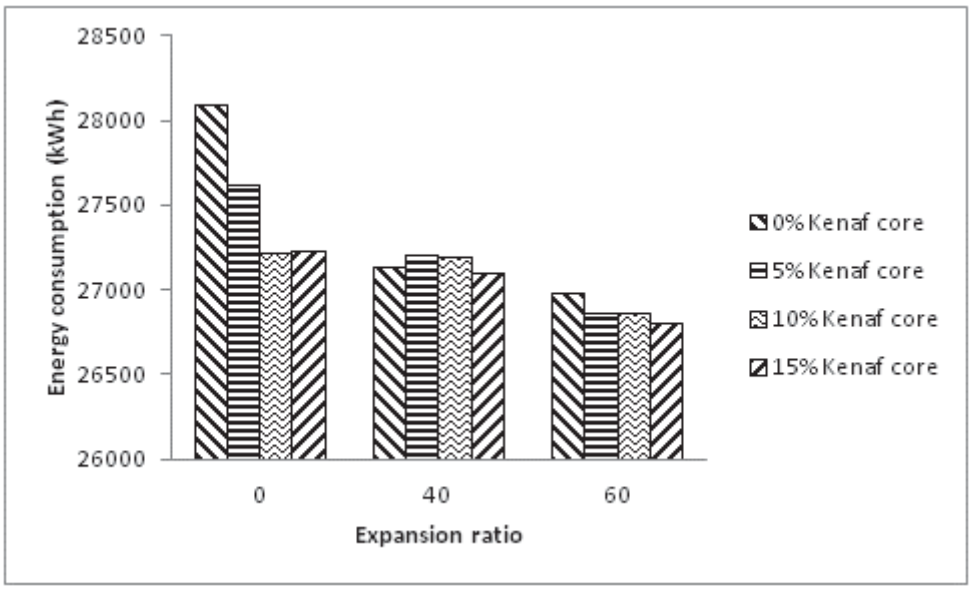
28500
28000
27500
27000
26500
26000
Energy consumption (kWh)
0
40
60
Expansion ratio
0% Kenaf core
5% Kenaf core
10% Kenaf core
15% Kenaf core

D

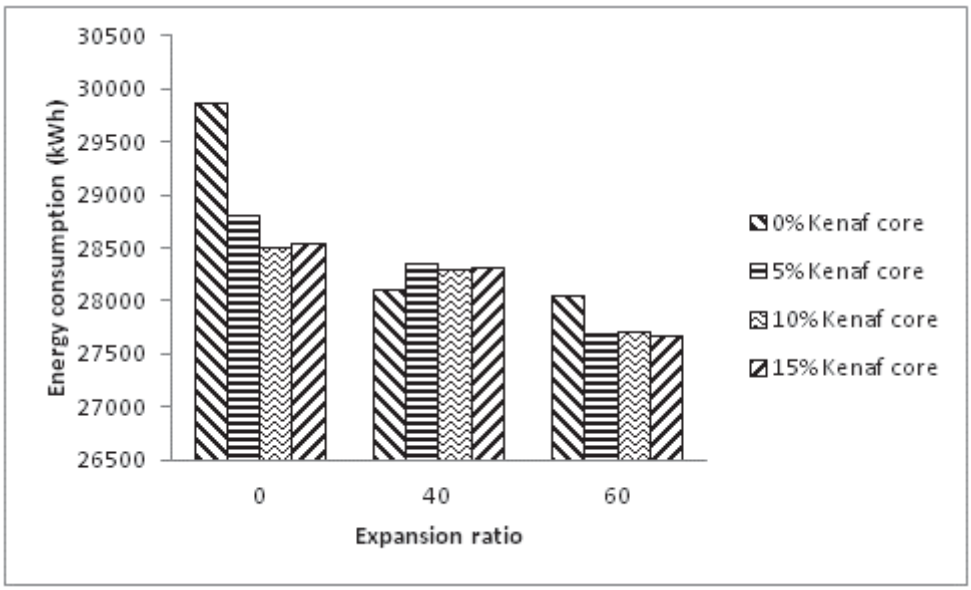
30500
30000
29500
29000
28500
28000
27500
27000
26500
Energy consumption (kWh)
0
40
60
Expansion ratio
0% Kenaf core
5% Kenaf core
10% Kenaf core
15% Kenaf core

E

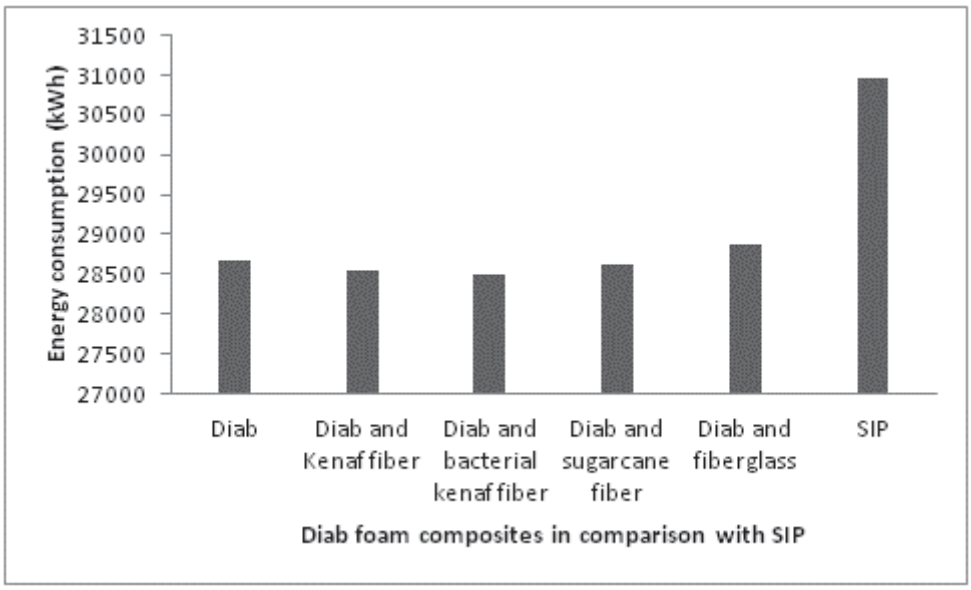
31500
31000
30500
30000
29500
29000
28500
28000
27500
27000
Energy consumption (kWh)
Diab
Diab and Kenaf fiber
Diab and bacterial kenaf fiber
Diab and sugarcane fiber
Diab and fiberglass
SIP
Diab foam composites in comparison with SIP

F

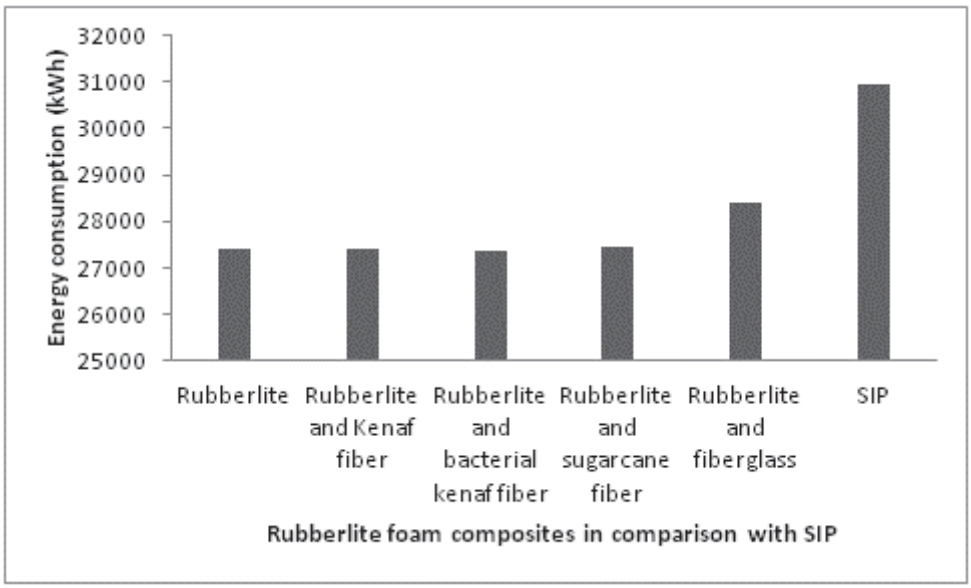


G

*Figure 5-10* (A) Annual energy consumption for PU foam with 0, 5, 10, and 15 % kenaf core loading, (B) annual energy consumption for sandwich foam composites with kenaf fiber panel, (C) for sandwich foam composites with bacterial kenaf fiber panel, (D) for sandwich foam composites with sugarcane fiber panels, (E) for sandwich foam composites with fiberglass panels, (F) and (G) Diab™ and Rubberlite™ foam composites when compared to SIP

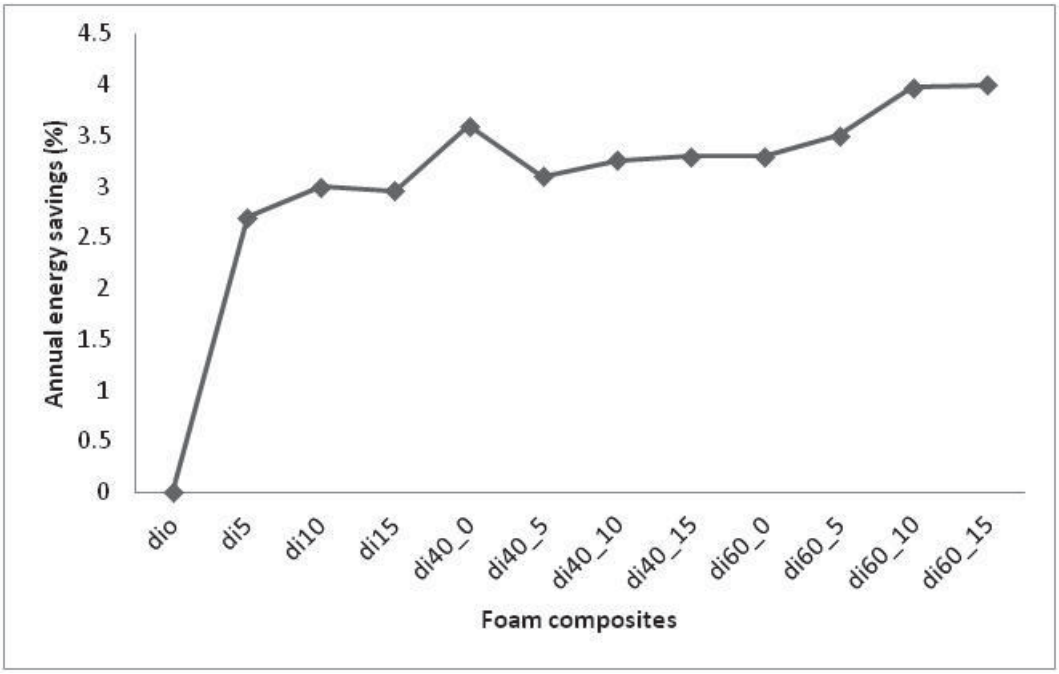
Annual energy savings (%)
4.5
4
3.5
3
2.5
2
1.5
1
0.5
0
dio
di5
di10
di15
di40_0
di40_5
di40_10
di40_15
di60_0
di60_5
di60_10
di60_15
Foam composites

A

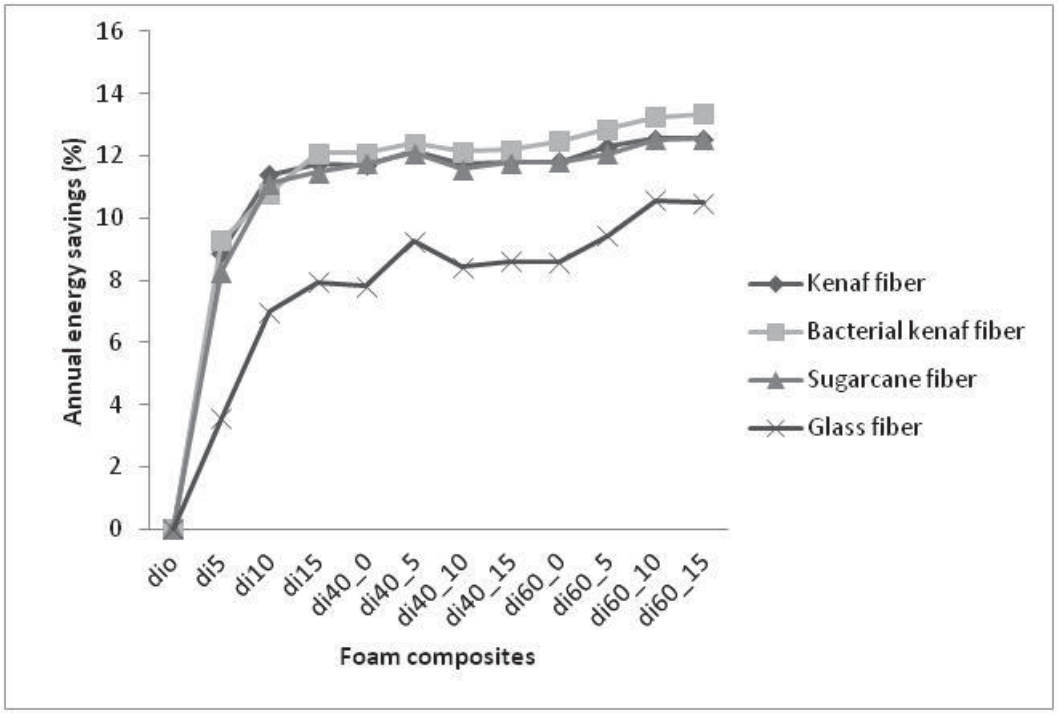
Annual energy savings (%)
16
14
12
10
8
6
4
2
0
dio
di5
di10
di15
di40_0
di40_5
di40_10
di40_15
di60_0
di60_5
di60_10
di60_15
Foam composites
Kenaf fiber
Bacterial kenaf fiber
Sugarcane fiber
Glass fiber

B

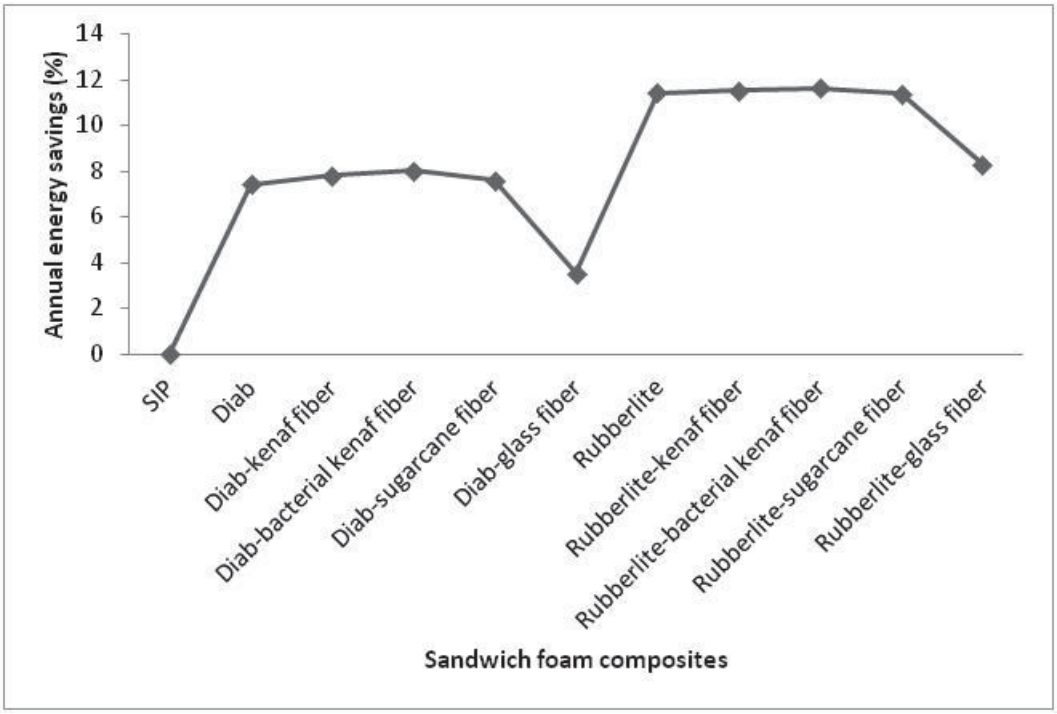


C

*Figure 5-11* Annual energy savings in percentage for (A) foam composites with kenaf core with reference as pure PU, (B) foam composites with sandwich panels made of kenaf fiber, bacterial kenaf fiber, sugarcane fiber, and glass fiber, and (C) sandwich foam composites with commercial Diab™ and Rubberlite™ foams with sandwich panels.

## 5.6 Conclusion

The constrained volume expansions of the foam composites have improved thermal resistance. Higher the constrain, higher is the pressure generated during the foam expansion and curing. The pore size reduced for 40, and 60 % volume constrained expansion as compared to free expansion. It is shown here that smaller the pore size, lower is the thermal conductivity, and therefore, better thermal properties of the foams. This is attributed to the lower gas conduction. The aging of foams for 90 days has a negligible effect on thermal conductance for the constrained foams; specifically the 60 % one showed a very small deviation from the thermal conductivity of

non aged. This is due to the urea linkages that form into hard domains in the polyurethane matrix reducing the gas diffusion as seen from AFM images. Raman spectroscopy shows that the higher the urea-to-urethane ratio lower is the reduction in thermal conductivity. Further, the kenaf fiber panels, bacterial kenaf fiber panels, sugarcane panels, and fiberglass panels additionally improve the thermal properties of the sandwich foam composites. Among all listed above bacterial kenaf fiber panels have given best thermal resistance and has proved to be a good energy saving options followed by kengro kenaf fiber and sugarcane fibers panels, and least by glass fibers.

## 5.7 References


[1] Saidur R, Masjuki HH, Jamaluddin MY. An application of energy and exergy analysis in residential sector of Malaysia. Energy Policy 2007;35(2):1050–63.

[2] E. Mazria, Architecture 2030, The 2030 Challenge, http://architecture2030.org/ current situation/building sector.html, 2007-8-5.

[3] Energy Efficiency and Renewable Energy, U.S. Department of Energy 2011. Building energy data book. Chap. 1: Building Sector.

[4] Thirumal, M., Dipak Khastgir, Nikhil K. Singha, B. S. Manjunath, and Y. P. Naik. "Effect of foam density on the properties of water blown rigid polyurethane foam." Journal of applied polymer science 108, no. 3 (2008): 1810-1817.

[5] Cao, Xia, L. James Lee, Tomy Widya, and Christopher Macosko. "Polyurethane/clay nanocomposites foams: processing, structure and properties." Polymer 46, no. 3 (2005): 775-783.

[6] Tien, Y. I., and K. H. Wei. "High-tensile-property layered silicates/polyurethane nanocomposites by using reactive silicates as pseudo chain extenders." Macromolecules 34, no. 26 (2001): 9045-9052.

[7] Seo, W. J., J. H. Park, Y. T. Sung, D. H. Hwang, W. N. Kim, and H. S. Lee. "Properties of water-blown rigid polyurethane foams with reactivity of raw materials." Journal of applied polymer science 93, no. 5 (2004): 2334-2342.

[8] Xu, Zhongbin, Xiling Tang, Aijuan Gu, and Zhengping Fang. "Novel preparation and mechanical properties of rigid polyurethane foam/organoclay nanocomposites." Journal of applied polymer science 106, no. 1 (2007): 439-447.

[9] Yang, Zhen-Guo, Bin Zhao, Sang-Lu Qin, Zheng-Fei Hu, Zhong-Kao Jin, and Jian-Hua Wang. "Study on the mechanical properties of hybrid reinforced rigid polyurethane composite foam." Journal of applied polymer science 92, no. 3 (2004): 1493-1500.

[10] Harikrishnan, G., and D. V. Khakhar. "Effect of monomer temperature on foaming and properties of flexible polyurethane foams." Journal of applied polymer science 105, no. 6 (2007): 3439-3443.

[11] Oertel, Günter, and Lothar Abele. Polyurethane handbook: chemistry, raw materials, processing, application, properties. Hanser Publishers. Distributed in USA by Scientific and Technical Books, Macmillan, 1985.

[12] Antolini, B., F. Bianchi, M. Bottazzi, M. Careri, and M. Musci. "Development and validation of novel DH-GC-ITMS methods for the determination of Freon F-141b in formulated polyol and rigid polyurethane foam." Chromatographia 60, no. 5-6 (2004): 323-327.

[13] Guo, Andrew, Ivan Javni, and Zoran Petrovic. "Rigid polyurethane foams based on soybean oil." Journal of Applied Polymer Science 77, no. 2 (2000): 467-473.

[14] Hu, Yan Hong, Yun Gao, De Ning Wang, Chun Pu Hu, Stella Zu, Lieve Vanoverloop, and David Randall. "Rigid polyurethane foam prepared from a rape seed oil based polyol." Journal of applied polymer science 84, no. 3 (2002): 591-597.

[15] Javni, Ivan, Zoran S. Petrović, Andrew Guo, and Rachel Fuller. "Thermal stability of polyurethanes based on vegetable oils." Journal of Applied Polymer Science 77, no. 8 (2000): 1723-1734.

[16] Bledzki, Andrzej K., Wenyang Zhang, and Andris Chate. "Natural-fibre-reinforced polyurethane microfoams." Composites Science and Technology 61, no. 16 (2001): 2405-2411.

[17] Bledzki, Andrzej K., Wenyang Zhang, and Omar Faruk. "Microfoaming of flax and wood fibre reinforced polypropylene composites." Holz als Roh-und Werkstoff 63, no. 1 (2005): 30-37.

[18] Matuana, Laurent M., and Fatih Mengeloglu. "Microcellular foaming of impact-modified rigid PVC/wood-flour composites." Journal of Vinyl and Additive Technology 7, no. 2 (2001): 67-75.

[19] The US Department of Energy. Insulation fact sheet with addendum on moisture control, DOE/CE-0180, USA, 2002

[20] Niachou A, Papakonstantinou K, Santamouris M, Tsangrassoulis A, Mihalakakou G. Analysis of the green roof thermal properties and investigation of its energy performance. Journal of Energy Buildings 2001;33:719–29.

[21] Sozer H. Improving energy efficiency through the design of the building envelope. Build Environ 2010;45:2581-93.

[22] N. Lechner, Heating, Cooling, Lighting: Design Methods for Architects, 2nd ed., John Wiley and Sons, Inc., New York, 2001.

[23] Seunghwan Yoo, Hakgeun Jeong, Byung-Lip Ahn, Hyesim Han, Donghyun Seo, Junghoon Lee, Cheol-Yong Jang, Thermal transmittance of window systems and effects on building heating energy use and energy efficiency ratings in South Korea, Energy and Buildings, Volume 67, December 2013, Pages 236-244

[24] Modesti, Michele, Alessandra Lorenzetti, and Stefano Besco. "Influence of nanofillers on thermal insulating properties of polyurethane nanocomposites foams." Polymer Engineering & Science 47, no. 9 (2007): 1351-1358.

[25] Mills, Nigel. Polymer foams handbook: engineering and biomechanics applications and design guide. Butterworth-Heinemann, 2007.

[26] Wang, Shi-Kwun, and Chong Sook Paik Sung. "Fluorescence and IR characterization of cure in polyurea, polyurethane, and polyurethane-urea." Macromolecules 35, no. 3 (2002): 883-888.

[27] Seo, W. J., H. C. Jung, J. C. Hyun, W. N. Kim, Y-B. Lee, K. H. Choe, and S-B. Kim. "Mechanical, morphological, and thermal properties of rigid polyurethane

foams blown by distilled water." Journal of applied polymer science 90, no. 1 (2003): 12-21.

# CHAPTER 6

# LIFE-CYCLE ASSESSMENT

## 6.1 Introduction

World Health Organization (WHO) studied the climate-health assessment till 2000 [1] which showed global burden, a projection to 2030 of health impact due to climate change have also been modeled by WHO [2]. Climate change brings about fluctuations in weather and affects health such as lung and heart diseases that are due to these fluctuations [3]. Ozone hole was first observed in 1979 over Antarctic pole, now show an increase in hole in 2009 (Figure 6-1 A), the Montreal protocol although is working but it's very slow to restore the ozone layer to the thickness that was measured in 1980 [4]. As a result skin cancer and pigmentation is seen on the exposed skin due to ultraviolet radiation (UVR) [5,6]. As the concentrations of chlorine decreases in the atmosphere, in near future $N_2O$ which is a greenhouse gas may pose a concern for ozone depletion in 21$^{st}$ century [7,8]. Increasing level of $CO_2$ increases the acid level of water. Acidification of seawater shows to interrupt processes such as calcification and cellular physiology that affects the microorganism population [9]. Water acidification due to decrease in pH can trigger other complex processes like leaching out metals from rocks [10]. These metal ions in water pose a severe problem of metal-induced toxicity and carcinogenicity [11]. A global emissions study for the year 1992 and a projection to 2015 shows an increase in emissions in teragrams (Tg) per year that show alarming numbers. Volatile organic compounds (VOC) were shown to increase by 20 % between years 1992 to 2015. In regions outside Europe and North America emissions of S and $NO_x$ showed an increase by 31 and 37 % respectively [12]. Although an effort can be

made to study and understand the effect of all the emissions and impact categories separately, however the cause and effects are intertwined. This makes the analysis on a whole a very complex system and has to be simplified. It is necessary to consciously make efforts towards choosing the right materials for processing and construction as this has a larger impact on ecosystem and eventually human health.

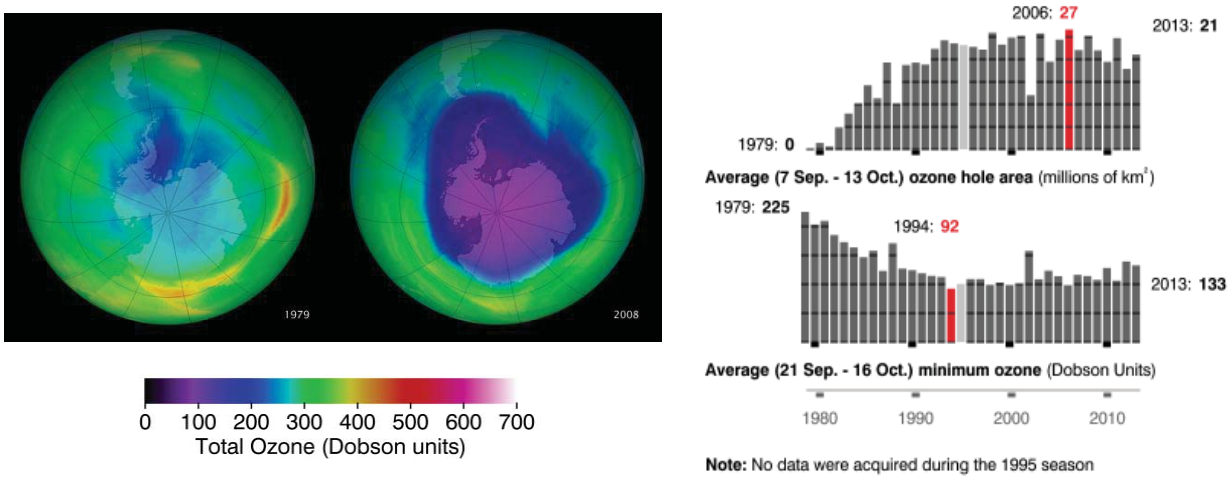


A B

*Figure 6-1* (A) Total ozone over Antarctic pole (purple and blue show least ozone, and green and red show more ozone) and (B) 1980 to 2013 the data showing depletion of the ozone [13].

Lower environmental impact has motivated researchers towards making structural building materials for roofs and walls from plant based sources, lower thermal conductivity being the property of focus. Others advantages being low cost [14], renewability [15], and $CO_2$ sequestering [16]. Binderless cotton stalk fibreboards [17], and thermal insulating kenaf fiber boards [18] with 70 % less environmental impact when compared to polyester fibers are other options for building materials. Kenaf core low density particle board [19] gave a similar thermal conductivity as rockwool. Mixture of coconut coir and durian peel [20,21], hollow wheat straw [22], solid tissue waste and

corn peel [23] have been used, too, for particle board application. Recycled plastics show lower burden on the environment than virgin plastics [24,25].

Rigid polyurethane foams have been used as insulating material for building applications with their open and closed cells imparting to them a range of properties [26,27]. Vacuum insulated panels are shown to reduce power consumption [28]. Kenaf plant is grown in many parts of USA [29]; the plant grows to a height of 5 to 6 m in 6 months. Kenaf plant has woody core which is surrounded by bast fibers. The bast fibers of hemp and flax have shown to impart better thermal resistance due to their porous structure of fiber bundles [30]. The hydrophobic woody core has use in structural applications and can be used in rigid polyurethane foams to improve the mechanical properties [31]. Hydrophilic kenaf fibers as a reinforcement to polyester matrix has been proved to enhance mechanical strength of the composite boards [32].

Life-cycle assessment (LCA) is a methodology for accounting environmental impacts that are associated with products or services. LCA is developed from chemical engineering principles and energy analysis. In general terms, LCA involves taking a product and analyzing the product life cycle from the precursor to the disposal of the product this is termed as cradle-to-grave approach. However it can be applied to any stage of product life cycle; this selected boundary is defined as a functional unit.

Today according to the standards for LCA laid down by the International Organization for Standardization 14040 series (ISO 1997, 2000), LCA consists of four phases (Figure 6-1):

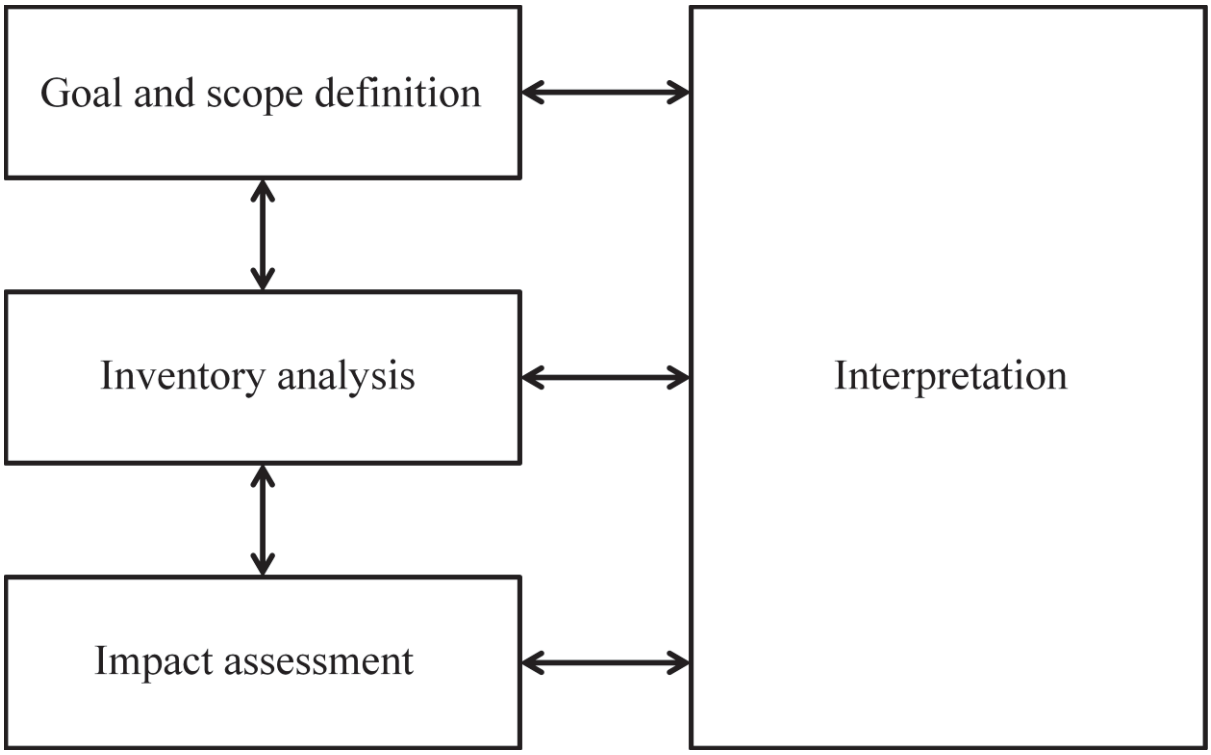


*Figure 6-2* Schematic representing four phases of LCA

### 6.1.1 Goal and Scope Definition

The purpose of the first phase is to define the goal and scope definition and the extent of the study that will be conducted. The functional unit is to be decided and defined in this stage. An assessment can contain the complete process or only a selected part or even selective impact category. When the goal is defined, the scope definition includes the boundary of the system and functional units are then defined.

### 6.1.2 Inventory Analysis

This is the second phase and involves recording of inventory for data collection and analysis. This is the most time consuming process of LCA as substantial list of raw materials, energy, and water that is the input to the unit process is made, as output

emissions to the air, water, and land is noted. These will include direct chemicals or any by-products of the reaction.

### 6.1.3 Impact Assessment

According to ISO this stage has two elements. Life-cycle impact assessment (LCIA) can be summarized as shown in Figure 6-2.

ISO 14042 (ISO 2000) define mandatory and optional elements as,

1. Mandatory elements:
    - Classification: Inventory data is assigned to various environmental impact categories, such as global warming, acidification, toxicology, ozone depletion, and ecological impacts such as terrestrial and aquatic eutrophication.
    - Characterization: Using characterization factor for each impact category, category indicator (CI) are calculated using characterization models.
2. Optional elements:
    - Normalization: Effect of CI results on reference area selected and then characterized by same characterization technique.
    - Grouping: In this grouping is done of impact categories in order of their impact, for example high, medium, and low priority.
    - Weighting: Converting category indicator values of different impact categories based on value to a common scale. This can indicate towards single indicator.

### 6.1.4 Interpretation

LCA being an iterative process can sometimes change the or slightly vary the goal and scope of the defined problem and might need further adjustments in inventory and therefore with defined impacts. The whole purpose of this study is to scientifically arrive towards a recommendation of the less environmental impact product.

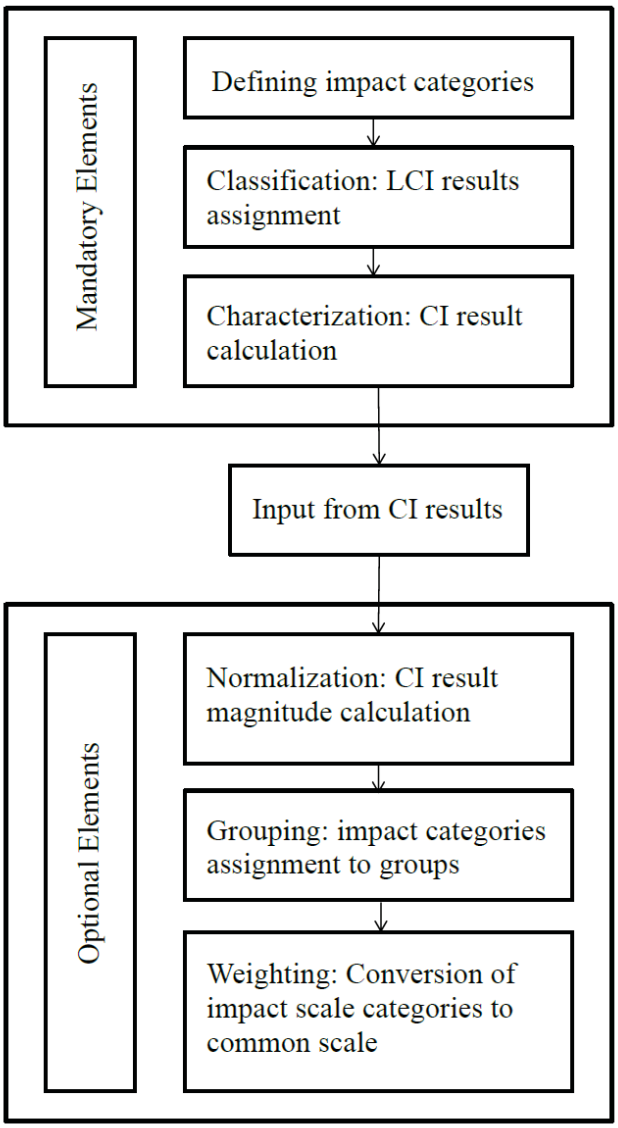


*Figure 6-3* Life-cycle impact assessment (LCIA) elements, where CI is category indicator

## 6.2 Category Indicator and Characterization Factors

### 6.2.1 Climate Change

Climate change is also called as the greenhouse effect and is due to the mechanism called as radiative forcing [33]. In this the absorption of infrared spectra is between 10 to 15 μm, which is also the spectral window of the atmosphere. Indirect effects other than global warming are the uncertainty in hurricanes that have been observed with regards to the weather impact [34].

$$GWP = \sum_i (m_i \times GWP_i)$$

Where GWP is the global warming potential, $m_i$ is the mass of greenhouse gases emission *i*, and $GWP_i$ is the characterization factor of emission *i*.

### 6.2.2 Stratospheric Ozone Depletion

Rowland and Molina in 1973 discovered that the CFC-11 readily reacts with ultraviolet light and gives off chlorine which leads to ozone depletion. Later they won Nobel Prize in chemistry for the work in 1995 [35]. The ozone hole over Antarctic was related to the same effect of homogenous catalysis as discovered by Rowland and Molina [36].

$$ODP_i = (global\ \Delta O_3\ due\ to\ i)/(global\ \Delta O_3\ due\ to\ CFC-11)$$

$$ODP = \sum_i (m_i \times ODP_i)$$

Where ODP is the stratospheric ozone depletion, $m_i$ is the mass of ozone-depleting gas emission *i*, and $ODP_i$ is the characterization factor of emission *i*.

### 6.2.3 Smog Potential

Los Angeles smog is the generic term for photochemical fog. The reaction close to ground with ozone is a complex reaction depending on the nitrogen oxides, OH-reactive hydrocarbons (HCs) and carbon monoxide.

$$POPC_{reg} = \sum_i (m_i \times POPC_i)$$

Where $POPC_{reg}$ is the photooxidant formation potential, regional; $m_i$ is the mass of aquatic eutrophying emission *i*, and $POPC_i$ is the characterization factor of emission *i*.

### 6.2.4 Acidification

Acidification increases the hydrogen ion concentration of the soil and water. The leaching of nutrients [37] from the soil is the mechanism by which the acidity is increased. Loss of aquatic life is observed due to acidification [38]. Major acidifying emissions are oxides of nitrogen, and sulphur and ammonia emissions for regional characterization.

$$X + .. \rightarrow \vartheta H^+ + ..$$

$$AP_{reg} = \sum_i (m_i \times AP_i)$$

Where X is pollutant, H+ is hydrogen ions, υ is stoichiometric coefficient, AP is the aquatic acidification potential, regional; $m_i$ is the mass of acidifying emission *i*, and $EP_i$ is the characterization factor of emission *i* within acidification.

### 6.2.5 Eutrophication

#### 6.2.5.1 Terrestrial Eutrophication

Terrestrial eutrophication has a negative impact on the animal and plant species. Increasing loads of nitrogen in an ecosystem can set an imbalance to the system. A recent study shows that this is not only in North America and Europe but also in tropical and subtropical regions [39]. Key emissions to be considered for terrestrial eutrophication are ammonia and nitrogen oxides.

$$TEP_{reg} = \sum_i (m_i \times EP_i)$$

Where TEP is the terrestrial eutrophication potential, regional; $m_i$ is the mass of eutrophying emission *i*, and $EP_i$ is the characterization factor of emission *i* within terrestrial eutrophication.

#### 6.2.5.2 Aquatic Eutrophication

Aquatic eutrophication can be defined as the increase in nutrient in water. This gives rise to a complex chain of events that throws the ecosystem out of balance [40].

$$AEP = \sum_i (m_i \times EP_i)$$

Where AEP is the aquatic eutrophication potential, $m_i$ is the mass of aquatic eutrophying emission *i*, and $EP_i$ is the characterization factor of emission *i* based on the Redfield ratio.

## 6.3 Method

The functional unit was considered to be the complete ZOE building in use. The time horizon for the building was taken as 100 y. The main aim of this work was to study

the environmental impact of heating and cooling loads when the material for building wall construction is changed from traditional SIP to foam composites of rigid PU and panels from natural fibers such as kenaf and sugarcane. The environmental impact was evaluated on the six criteria for instance fossil fuel consumption, global warming potential, acidification potential, eutrophication potential, ozone depletion, and smog potential. The phases that were considered were transportation, usage, de-construction and demolition, and transport.

## 6.4 Results and Discussion

### 6.4.1 Life Cycle Interpretation for Environmental Impact

LCA is done for three systems one for foam and the other two for sandwich foam composites. In this analysis, the pure foam (Table 5) is a reference and in most of the cases shows highest impact on the environment. For example, (Table 6), in the case of kenaf fiber panel foam composites, the environmental impact has been reduced for the 15 % kenaf core loading by almost 4 % in fossil fuel consumption, global warming potential, acidification potential, HH particles, eutrophication potential, and smog potential. Impact on ozone depletion is negligible. Bacterial kenaf fiber panel sandwich foam composites (Table 7) show almost 6 % reduction on the environmental impact factors when compared to kengro kenaf fiber. Sugarcane, on the other hand, has the lowest impact on environment. The 15 % kenaf core loaded sugarcane fiber panel with 60 volume expansion reduced the impact by almost 14 % in all cases except for ozone depletion as seen from Table 8. This lower impact is due to lower utilization of energy in order to maintain the indoor temperature of the ZOE. Sandwich composites with fiberglass panels show (Table 9) highest energy consumption of the four foam types as

well as higher impact on the environment. Among the fiberglass panels, the one with a 15 % kenaf core loading gives 4 to 5 % lesser environmental burden than the 0 % kenaf core with a free expansion.

Fig. 4 (F) shows the comparison between commercial foams like SIP and foam composites made from Diab™ and Rubberlite™. When; SIP environmental effects are taken as a reference with 100 %, foam composites with Diab™ and Rubberlite™ give ~ 5% less environmental impact.

## 6.5 Conclusion

The insulation material for the wall was replaced by the foam composites with kenaf core loadings. Further calculations were done with adding panels of kenaf fibres, enzymatic kenaf fibres, sugarcane fibres, glassfibres. Commercial foams like rubberlite and diab with combination of above mentioned panels were assessed. SIP with conventional EPS showed highest environmental impact. The lowest impact was shown by bacterial retted kenaf fibres.

Table 6-1

*Environmental impact for foam composites with kenaf core*

| | PU foam | | | | | | | | | | | |
|---|---|---|---|---|---|---|---|---|---|---|---|---|
| Volume expansion | 0 | | | | 40 | | | | 60 | | | |
| Kenaf core (%) | 0 | 5 | 10 | 15 | 0 | 5 | 10 | 15 | 0 | 5 | 10 | 15 |
| Fossil Fuel Consumption (MJ) | 19038437.39 | 19157706.73 | 19000000.00 | 19100000.00 | 19200000.00 | 19100000.00 | 19061155.36 | 19027078.40 | 19157706.73 | 19215017.97 | 19130341.90 | 18988354.59 |
| Global Warming Potential (kg CO2 eq) | 1553769.37 | 1563501.03 | 1550000.00 | 1560000.00 | 1570000.00 | 1560000.00 | 1555623.02 | 1552842.54 | 1563501.03 | 1568177.29 | 1561268.23 | 1549682.91 |
| Acidification Potential (kg SO2 eq) | 12161.28 | 12237.44 | 12200.00 | 12200.00 | 12300.00 | 12200.00 | 12175.79 | 12154.03 | 12237.44 | 12274.04 | 12219.97 | 12129.30 |
| HH Particulate (kg PM2.5 eq) | 1495.91 | 1505.29 | 1500.00 | 1500.00 | 1510.00 | 1500.00 | 1497.70 | 1495.02 | 1505.29 | 1509.79 | 1503.14 | 1491.98 |
| Eutrophication Potential (kg N eq) | 116.69 | 117.35 | 117.00 | 117.00 | 118.00 | 117.00 | 116.81 | 116.62 | 117.35 | 117.67 | 117.20 | 116.41 |
| Ozone Depletion Potential (kg CFC-11 eq) | 0.00 | 0.00 | 0.00 | 0.00 | 0.00 | 0.00 | 0.00 | 0.00 | 0.00 | 0.00 | 0.00 | 0.00 |
| Smog Potential (kg O3 eq) | 49681.35 | 50193.15 | 49900.00 | 50000.00 | 50300.00 | 50100.00 | 49940.74 | 49851.66 | 50193.15 | 50342.97 | 50121.61 | 49750.43 |

Table 6-2

*Environmental impact for sandwich foam composites with kenaf fiber panels*

| | Sandwiched foam composite (Kenaf fiber) | | | | | | | | | | | |
|---|---|---|---|---|---|---|---|---|---|---|---|---|
| Volume expansion | 0 | | | | 40 | | | | 60 | | | |
| Kenaf core (%) | 0 | 5 | 10 | 15 | 0 | 5 | 10 | 15 | 0 | 5 | 10 | 15 |
| Fossil Fuel Consumption (MJ) | 18426084.83 | 17813732.27 | 18162246.59 | 18193741.96 | 18365675.68 | 18344506.67 | 18271189.58 | 18271189.58 | 18223688.37 | 18119908.55 | 18097706.90 | 17705821.92 |
| Global Warming Potential (kg CO2 eq) | 1503805.05 | 1453840.73 | 1482277.42 | 1484847.26 | 1498876.02 | 1497148.76 | 1491166.52 | 1491166.52 | 1487290.71 | 1478822.89 | 1477011.37 | 1445035.89 |
| Acidification Potential (kg SO2 eq) | 11770.27 | 11379.25 | 11601.79 | 11621.90 | 11731.69 | 11718.17 | 11671.36 | 11671.36 | 11641.03 | 11574.76 | 11560.58 | 11310.34 |
| HH Particulate (kg PM2.5 eq) | 1447.78 | 1399.64 | 1427.04 | 1429.52 | 1443.03 | 1441.37 | 1435.60 | 1435.60 | 1431.87 | 1423.71 | 1421.97 | 1391.16 |
| Eutrophication Potential (kg N eq) | 113.28 | 109.87 | 111.81 | 111.99 | 112.94 | 112.83 | 112.42 | 112.42 | 112.15 | 111.58 | 111.45 | 109.27 |
| Ozone Depletion Potential (kg CFC-11 eq) | 0.00 | 0.00 | 0.00 | 0.00 | 0.00 | 0.00 | 0.00 | 0.00 | 0.00 | 0.00 | 0.00 | 0.00 |
| Smog Potential (kg O3 eq) | 48260.55 | 46679.74 | 47590.82 | 47673.16 | 48122.63 | 48067.29 | 47875.62 | 47875.62 | 47751.44 | 47480.14 | 47422.10 | 46397.64 |

Table 6-3

*Environmental impact for sandwich foam composites with bacterial kenaf fiber panels*

| | Sandwiched foam composite (Bacterial kenaf fiber) | | | | | | | | | | | |
|---|---|---|---|---|---|---|---|---|---|---|---|---|
| Volume expansion | 0 | | | | 40 | | | | 60 | | | |
| Kenaf core (%) | 0 | 5 | 10 | 15 | 0 | 5 | 10 | 15 | 0 | 5 | 10 | 15 |
| Fossil Fuel Consumption (MJ) | 18180317.70 | 17569514.10 | 17697560.84 | 17770361.60 | 18050722.01 | 17927838.44 | 17777590.05 | 17753839.44 | 17589650.48 | 17356791.29 | 17311871.66 | 17111540.47 |
| Global Warming Potential (kg CO2 eq) | 1483751.92 | 1433913.99 | 1444361.84 | 1450301.95 | 1473177.68 | 1463151.12 | 1450891.74 | 1448953.84 | 1435557.00 | 1416557.07 | 1412891.90 | 1396546.07 |
| Acidification Potential (kg SO2 eq) | 11613.33 | 11223.30 | 11305.07 | 11351.55 | 11530.58 | 11452.11 | 11356.17 | 11341.00 | 11236.16 | 11087.47 | 11058.79 | 10930.86 |
| HH Particulate (kg PM2.5 eq) | 1428.46 | 1380.45 | 1390.51 | 1396.24 | 1418.27 | 1408.61 | 1396.60 | 1394.94 | 1382.03 | 1363.73 | 1360.20 | 1344.45 |
| Eutrophication Potential (kg N eq) | 111.91 | 108.51 | 109.22 | 109.63 | 111.19 | 110.51 | 109.67 | 109.54 | 108.62 | 107.33 | 107.08 | 105.96 |
| Ozone Depletion Potential (kg CFC-11 eq) | 0.00 | 0.00 | 0.00 | 0.00 | 0.00 | 0.00 | 0.00 | 0.00 | 0.00 | 0.00 | 0.00 | 0.00 |
| Smog Potential (kg O3 eq) | 47638.06 | 46041.31 | 46376.05 | 46566.36 | 47299.28 | 46978.04 | 46585.26 | 46523.17 | 46093.95 | 45485.21 | 45367.78 | 44844.08 |

Table 6-4

*Environmental impact for sandwich foam composites with sugarcane panels*

| | Sandwiched foam composite (sugarcane fiber) | | | | | | | | | | | |
|---|---|---|---|---|---|---|---|---|---|---|---|---|
| Volume expansion | 0 | | | | 40 | | | | 60 | | | |
| Kenaf core (%) | 0 | 5 | 10 | 15 | 0 | 5 | 10 | 15 | 0 | 5 | 10 | 15 |
| Fossil Fuel Consumption (MJ) | 18131783.86 | 17767780.02 | 17737833.60 | 17550926.67 | 17713050.36 | 17565383.56 | 17351628.11 | 17109475.20 | 16899650.30 | 16899650.30 | 16217278.56 | 15765500.74 |
| Global Warming Potential (kg CO2 eq) | 1479791.85 | 1450091.30 | 1447647.85 | 1432397.36 | 1445625.69 | 1433576.96 | 1416135.79 | 1396377.56 | 1379273.41 | 1379273.41 | 1323579.63 | 1286717.26 |
| Acidification Potential (kg SO2 eq) | 11582.34 | 11349.91 | 11330.78 | 11211.43 | 11314.96 | 11220.67 | 11084.17 | 10929.55 | 10795.69 | 10795.69 | 10359.83 | 10071.35 |
| HH Particulate (kg PM2.5 eq) | 1424.65 | 1396.03 | 1393.68 | 1378.99 | 1391.73 | 1380.12 | 1363.32 | 1344.29 | 1327.81 | 1327.81 | 1274.16 | 1238.65 |
| Eutrophication Potential (kg N eq) | 111.64 | 109.62 | 109.45 | 108.41 | 109.31 | 108.49 | 107.30 | 105.95 | 104.78 | 104.78 | 100.99 | 98.47 |
| Ozone Depletion Potential (kg CFC-11 eq) | 0.00 | 0.00 | 0.00 | 0.00 | 0.00 | 0.00 | 0.00 | 0.00 | 0.00 | 0.00 | 0.00 | 0.00 |
| Smog Potential (kg O3 eq) | 47511.19 | 46559.61 | 46481.33 | 45992.72 | 46416.54 | 46030.51 | 45471.71 | 44838.68 | 44290.68 | 44290.68 | 42506.31 | 41325.27 |

Table 6-5

*Environmental impact for sandwich foam composites with fiberglass panels*

| | Sandwiched foam composite (fiberglass) | | | | | | | | | | | |
|---|---|---|---|---|---|---|---|---|---|---|---|---|
| Volume expansion | 0 | | | | 40 | | | | 60 | | | |
| Kenaf core (%) | 0 | 5 | 10 | 15 | 0 | 5 | 10 | 15 | 0 | 5 | 10 | 15 |
| Fossil Fuel Consumption (MJ) | 19613615.09 | 19599158.20 | 19692611.66 | 19709650.14 | 19764379.80 | 19241866.48 | 19220697.47 | 19159255.68 | 19226376.96 | 19263551.82 | 18714190.00 | 18694053.61 |
| Global Warming Potential (kg CO2 eq) | 1600700.44 | 1599520.84 | 1607146.09 | 1608536.32 | 1613001.94 | 1570367.97 | 1568640.70 | 1563627.42 | 1569104.11 | 1572137.36 | 1527312.71 | 1525669.70 |
| Acidification Potential (kg SO2 eq) | 12528.56 | 12519.33 | 12579.01 | 12589.89 | 12624.83 | 12291.18 | 12277.67 | 12238.43 | 12281.29 | 12305.03 | 11954.24 | 11941.38 |
| HH Particulate (kg PM2.5 eq) | 1541.12 | 1539.99 | 1547.33 | 1548.67 | 1552.97 | 1511.90 | 1510.24 | 1505.41 | 1510.68 | 1513.61 | 1470.42 | 1468.84 |
| Eutrophication Potential (kg N eq) | 119.89 | 119.81 | 120.33 | 120.42 | 120.73 | 117.82 | 117.70 | 117.36 | 117.73 | 117.94 | 114.88 | 114.77 |
| Ozone Depletion Potential (kg CFC-11 eq) | 0.00 | 0.00 | 0.00 | 0.00 | 0.00 | 0.00 | 0.00 | 0.00 | 0.00 | 0.00 | 0.00 | 0.00 |
| Smog Potential (kg O3 eq) | 51384.98 | 51347.18 | 51591.49 | 51636.03 | 51779.10 | 50413.16 | 50357.82 | 50197.20 | 50372.66 | 50469.85 | 49033.71 | 48981.07 |

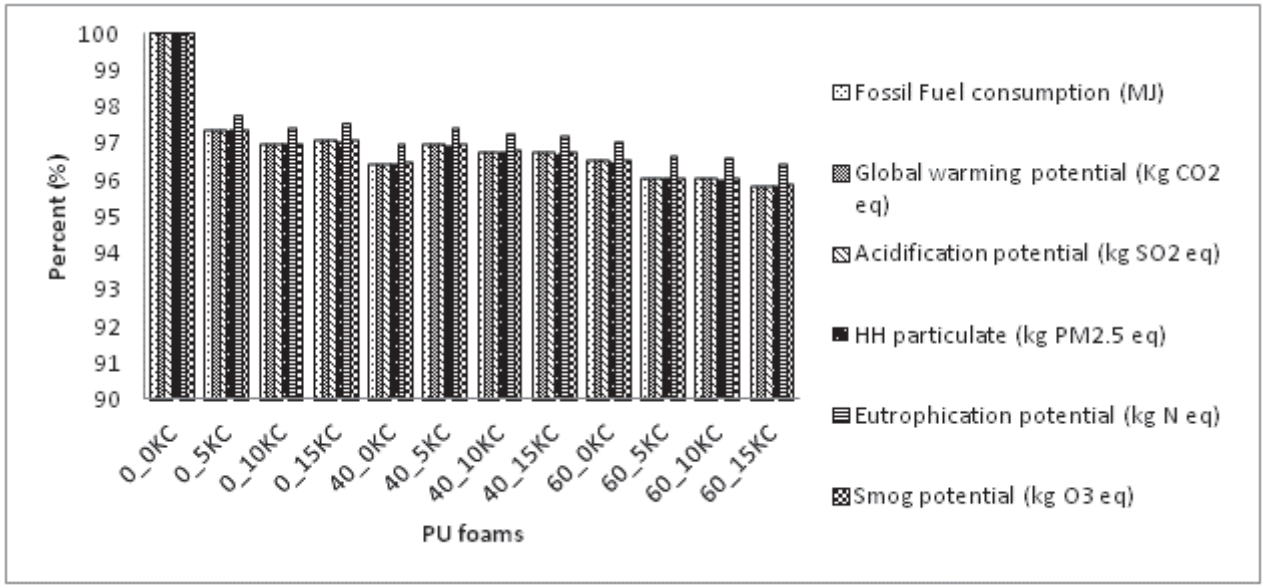
100
99
98
97
96
95
94
93
92
91
90
Percent (%)
0_0KC
0_5KC
0_10KC
0_15KC
40_0KC
40_5KC
40_10KC
40_15KC
60_0KC
60_5KC
60_10KC
60_15KC
PU foams
Fossil Fuel consumption (MJ)
Global warming potential (Kg CO2 eq)
Acidification potential (kg SO2 eq)
HH particulate (kg PM2.5 eq)
Eutrophication potential (kg N eq)
Smog potential (kg O3 eq)

**A**

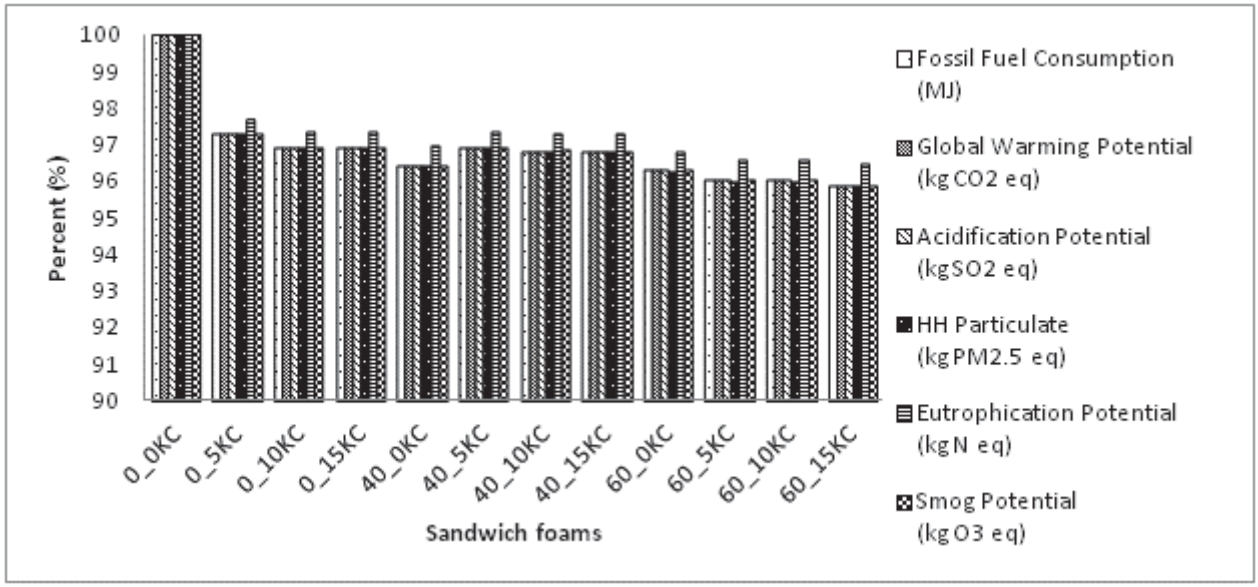
100
99
98
97
96
95
94
93
92
91
90
Percent (%)
0_0KC
0_5KC
0_10KC
0_15KC
40_0KC
40_5KC
40_10KC
40_15KC
60_0KC
60_5KC
60_10KC
60_15KC
Sandwich foams
Fossil Fuel Consumption (MJ)
Global Warming Potential (kg CO2 eq)
Acidification Potential (kgSO2 eq)
HH Particulate (kgPM2.5 eq)
Eutrophication Potential (kgN eq)
Smog Potential (kg O3 eq)

**B**

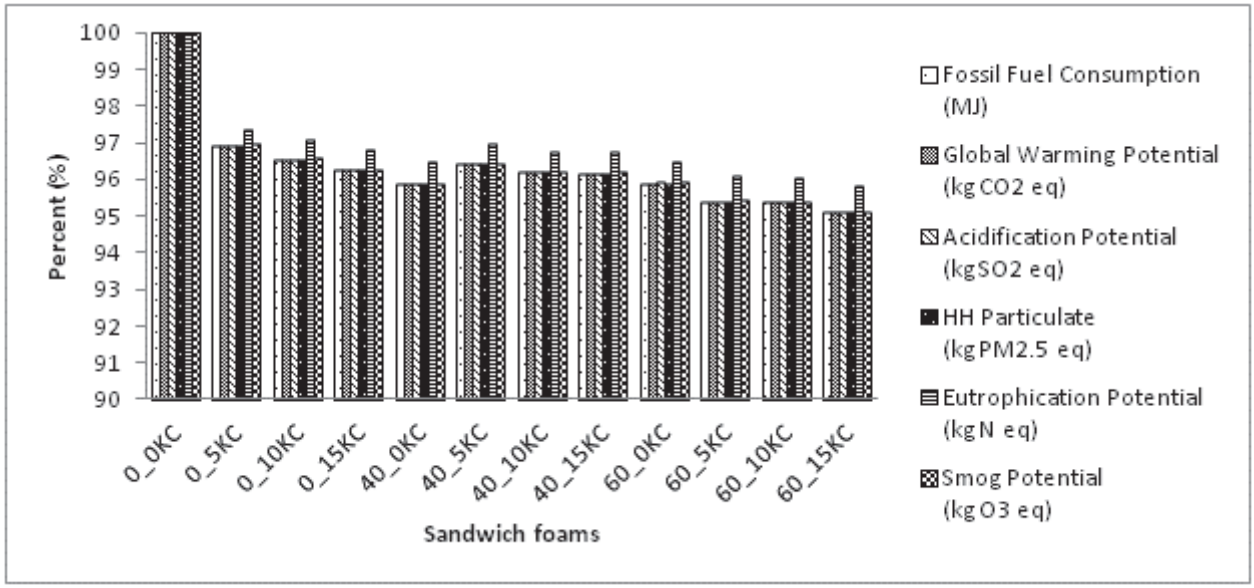
100
99
98
97
96
95
94
93
92
91
90
Percent (%)
0_0KC
0_5KC
0_10KC
0_15KC
40_0KC
40_5KC
40_10KC
40_15KC
60_0KC
60_5KC
60_10KC
60_15KC
Sandwich foams
Fossil Fuel Consumption (MJ)
Global Warming Potential (kg CO2 eq)
Acidification Potential (kgSO2 eq)
HH Particulate (kgPM2.5 eq)
Eutrophication Potential (kgN eq)
Smog Potential (kgO3 eq)

**C**

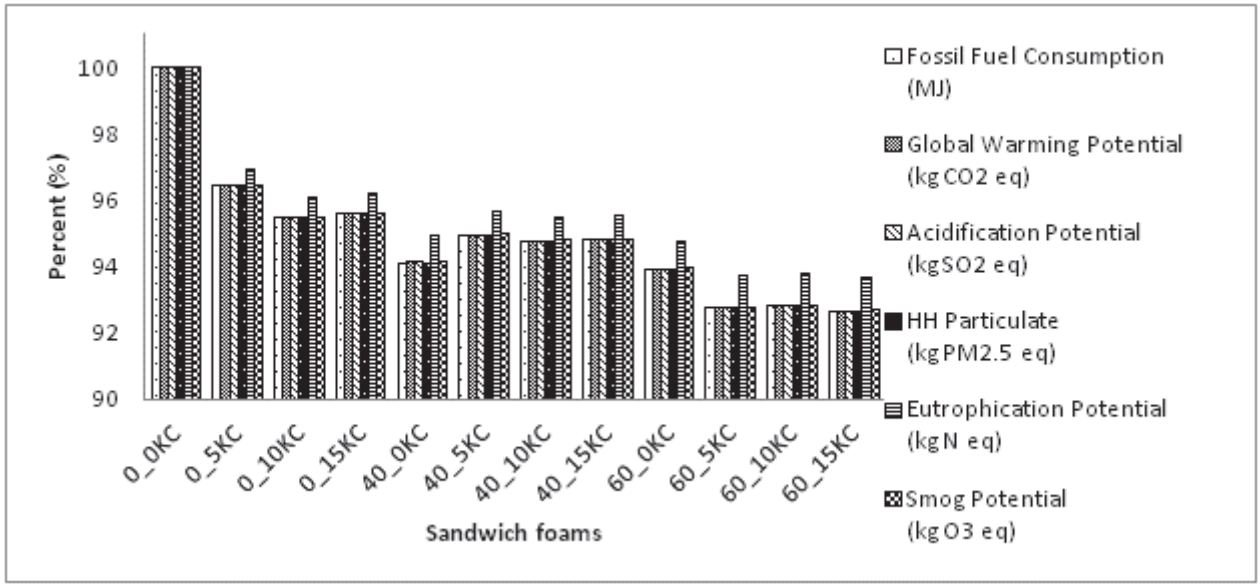
100
98
96
94
92
90
Percent (%)
0_0KC
0_5KC
0_10KC
0_15KC
40_0KC
40_5KC
40_10KC
40_15KC
60_0KC
60_5KC
60_10KC
60_15KC
Sandwich foams
Fossil Fuel Consumption (MJ)
Global Warming Potential (kg CO2 eq)
Acidification Potential (kgSO2 eq)
HH Particulate (kgPM2.5 eq)
Eutrophication Potential (kgN eq)
Smog Potential (kgO3 eq)

**D**

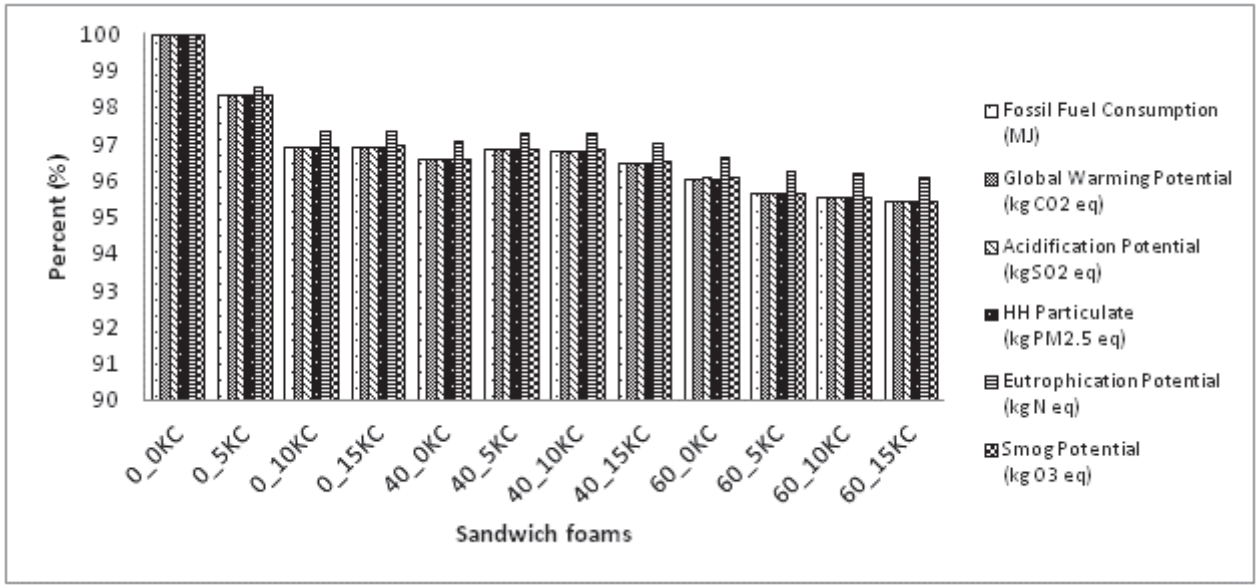


**E**

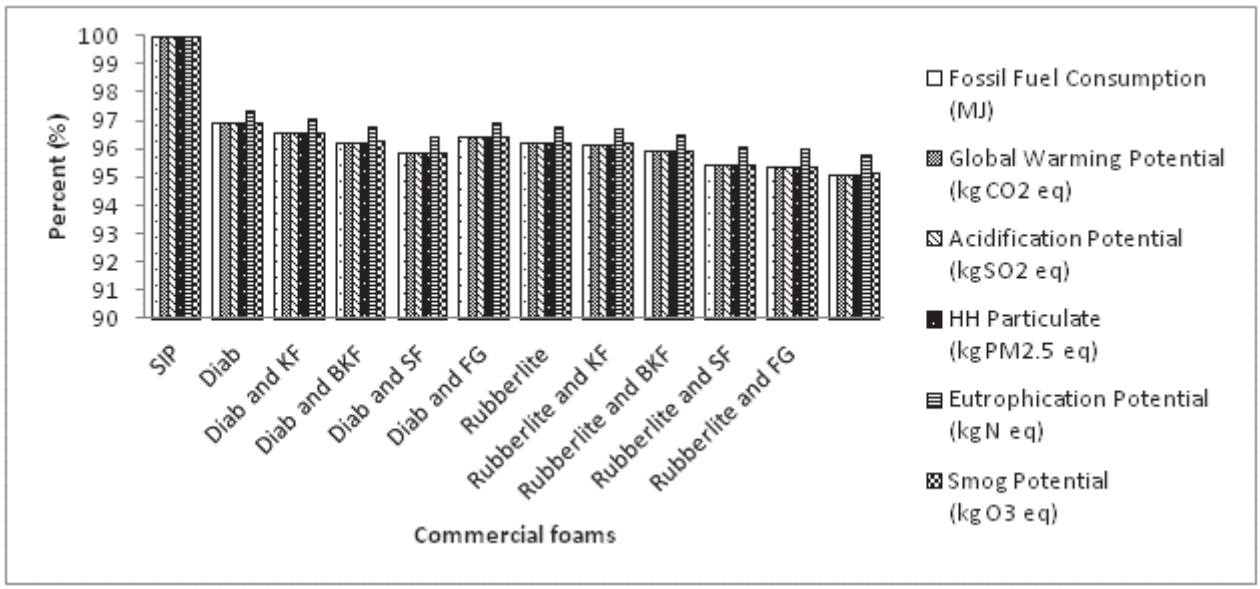


**F**

*Figure 6-4* Normalized environmental impact with reference to 0_0KC as 100 percent (A) for PU foam composites, (B) for Sandwich foam composites with Kengro kenaf fibers, (C) for sandwich foam composites with bacterial kenaf fibers, (D) for sandwich foam composites with sugarcane fibers, (E) for sandwich foam composites with fiberglass, and (F) for commercial foam composites.

## 6.6 References


[1] World Health Organization. "The World health report: 2002: reducing risks, promoting healthy life: overview." (2002).

[2] McMichael, A. J. "Impact of climatic and other environmental changes on food production and population health in the coming decades." Proceedings of the nutrition Society 60, no. 02 (2001): 195-201.

[3] Patz, Jonathan A., Diarmid Campbell-Lendrum, Tracey Holloway, and Jonathan A. Foley. "Impact of regional climate change on human health." Nature 438, no. 7066 (2005): 310-317.

[4] Salby, Murry, Evgenia Titova, and Lilia Deschamps. "Rebound of Antarctic ozone." Geophysical Research Letters 38, no. 9 (2011).

[5] Jablonski, Nina G., and George Chaplin. "Human skin pigmentation as an adaptation to UV radiation." Proceedings of the National Academy of Sciences 107, no. Supplement 2 (2010): 8962-8968.

[6] Narayanan, Deevya L., Rao N. Saladi, and Joshua L. Fox. "Review: ultraviolet radiation and skin cancer." International journal of dermatology 49, no. 9 (2010): 978-986.

[7] Konopka, Paul, Andreas Engel, Bernd Funke, Rolf Müller, Jens- Uwe Grooß, Gebhard Günther, Thomas Wetter et al. "Ozone loss driven by nitrogen oxides and triggered by stratospheric warmings can outweigh the effect of halogens." Journal of Geophysical Research: Atmospheres (1984–2012) 112, no. D5 (2007).

[8] Ravishankara, A. R., John S. Daniel, and Robert W. Portmann. "Nitrous oxide (N2O): the dominant ozone-depleting substance emitted in the 21st century." science 326, no. 5949 (2009): 123-125.

[9] Porzio, Lucia, Maria Cristina Buia, and Jason M. Hall-Spencer. "Effects of ocean acidification on macroalgal communities." Journal of Experimental Marine Biology and Ecology 400, no. 1 (2011): 278-287.

[10] Moiseenko, T. I., and N. A. Gashkina. "Zonal features of lake acidification." Water resources 38, no. 1 (2011): 47-62.

[11] Jomova, Klaudia, and Marian Valko. "Advances in metal-induced oxidative stress and human disease." Toxicology 283, no. 2 (2011): 65-87.

[12] Bouwman, A. F., D. P. Van Vuuren, R. G. Derwent, and M. Posch. "A global analysis of acidification and eutrophication of terrestrial ecosystems." Water, Air, and Soil Pollution 141, no. 1-4 (2002): 349-382.

[13] http://ozonewatch.gsfc.nasa.gov/

[14] Akil HM, Omar MF, Mazuki AAM, Safiee S, Ishak ZAM, Abu Bakar A. Kenaf fiber reinforced composites: A review. Mater Des 2011;32:4107-21.

[15] Ochi S. Mechanical properties of kenaf fibers and kenaf/PLA composites. Mech Mater 2008;40:446-52.

[16] Paridah MT, Basher AB, SaifulAzry S, Ahmed Z. Retting process of some bast plant fibres and its effect on fibre quality: A review. BioResources 2011;6:5260-81.

[17] Xiao-yan Zhou, Fei Zheng, Hua-guan Li, Cheng-long Lu, An environment-friendly thermal insulation material from cotton stalk fibers, Energy and Buildings, Volume 42, Issue 7, July 2010, Pages 1070-1074

[18] Fulvio Ardente, Marco Beccali, Maurizio Cellura, Marina Mistretta, Building energy performance: A LCA case study of kenaf-fibres insulation board, Energy and Buildings, Volume 40, Issue 1, 2008, Pages 1-10

[19] J.Y. Xu, R. Sugawara, R. Widyorini, G.P. Han, S. Kawai, Manufacture and properties of low-density binderless particleboard from kenaf core, Journal of Wood Science 50 (2004) 62–67.

[20] J. Khedari, N. Nankongnab, J. Hirunlabh, S. Teekasap, New low-cost insulation particleboards from mixture of durian peel and coconut coir, Building and Environment 39 (1) (2004) 59–65.

[21] J. Khedari, N. Nankongnab, J. Hirunlabh, S. Teekasap, New insulating particleboards from durian and coconut coir, Building and Environment 38 (3) (2003) 435–441.

[22] X.Y. Zhou, J. Li, D.G. Zhou, Thermal transfer properties of low density wheat strawboard, Journal of Nanjing Forestry University (Natural Sciences Edition) 28 (6) (2004) 1–4.

[23] P. Lertsutthiwong, S. Khunthon, K. Siralertmukul, K. Noomun, S. Chandrkrachang, New insulating particleboards prepared from mixture of solid wastes from tissue paper manufacturing and corn peel, Bioresource Technology 99 (11) (2008) 4841– 4845.

[24] V. Krivtsov, P.A.Wa¨ger, P. Dacombe, P.W. Gilgen, S. Heaven, L.M. Hilty, C.J. Banks, Analysis of energy footprints associated with recycling of glass and plastic—case studies for industrial ecology, Ecological Modelling 174 (2004) 175–189.

[25] A.C.Woolridge, G.D.Ward, P.S. Phillips, M. Collins, S. Gandy, Life cycle assessment for reuse/recycling of donated waste textiles compared to use of virgin material: an UK energy saving perspective, Resources Conservation and Recycling 46 (2006) 94–103.

[26] Modesti M, Adriani V, Simioni F. Chemical and physical blowing agents in structural polyurethane foams: Simulation and characterization. Polymer Engineering & Science 2000;40:2046-57.

[27] Yeganeh H, Razavi-Nouri M, Ghaffari M. Investigation of thermal, mechanical, and electrical properties of novel polyurethanes/high molecular weight polybenzoxazine blends. Polym Adv Technol 2008;19:1024-32.

[28] Tao W, Chang C, Lin J. An Energy-Efficiency, Performance Study of, Vacuum Insulation Panels. Journal of Cellular Plastics 2000;36:441-50.

[29] Parikh DV, Calamari TA, Sawhney APS, Blanchard EJ, Screen FJ, Warnock M et al. Improved Chemical Retting of Kenaf Fibers. Textile Research Journal 2002;72:618-24.

[30] Kymäläinen, Hanna-Riitta, and Anna-Maija Sjöberg. "Flax and hemp fibres as raw materials for thermal insulations." Building and environment 43, no. 7 (2008): 1261-1269.

[31] Nar, M., Webber, C. and Anne D'Souza, N. (2014), Rigid polyurethane and kenaf core composite foams. Polym Eng Sci. doi: 10.1002/pen.23868

[32] Bing Yang, Sheldon Shi, Michael Allen, Brian Ayre, Chuck Webber, Nandika Anne D'Souza, Kenaf VS. sugarcane Polyester Composite, Composite Part A

[33] Hyde, William T., and Thomas J. Crowley. "Probability of future climatically significant volcanic eruptions." Journal of climate 13, no. 9 (2000).

[34] Solomon, Susan, Rolando R. Garcia, F. Sherwood Rowland, and Donald J. Wuebbles. "On the depletion of Antarctic ozone." Nature 321, no. 6072 (1986): 755-758.

[35] Prather, Michael J., and Donald R. Blake. "F. Sherwood Rowland (1927-2012)." Nature 484, no. 7393 (2012): 168-168.

[36] Crutzen, Paul J., and Frank Arnold. "Nitric acid cloud formation in the cold Antarctic stratosphere: A major cause for the springtime 'ozone hole'." (1986): 651-655.

[37] Hruška, J., F. Oulehle, P. Šamonil, J. Šebesta, K. Tahovská, R. Hleb, J. Houška, and J. Šikl. "Long-term forest soil acidification, nutrient leaching and vegetation development: Linking modelling and surveys of a primeval spruce forest in the Ukrainian Transcarpathian Mts." Ecological Modelling 244 (2012): 28-37.

[38] Gibson, R., R. Atkinson, J. Gordon, I. Smith, and D. Hughes. "Impact of ocean warming and ocean acidification on marine invertebrate life history stages: vulnerabilities and potential for persistence in a changing ocean." Oceanogr Mar Biol Annu Rev 49 (2011): 1-42.

[39] Busch, Gerald, Gerhard Lammel, Friedrich O. Beese, Johann Feichter, Frank J. Dentener, and Geert-Jan Roelofs. "Forest ecosystems and the changing patterns of nitrogen input and acid deposition today and in the future based on a scenario." Environmental Science and Pollution Research 8, no. 2 (2001): 95-102.

[40] Khan, Fareed A., Fauzia Naushin, Farha Rehman, Ather Masoodi, Mudasir Irfan, Farah Hashmi, and Abid A. Ansari. "Eutrophication: Global Scenario and Local Threat to Dynamics of Aquatic Ecosystems." In Eutrophication: Causes, Consequences and Control, pp. 17-27. Springer Netherlands, 2014.

# CHAPTER 7

# CONCLUSION

## 7.1 Effect of Expansion Ratio on Cell Size, Distribution, Foam Density on PU and Kenaf Core Reinforced Foams

Polyurethane foams were processed using a unique approach of introducing constraint during foaming to influence performance, Foam cell sizes were affected by the constraints method. It was seen that constrained expansion gave an increase in cell diameter for pure PU. The cell size increased from 316 μm to 350 to 583 μm for free to 40 to 60 % constrained expansion. This was due to the higher pressure generated during the expansion resulting in cell fusion and coalescence together to give higher cell size before gelling and curing of the PU. The Cell size distribution results showed that the free foaming had a cell distribution curve which was broad indicating the cell sizes varied with a smooth incremental decrease. 40 % showed a broader distribution for smaller cell sizes but tended to show a peak for high cell size. For 60 % showed a higher frequency for large diameter cell with a broad distribution for smaller cell sizes.

Foam densities increased for constrained expansion for 40 and 60. It was 0.271 g/cc and 0.197 g/cc respectively. Free foaming showed on the other hand a lowest density with 0.063 g/cc. This was due to the coalescing of the foams cells that gave higher cell sizes and thus lower foam densities with increased constraint.

Kenaf core loading with 5, 10 and 15 % for the foams with free expansion showed very little control on the cell morphology and therefore the densities. Free foaming with 5 % showed highest cell size of ~650 μm, 10 and 15 % showed ~250 and ~293 μm cell size. This affected the densities invariably from 0.0092 to 0.0085 to 0.107

g/cc for 5, 10 and 15 % loading. The cell size distribution was shown to have broader distribution. Void fraction was seen to decrease as kenaf core loading increased. The kenaf core resided within the cells and did not contribute to cell nucleation. Rather the kenaf core under free expansion conditions provided a barrier to uniform foaming of the PU. On the other hand, constrained expansion imparted good control over cell morphologies of the foam composites. For 40 % constrained expansion it is seen that the cell size decreases as the kenaf core loading increases. Foam densities increased for higher loading from 0.484 g/cc to 0.899 g/cc. and void fraction decreases from 74 % to 57 % as the kenaf core loading increased from 5 to 15 %.

A 60 % constrained expansion showed a trend similar to the 40 % constrained expansion. Cell sizes decreased from 300 to 250 to 150 μm as the kenaf core loading increased from 5 to 10 and 15 %. This trend is seen due to ability of kenaf core to initiate cell nucleation under the constraint.Higher the fraction of kenaf core particles, higher is the number of cells and therefore smaller is the cell size. This nucleating behaviour can be seen from the increase in cell density that has increased as the loading of kenaf core increased. The void fraction has tended to decrease with the higher constrained expansion of 60 % when compared to 40 % and it decreases from 67 % to 59 % to 54 % for 5 to 10 to 15 % loading of kenaf core.

## 7.2 Effect of Kenaf Core on Performance

### 7.2.1 Mechanical

The effect of constrained expansion of 40 and 60 % has improved mechanical properties as compression and flexural modulus when compared to free foaming. An increase from 21 MPa to 22 MPa for 40 % and 24 MPa for 60 % constrained expansion

was seen in compression modulus. An increase in compressive strength from 1 to 1.1 to 1.2 MPa for free expansion and 40 and 60 % expansion ratio respectively was obtained. A positive impact was seen on flexural modulus too with an increase from 7.5 to 8.2 to 10 MPa and peak load reached to 40, 41 and 45 N for free expansion, 40 and 60 % constrained expansion of the foams respectively. Thus a novel method of constrained volume expansion was employed successfully to improve the mechanical performance of the foams.

Kenaf core at 5, 10 and 15 % by weight of PU was added to PU in an attempt to impart reinforcement. For free expansion, the kenaf core showed a negative impact on mechanical properties . For compressive properties 5 % showed lower compression modulus of ~18 MPa. 10 % showed a very low modulus of 5 MPa.This was attributed to the kenaf core particles occupying the space inside the cells that did not reinforce the foam composite as seen by SEM images. 15 % showed a synergistic effect of 5 and 10 % loading. It showed an increase of compressive modulus due to the kenaf core in the cell walls but also did not improve mechanical performance due to the kenaf core residing in the cell space . A similar trend is seen for compressive strength. Flexural modulus and peak load showed an increase for 5, 10 and 15 % loading, However these were seen to decrease when compared to pure PU. This is again attributed to the kenaf core not acting as a reinforcing agent when free foaming is employed.

The 40 % constrained expansion PU showed an increase for the loading for 5, 10 and 15 % on compressive modulus indicating reinforcement due to embedding it in cell walls. However when compared to pure PU the modulus and strength showed a decrease. The flexural properties showed an increase with kenaf core loadings and

showed an increase when compared to pure foam. This showed that the kenaf core has improved flexural properties more than compressive. The same trend was seen for the 60 % constrained expansion. Kenaf core was shown to give a reinforcement effect for the foam composites by reinforcing the cell walls. Resistance to deformation was obtained for both compressive and as well as flexural loading.

The processing of the foams such as free foam expansion and constrained expansion have resulted in foams with varying cell sizes and foam densities. This has clearly influenced mechanical properties, one of them being compressive modulus. Hence modelling of foams was done with varying cell structures that included open porosity, closed porosity and bulk cells. These cell structures have influenced the uniaxial compressive strength of the foams. The combination of bulk and closed cells has shown to give higher initial stress when compared to combination of bulk and open cells. However 100 % open cell structure gave a higher stress response; this was attributed to the material that flows to the vertices while foaming and when the cells go from closed cells to open cell structure. This extra material gives extra strength to the foam structure. However when combined with bulk it's seen that closed and bulk material combination gave higher strength. It is noted that as the open porosities increased for free foaming to constrained expansion from 15 to 19 to 26 % it showed an increase in compressive modulus experimentally. A similar trend is seen for open porosities from simulation results for combinations for bulk and open pores the modulus increased as the open pores increased from 25 to 75 % from 5.94 to 7.06 %.

### 7.2.2 Acoustic

Sound absorption of the foams was seen to be influenced by cell size, higher the cell size higher was the sound absorption. Hence highest sound absorption was recorded for the foams that had cell size of ~600 µm of 0.88 at lower frequencies of 500 Hz. Medium and large frequencies that is at 2000 and 4000 Hz showed a similar trend that was seen at 500 Hz. As the cell diameter decreased the sound absorption decreased for example for 15 % kenaf loading with a cell diameter of ~150 µm showed lower sound absorption of ~0.74 at lower frequency and ~0.65 for medium and higher frequencies. Reflection of the material showed an opposite behaviour to that of sound absorption. As the cell size decreased the reflection increased. Whereas transmission loss was seen to be independent of the cell size and was correlated to the viscoelastic property of the material as measured by the tan δ. It showed higher the tan δ higher was the ability to show sound transmission loss, and hence showed higher sound insulation property. Kenaf core that occupied the cell space was shown to increase the sound absorption. This was due to the sound energy getting converted into kinetic energy that was consumed by the kenaf core particles for vibrations. This was seen for 10 and 15 % kenaf core loaded free foam samples.

### 7.2.3 Thermal Conductivity and Insulation Effectiveness

Thermal conductivity of the foam composites is influenced by cell size. Lower the cell size lower is the thermal conductivity. This is because the lower cell size has given rise to higher number of smaller cells. These gas filled cells restrict the movement of gas thereby slowing down the heat transfer from one face through the material to the other side. Hence it was seen that the lowest cell size with 150 µm had lowest thermal

conductivity of 0.0259 W/m-K. Panels made out of kenaf fibers, sugarcane fibers, fibreglass further reduced thermal conductivity of which sugarcane fibers showed the lowest thermal conductivity followed by bacterial kenaf fibers, fibreglass, and kengro kenaf fibers. Thus sandwich foam panels have shown to decrease thermal conductivity for the foam composites.,

### 7.2.4 Building Information Modeling

Net zero energy buildings energy consumption was studied using the foam composites and sandwich panels made from the fibers. The conventional SIP material was replaced for wall insulation with the foam composites and sandwich panels using the measured thermal conductivity. It was seen that SIP showed the highest energy consumption, bacterial retted kenaf panels when used with foam composites and commercial foams such as Diab™ and Rubberlite™ showed higher energy savings.

### 7.2.5 Life Cycle Assessment

Life cycle assessments for the materials in building were conducted using a time horizon of 100 years. The insulation material for the wall was replaced by the foam composites with kenaf core loadings. Further calculations were done with adding panels of kenaf fibers, enzymatic kenaf fibres, sugarcane fibres, glassfibres. Commercial foams like Rubberlite™ and Diab™ with combination of above mentioned panels were assessed. SIP with conventional EPS showed highest environmental impact. The lowest impact was shown by bacterial treated kenaf fibres.